NONEQUILIBRIUM UNIMOLECULAR REACTIONS
of
CHEMICALLY ACTIVATED FLUOROBUTANE

by

HYH WON CHANG

B. S. Yonsei University, Seoul, Korea, 1961

A MASTER'S THESIS

submitted in partial fulfilment

of the requirements for the degree

MASTER OF SCIENCE

Department of Chemistry

KANSAS STATE UNIVERSITY

Manhattan, Kansas

1965

approved by:

major professor

TABLE OF CONTENTS

LIST OF TABLES

LIST OF FIGURES

INTRODUCTION

The main purpose of this study was to obtain well defined nonequilibrium unimolecular reaction rate constants for HF elimination from CH_3CH_2F and CH_2FCH_2F. Due to problems of heterogeneous reactions, the conventional thermal activation studies of fluorine substituted ethane do not give good unimolecular rate constants from which the critical energies and enthalpies of activation can be obtained. Therefore, one objective was to establish the critical energy for CH_3CH_2F and CH_2FCH_2F from the nonequilibrium rate constants. In order to do this the experimental results were combined with the calculations from the quantum statistical theory of unimolecular reactions, commonly called the RRKM (Rice-Ramsperger-Kassel-Marcus) formulation. In terms of the RRKM formulation, the specific rate constant k_ϵ is given by

$$k_\epsilon = \frac{\sigma Z_1^+ \Sigma P\,(\epsilon_{vr}^+)}{h Z_1^* N^*\,(\epsilon_{vr})}$$

where Z_1^+, Z_1^* : Partition function for adiabatic degrees of freedom of the complex and molecule, respectively;

$\Sigma P\,(\epsilon_{vr}^+)$: Sum of energy eigenstates of the active degrees of freedom for the complex at energy ϵ_{vr}^+;

$N\,(\epsilon_{vr}^+)$: The density of energy eigenstates of the active degrees of freedom of the complex and molecule, respectively;

σ : The reaction path degeneracy;

ϵ : Active energy of the molecule;

ϵ^+ : Active energy of the activated complex;

ϵ_o : Critical energy of the reaction, thus $\epsilon^+ = \epsilon - \epsilon_o$;

The RRKM formulation is reliable if the thermochemistry is known and

enough data are available to provide a good model for the activated complex that represents the unimolecular reaction. For instance studies of unimolecular reactions of alkyl radicals (CH_3CH_2, $CH_3CH_2CH_2$, sec-C_4H_9) showed not only a good agreement between calculated and experimental results, but also showed that common features of the model exist in the same kind of reactions (1). In this laboratory a good model has been developed for the HCl elimination from energized chloroethane (2). This model was called a four centered model to emphasize the feature that the reaction involves simultaneous breaking of C-Cl and C-H bonds and formation of the C-C double bond and H-Cl bond. This four centered model has been refined and tested by matching the calculated results of CH_3CH_2Cl, CH_2ClCH_2Cl, CH_3CH_2Br, CH_2BrCH_2Br, CH_2ClCH_2Br, CD_3CD_2Cl, and CD_2ClCD_2Cl (3) (4) (5) to experimental data. Since a good model exists for four centered HX elimination reactions, if chemically activated molecules can be produced with reasonably well known energies the experimental rate constants can be used to fix the critical energies. A similar use has been made of the RRKM formulation for the evaluation of thermochemical quantities for the competitive unimolecular decomposition of chemically activated alkyl radicals (6).

Vibrationally excited CH_3CH_2F and CH_2FCH_2F, containing about 90 kcal mol^{-1} of energy due to release of potential energy of the C-C bond, were formed from the combination of CH_3 and CH_2F radicals which were generated from mercury photosensitization of CH_2FCl and co-photolysis of CH_3COCH_3 and CH_2FCOCH_2F. Since previous data on these energized molecules published in literatures (7) (8) (9) are not in agreement, a requirement of the present study was to obtain reliable data to eliminate the conflicts. This was achieved by studying the nonequilibrium reactions in a different activation system, that is, Hg-photosensitized reaction. Since the

activation energies for the HF elimination reaction from CH_3CH_2F and CH_2FCH_2F are less than 90 kcal mol^{-1} (expected to be 60 $\pm$ 10 kcal mol^{-1}), these vibrationally excited molecules will either decompose or be stabilized by collision. By measuring the amounts of decomposition and stabilization products, experimental decomposition rate constants at two temperatures for CH_2FCH_2F and one temperature for CH_3CH_2F were carefully measured.

In addition to determining critical energies from the matching of RRKM calculations to the experimental results, a second purpose was to compare the RRKM calculations to a previous RRK estimation. The RRK (Rice-Ramsperger-Kassel) theory gives the following rate constant expression for a unimolecular reaction.

$$k_a = A_r \left(\frac{E - E_o}{E} \right)^{s-1}$$

where A_r is a constant called the frequency factor, E_o is a critical energy of the decomposition reaction, E is the energy content of the energized molecule and s is the number of effective classical oscillator. The critical energies for CH_2FCH_2F and CH_3CH_2F have been determined by Benson and Haugen (10) and Pritchard and Thommarson(8), respectively, by using the classical RRK theory of unimolecular reactions. This was done by adjusting the parameters (E_o, s and A_r) in the RRK equation in order to obtain agreement between the rate constants calculated from the RRK equation and the early experimental values (8) (9). As applied by the above authors, the RRK treatment requires the parameter, s to vary from 10.5 for CH_3CH_2F to 16.5 for CHF_2CF_3 (10). There is some doubt as to whether or not the number of effective classical oscillator should really change in the series of halogen substituted ethanes, and this point

was investigated.

A third purpose of this study was to measure the temperatue dependence of the chemical activation rate constant and compare this dependence with the calculated results from the RRKM formulation. In this comparison, the temperature dependence of the collisional cross section should be considered since it enters into the expression for the experimental rate constant; much of the work in the literature has ignored this. For a unit deactivation mechanism the calculated RRKM apparent rate constant, k_a, depends only upon energy content of the activated molecule, which is governed by the energy distribution function, $f(\epsilon)$, of the activated molecules as shown in the following equation

$$k_a = \omega \frac{\int_{\epsilon_{min}}^{\infty} \frac{k_\epsilon}{k_\epsilon + \omega} f(\epsilon) d\epsilon}{\int_{\epsilon_{min}}^{\infty} \frac{\omega}{k_\epsilon + \omega} f(\epsilon) d\epsilon}$$

where ω is the collisional frequency.

At high pressure where $\omega \gg k_\epsilon$ the above expression reduces to

$$k_a = \int_{\epsilon_{min}}^{\infty} k_\epsilon f(\epsilon) d\epsilon$$

If $f(\epsilon)$ and k_ϵ are calculated from models, the experimental and calculated apparent rate constants can be compared at various temperatures. This kind of test of the theory has been done only for butyl radicals by Rabinovitch and co-workers (11). For instance, in the H + butene - 1 case increasing the temperature from -78°C to 27°C caused the rate constants to increase by a factor of 2.2. This rate constant increase corresponds to a change from 10.98 to 12.4 kcal mol^{-1} for the average excess energy above ϵ_o of the

radicals. Assuming that the collisional deactivation mechanism is unchanged, varying the temperature in a nonequilibrium system only affects the amount of energy in the molecule undergoing reaction. Since the specific rate constant in RRKM formulation depends only upon energy, varying the energy is one way of testing the theory.

The final purpose of this study was to measure the collisional deactivation probabilities of CH_2FCH_2F. This was done by comparing the competition between unimolecular reaction and collisional deactivation at low pressures. It was of special interest to learn if the collisional deactivation probabilities are temperature dependent. Previously, a simple stepladder model for collisional deactivation was used for CH_2ClCH_2Cl (12). The same type of model was utilized in this study. These collisional efficiency results are especially pertinent for the practical purpose of comparing rate constants deduced from other nonequilibrium unimolecular reaction studies of fluoroethane in the literature. Furthermore, such data are needed for developing theories of the intramolecular energy transfer in polyatomic molecules.

EXPERIMENTAL

Reagents. The following reagents were used;

CH_2=CHF, CH_2FCl	(Gifts from E. I. du Pont de Nemours)
C_3H_6	(Matheson Scientific Inc.)
CHFClCHFCl	(Pierce Chemical Co.)
CH_3COCH_3	(Fischer Scientific Co.)
CH_2FCOCH_2F	(Pfaltz & Bauer Inc.)
CH_2FCH_2F	(Prepared by author)

Apparatus and Gas Handling Techniques. Gas handling was done in a conventional vacuum system which was operated at pressures of 10^{-3} - 10^{-4} mm. Most gas measurements were made with a gas burrette equipped with greaseless Springham valves having viton-A diaphragms. Since acetone reacts with the viton diaphragm, the ketones were handled with a calibrated pyrex line which was fitted with greased stopcocks.

The Hg photosensitization experiments were carried out in quartz vessels which ranged in size from 35 to 254 cc. The types of vessels are shown in fig. 1; the sealed vessel was used for the higher temperature photosensitization. The pressure of interest was obtained by varying the size of vessels with nearly constant sample size, 2 cc at standard temperature and pressure. This was done because the gas chromatography (to be called g. c.) columns can conveniently handle this quantity of gas, and they were calibrated for this size of sample.

Two different lamps were used for the light source:
(a) General Electric's 15 watt Germicidal lamp for Hg photosensitization. The output of the lamp is mostly 2537 Å as shown in fig. 2.

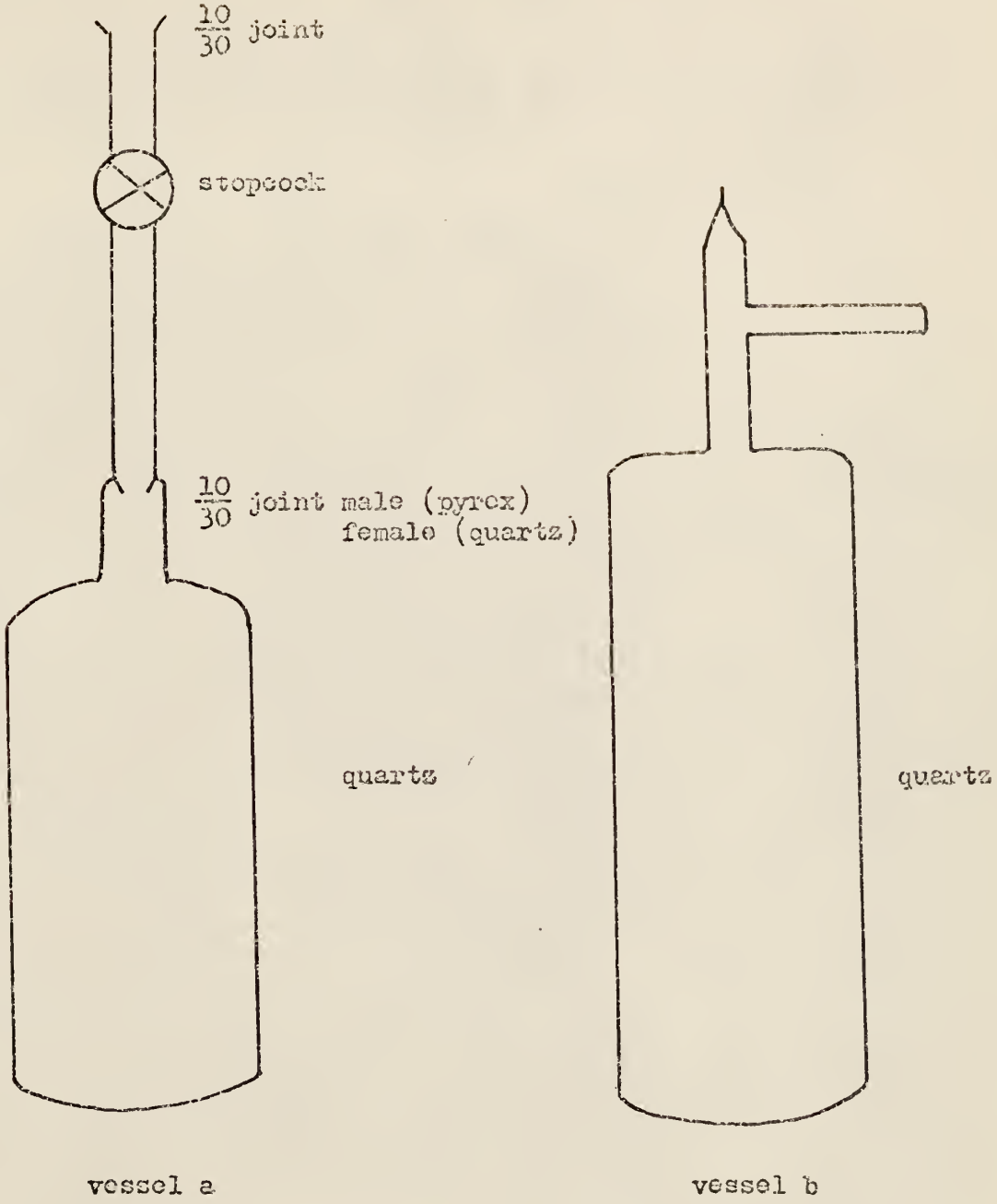

Fig. 1 Reaction vessels.

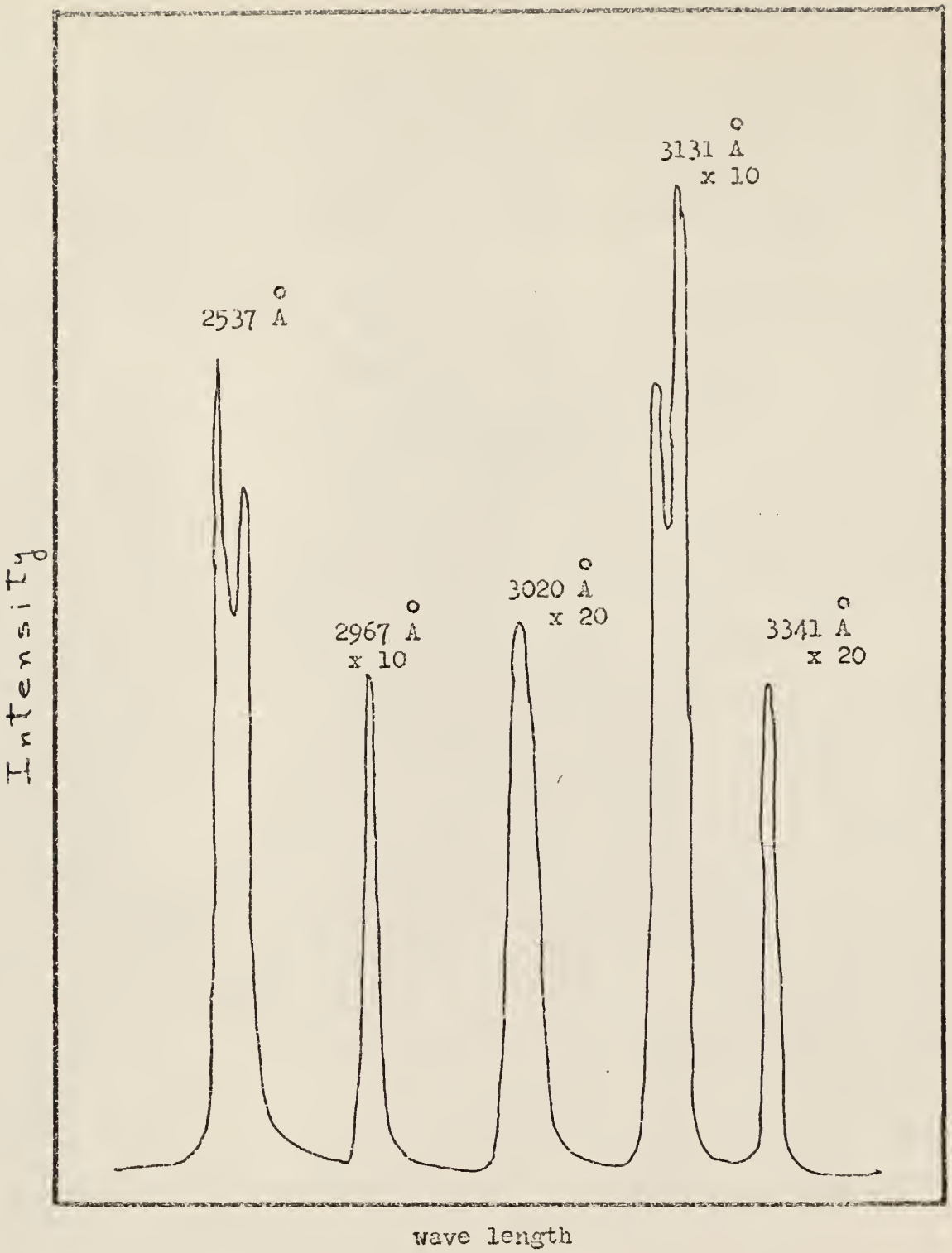

Fig. 2 Output of the lamp (a).

(b) General Electric's High Pressure mercury unfiltered, water cooled A-H6 lamp with quartz water jacket for the photolysis of the ketones. Ketones in a pyrex vessel absorb mostly at 3130 Å (13) from the output of this lamp.

The gases were analyzed by Perkin Elmer Model 820 g. c. with a four filament differential hot wire thermal conductivity detector. Helium was used as the carrier gas. The columns used were 16' x ¼" Porapak S column (column A) and 16' x ¼" ethylene glycol saturated with silver nitrate (column B). Column A was used for the analysis of the Hg photosensitization products. Columns A. and B were used for the analysis of the products from the ketone photolyses. For some experiments a 1½' x ¼" Porapak S column was connected with a Ethylene Glycol column by swagelock fittings.

The individual products trapped from the g. c. effluent were identified from their mass spectrum obtained with an Electronics Associates Inc. Quad 250 Residual gas analyzer and by comparison with retention times of known compounds.

An oven was made from a tin cylinder (3" diameter, 13" length) wrapped with chromel A wire and covered with pipe insulator. The reaction vessel shown in fig. 1-b was illuminated through a ½" x 9" slit in the side of the oven. The oven temperature was controlled by a powerstat and was measured with a thermometer which was placed inside the oven. With this apparatus it was possible to reproduce the oven temperature within 5°C accuracy.

Hg Photosensitization Procedure of CH_2FCl at 300°K. About 1.8 cc of CH_2FCl, 0.2 cc of C_3H_6 and a few drops of Hg were transferred to the reaction vessel which also contained some glass beads. In some cases the

C_3H_6 was not added. The vapor pressure of Hg at this temperature is 2×10^{-4} cm. After thorough mixing by mechanical shaking, the vessel was illuminated for 15 to 30 min. by the lamp described above, and the entire reaction mixture was analyzed by g. c. in the following way. The temperature of the g. c. column was initially set at 70° C, and the sample was injected. After 34 min. the temperature was raised to 110° C. The retention times of the major compounds under these conditions were:

C_2H_3F-5 min. 36 sec; C_3H_6-14 min.; CH_2FCl-25 min.; $C_2H_4F_2$-36 min..

Eventually a better procedure was developed. This consisted of setting the column at 70° C and increasing the temperature to 100° C after 8 min.. The retention times were as follows:

C_2H_3F-5 min. 36 sec; C_3H_6-10 min. 24 sec; CH_2FCl-14 min; $C_2H_4F_2$-19min. 36 sec.

Hg Photosensitization procedure at 473°K. The gas handling techniques and the reactants were the same as in the previous method. The gases were sealed into the quartz cell and the entire vessel was placed in the oven with only the side arm outside of the oven, but it was shielded from the light. In this way the mercury vapor pressure was kept approximately at the room temperature value of 2×10^{-4} cm, but the portion of the vessel that was illuminated was maintained at 473°K. After photosensitization, the vessel was cracked open and the contents were transferred to the g. c. inlet. The analytical procedure was the same as before.

Photolysis of CH_3COCH_3 and CH_2FCOCH_2F at 358°K. In order to obtain chemically activated CH_3CH_2F, co-photolysis of CH_3COCH_3 and CH_2FCOCH_2F was done. Due to the fact that the extinction coefficient of CH_2FCOCH_2F is about five times larger than that of CH_3COCH_3 (13) at 3130 Å, the ratio of CH_2FCOCH_2F to CH_3COCH_3 was about 1 to 5 in all experiments. 2 cc of CH_3COCH_3 and 0.4 cc of CH_2FCOCH_2F were sealed into a pyrex vessel

containing glass beads for mixing. Because of the low vapor pressure of CH_2FCOCH_2F the vessel was heated to 85°C in the oven described before. The oven was heated by the light of the lamp and temperature was controlled by passing a stream of air over the oven. After photolysis the vessel was cracked open and the contents pumped into a glass wool trap at liquid nitrogen temperature. After pumping the CO away, which required less than one minute, the samples were transferred into the g. c. inlet.

The temperature programming scheme for analysis as a function of time after sample injection was 25°C initially, 70°C after 8 min. and 90°C after 30 min.. The retention times of the major compounds were $CH_3F + C_2H_4$ - 11 min.; C_2H_6 - 15 min., C_2H_5F - 27 min.; $C_2H_4F_2$ - 44 min.. Since CH_3F and C_2H_4 were not separated by column A it was necessary to collect these compounds from the helium effluent by passing the gas mixture ($CH_3F + C_2H_4$) through traps at liquid nitrogen temperature. These collected samples were then re-run through column B; the retention times of these two compounds on column B were:

$$CH_3F - 3 \text{ min.}; \quad C_2H_4 - 13 \text{ min.}.$$

In order to eliminate the possibility of loss of some of the C_2H_4 in the trapping procedure of the technique described above, a 1½' x ¼" Porapak S column in series with a ethylene glycol column was used for some experiments. The porapak S column was heated slightly above room temperature with chromel A wire connected to a powerstat in order to shorten the retention times. As usual the entire sample was run through the g. c., but unfortunately with this column it was not possible to observe products other than CH_3CH_2F and C_2H_4 because of the long retention times of other compounds. Ethylene glycol has a high vapor pressure so that the column can not be heated. The stabilization to decomposition ratio results were the same for each analytical method.

EXPERIMENTAL RESULTS

Hg Photosensitization of CH_2FCl

(a) Mechanism of reaction without propene. The high pressure (P> 10 cm-Hg) reaction products, CH_2FCH_2F, $CH_2FCHFCl$, $CHFClCHFCl$ and CH_3F suggest the following mechanism involving CH_2F and $CHFCl$ radicals:

$$Hg\,(^1S_o) + 2537\ \text{Å} = Hg\,(^3P_1) \qquad (1)$$

$$Hg\,(^3P_1) + CH_2FCl = CH_2F + Cl + Hg\,(^1S_o) \qquad (2a)$$

$$= CH_2F + HgCl \qquad (2b)$$

$$Cl + CH_2FCl = CHFCl + HCl \qquad (3)$$

$$CH_2F + CH_2FCl = CHFCl + CH_3F \qquad (4)$$

$$CH_2F + CH_2F = CH_2FCH_2F^* \xrightarrow{\omega} CH_2FCH_2F \quad (S) \qquad (5a)$$

$$\xrightarrow{k_a} HF + CH_2{=}CHF \quad (D) \qquad (5b)$$

$$CHFCl + CHFCl = CHFClCHFCl^* \xrightarrow{\omega} CHFClCHFCl \qquad (6a)$$

$$\xrightarrow{k_a} CHF{=}CFCl + HCl \qquad (6b)$$

$$\xrightarrow{k_a} CHCl{=}CFCl + HF \qquad (6c)$$

$$CHFCl + CH_2F = CHFClCH_2F^* \xrightarrow{\omega} CHFClCH_2F \qquad (7a)$$

$$\xrightarrow{k_a} CH_2{=}CFCl + HF \qquad (7b)$$

$$\xrightarrow{k_a} CHF{=}CFCl + HF \qquad (7c)$$

$$\xrightarrow{k_a} CHF{=}CHF + HCl \qquad (7d)$$

The asterisk denotes a molecule in its ground electronic state having ~90 kcal mol^{-1} of vibrational energy, ω and k_a are the collisional frequency and the rate constant of the unimolecular reaction, respectively, and S and D represent the stabilization product and decomposition product, respectively. Reaction 2a and 2b are expected because the cross section for Cl-R reaction with $Hg\,(^3P_1)$ is large (30 $Å^2$)(14). Similar reactions

have been observed by Gunning and co-workers (15) in the CHF_2Cl system. They have shown that the quantum yield of CHF_2 radicals from the mercury photosensitization of CHF_2Cl is greater than 0.94 mol einstein^{-1} (15). The chlorine atom rapidly abstracts an H atom in the absence of olefins. The H abstraction by chlorine is known to be faster than abstraction by radicals such as CH_2F. For instance the activation energy for H atom abstraction from CH_3Cl by Cl atoms is 2-3 kcal mol^{-1} (16a), while for abstraction by CH_3 and CF_3 radicals it is 9-12 kcal mol^{-1} (16b). The remaining reactions 5-7 are radical combination reactions.

This mechanism is analogous to that observed in the Hg photosensitization of CH_2Cl_2 (17). The mechanism shown above was established experimentally at high pressure where the yield of the decomposition product of the chemically activated haloethanes was small. Only reaction 5 is considered in the remainder of this thesis; reactions 6b, 6c, 7b, and 7c are included only in analogy with other studies of vibrationally excited haloethanes without identifying the decomposition products.

$CHFClCHFCl$ and CH_3F were identified by comparing their g. c. retention times with those of known compounds. CH_2FCH_2F and $CH_2FCHFCl$ were identified from the mass spectra of trapped product samples. As shown in Table I the main decomposition ions arise from HF and HCl elimination or C-C rupture of $CHFClCHFCl$, CH_2FCH_2F and $CH_2FCHFCl$.

The chlorine atoms produced in reaction 2a can add to the olefins produced in reactions 5b, 6b, 6c, 7b, 7c, and 7d, for example

$$Cl + CH_2{=}CHF \longrightarrow \dot{C}H_2CHFCl \quad \text{or} \quad ClCH_2\dot{C}HF \qquad (8)$$

The rest of the olefins would exhibit the same types of reaction. In the case of vinyl chloride, this reaction is about 10^3-10^4 times faster than

Table I Mass Spectra

unit: relative abundance

m/e	ion	CH_2FCH_2F	$CH_2FCHFCl$	$CHFClCHFCl$	$CH_2FCH_2CH{=}CH_2$	$CH_3CH_2CH_2Cl$
12	C	23				
13	CH	24				
14	CH_2	36				
15	CH_3	35				16
25	C_2H	35			12	
26	C_2H_2	71			49	
27	C_2H_3	260			26	56
28	C_2H_4	200			11	20
31	CF	83	11	10		
32	CHF	59			11	
33	CH_2F	1000	13			
39	$C{-}CH{=}CH_2$				69	24
41	$CH_2CH{=}CH_2$				100	45
43	$CH_3CH_2CH_2$	24			34	100
44	C_2HF	118	6	7		
45	C_2H_2F	27	39	5		
46	C_2H_3F	333	4		28	
47	C_2H_4F	106				
49	CH_2C		6	13		24
51	CH_2Cl		4	6		7
58						7
59	$CHFCH{=}CH_2$				56	
63	C_2H_4Cl					16
64	$C_2H_2F_2$	65	17			
65	$C_2H_3F_2$	71	100			
	C_2H_4Cl					4
66	$C_2H_4F_2$	130				
67	CHFCl		54	100		
69	CHFCl		15	31		
74	C_4H_7F				25	
78	C_3H_7Cl					6.8
79	CHFClC			25		
80	C_3H_7Cl					1.7
81	CHFClC			7		
99	CHFClCHF			35		
101	CHFCl			12		

hydrogen abstraction (18) by Cl from CH_2FCl. Also a reaction analogous to (8) has been observed in the Hg photosensitized decomposition of CH_2Cl_2, and made the direct measurement of olefin yield impossible. In order to eliminate reactions like (8), a chlorine atom scavenger, propene, was added to the system. The chlorine adds to the terminal position;

$$Cl + CH_3CH{=}CH_2 \longrightarrow CH_3\dot{C}HCH_2Cl \qquad (9)$$

and introduces chloropropyl radicals into the reaction system.

(B) Mechanism of reaction with propene. Previously it has been shown that the primary process of fluoroethane (19a) and fluoromethane (19b) in the quenching of H_g ($^3P_1$) was C-H fission. However, the product yields of CH_2FCl due to the C-H fission are below the limit of the detector system used in this study. This was established from the fact that the Hg photosensitization of CH_2FCl with 10 % propene gave yields of neither CHFClCHFCl nor $CH_2FCHFCl$. This establishes that CHFCl radicals are not being directly formed from reaction 3 or being formed to any large extent by reaction 4. CH_2FCH_2F was still produced in excellent yield along with minor amounts of other radical products. The Hg photosensitized decomposition of propene is known to give H and $\cdot CH_2CH{=}CH_2$ in the primary process (20); the reaction apparently goes through excited molecules which can be collisionally quenched. The $\dot{C}H_2CH{=}CH_2$, CH_2F and $CH_2\dot{C}HCH_2Cl$ radicals, which are the major compounds, may react to give a variety of compounds as shown in Table II. The mechanism was formulated primarily by analogy with the mercury photosensitization of CH_2Cl_2 and propene mixture, since complete product identification was not attempted in this work. Products in this scheme that were identified are $CH_2FCH_2CH{=}CH_2$ and $CH_3CH_2CH_2Cl$. Their mass spectrometric breakdown patterns are shown in Table I. The formation of $CH_3CH_2CH_2Cl$ from disproportionation of $CH_3\dot{C}HCH_2Cl$ radical is good evidence that propene

Table II Summary of Radical reactions of 90 % CH_2FCl and 10 % C_3H_6

Reactants	Combination products	Disproportionation products
$\dot{C}H_2F + \dot{C}H_2F$	CH_2FCH_2F[a]	none
$\dot{C}H_2F + CH_3\dot{C}HCH_2Cl$	$CH_2FCHCH_3CH_2Cl$[b]	(a) $CH_3F + CH_2{=}CH{-}CH_2Cl$ (b) $CH_3F + CH_3CH{=}CH_2Cl$ (c) $CH_2FCl + CH_3{-}CH{=}CH_2$
$CH_3\dot{C}HCH_2Cl$ $CH_3\dot{C}HCH_2Cl$	$C_6H_{12}Cl_2$[b]	(a) $CH_2{=}CH{-}CH_2Cl$[b] + $CH_3CH_2CH_2Cl$[a] (b) $CH_3CH{=}CHCl$ + $CH_3CHClCH_2Cl$[b] (c) $CH_3CH{=}CH_2$[b] + $CH_3CHClCH_2Cl$[b]
$\dot{C}H_2F + \dot{C}H_2CH{=}CH_2$	$CH_2F{-}CH_2CH{=}CH_2$[a]	none
$\dot{C}H_2CH{=}CH_2$	$C_6H_{11}Cl$[b]	(a) $CH_3CH{=}CH$ + $CH_3CH{=}CHCl$[b] (b) $CH_3CH{=}CH_2$ $CH_2ClCH{=}CH_2$[b]
$CH_3\dot{C}H{-}CH_2Cl$		

a. Identified by g. c. and mass spectrometric analysis.

b. Written by analogy with similar reaction systems.

reacted with the chlorine atoms. The complete scavenging of chlorine atoms by propene is indicated by the fact that no CHFCl radical combination products were observed. The details of this mechanism are by no means proven. However, enough is known to assume that the system can be used as a source of CH_2F radicals for production of activated CH_2FCH_2F and for studies of the latter.

(C) Chemical Activation Data. The species of main interest in this study was the vibrationally excited CH_2FCH_2F formed in reaction 5a. Activated CH_2FCH_2F molecules either decompose to give vinyl fluoride or are stabilized by collisional deactivation. Tables III & IV show typical yields for photosensitization of CH_2FCl and 10 % propene samples at various pressures. These data were obtained over a six month period, with different g. c. analytical conditions and with frequent empirical checks of the calibration of the sensitivity of the g. c..

Since k_a, the nonequilibrium rate constant, can be defined as $k_a = \omega D/S$ (21) and ω is linearly dependent on pressure, a plot of $CH_2{=}CHF/CH_2FCH_2F$ vs. 1/P should be a straight line for molecules with a small spread of internal energy. The slope is equal to the apparent nonequilibrium rate constant. Such a plot for the higher pressure data, where D/S is less than two, is shown in fig. 3. Linear least square analyses of the data gave a rate constant for the reaction 5b of 2.0 ± 0.1 cm at 300°K and 4.6 ± 0.2 cm at 473°K. Equation 10, together with collision diameters of 4.7, 5.0, and 4.5 Å for C_3H_6 (22), CH_2FCH_2F and CH_2FCl (the latter two were assumed to be the same as those for CH_3COCH_3 and CH_2Cl_2), respectively, gave $k_a = (2.0 \pm 0.1) \times 10^8$ sec^{-1} at 300°K and $k_a = (3.7 \pm 0.2) \times 10^8$ sec^{-1} at 473°K.

$$\omega = N\bar{v}\sigma^2\left(\frac{8\pi kT}{\mu}\right)^{\frac{1}{2}} \qquad (10)$$

where N is the concentration of reactant, k is Boltzmann constant, T is

Table III Typical data* for 1,2 $C_2H_4F_2$ decomposition (300°K).

Pressure cm of Hg	$C_2H_4F_2$ ($\times 10^2$ cc)	C_2H_3F ($\times 10^2$ cc)	$\frac{C_2H_4F}{C_2H_4F_2}$ (D/S)
10.20	2.96	0.675	0.228
4.95	4.63	2.12	0.460
3.37	3.30	1.68	0.509
3.13	1.36	0.878	0.646
2.07	6.08	5.76	0.942
1.84	2.90	3.30	1.14
1.73	4.5	4.77	1.06
1.25	3.60	6.10	1.70
1.05	3.28	6.39	1.95
1.05	3.13	6.29	2.01
1.05	2.07	4.93	2.38
0.965	3.61	9.12	2.53
0.928	0.929	2.31	2.49
0.898	2.06	6.60	3.20
0.695	1.46	6.60	4.40
0.637	0.5	3.35	6.70
0.592	0.306	2.25	7.35
0.58	1.9	10.7	5.63
0.548	0.403	3.93	9.75
0.548	0.222	2.36	10.6
0.497	0.639	5.66	8.86
0.476	0.264	3.04	11.5

* Yields in cc of product at STP.

Table IV Data* for 1,2 $C_2H_4F_2$ decomposition (473°K)

Pressure cm of Hg	C_2H_3F (x10^2 cc)	$C_2H_4F_2$ (x10^2 cc)	$\frac{C_2H_3F}{C_2H_4F_2}$ (D/S)
49.4	0.223	2.22	0.101
19.97	0.127	0.465	0.273
12.2	0.345	0.75	0.46
9.99	1.08	2.52	0.429
8.06	0.498	0.84	0.593
7.12	1.78	2.94	0.605
6.71	2.93	4.0	0.733
5.29	1.06	1.14	0.93
4.88	0.345	0.36	0.958
4.40	2.1	2.01	1.04
4.00	2.20	1.60	1.38
2.86	4.49	2.82	1.59
2.26	3.14	1.47	2.14
1.55	0.922	0.24	3.84
1.23	0.562	0.135	4.16
1.22	0.615	0.105	5.86
1.07	0.657	0.06	10.95

* Yields in cc of product at STP.

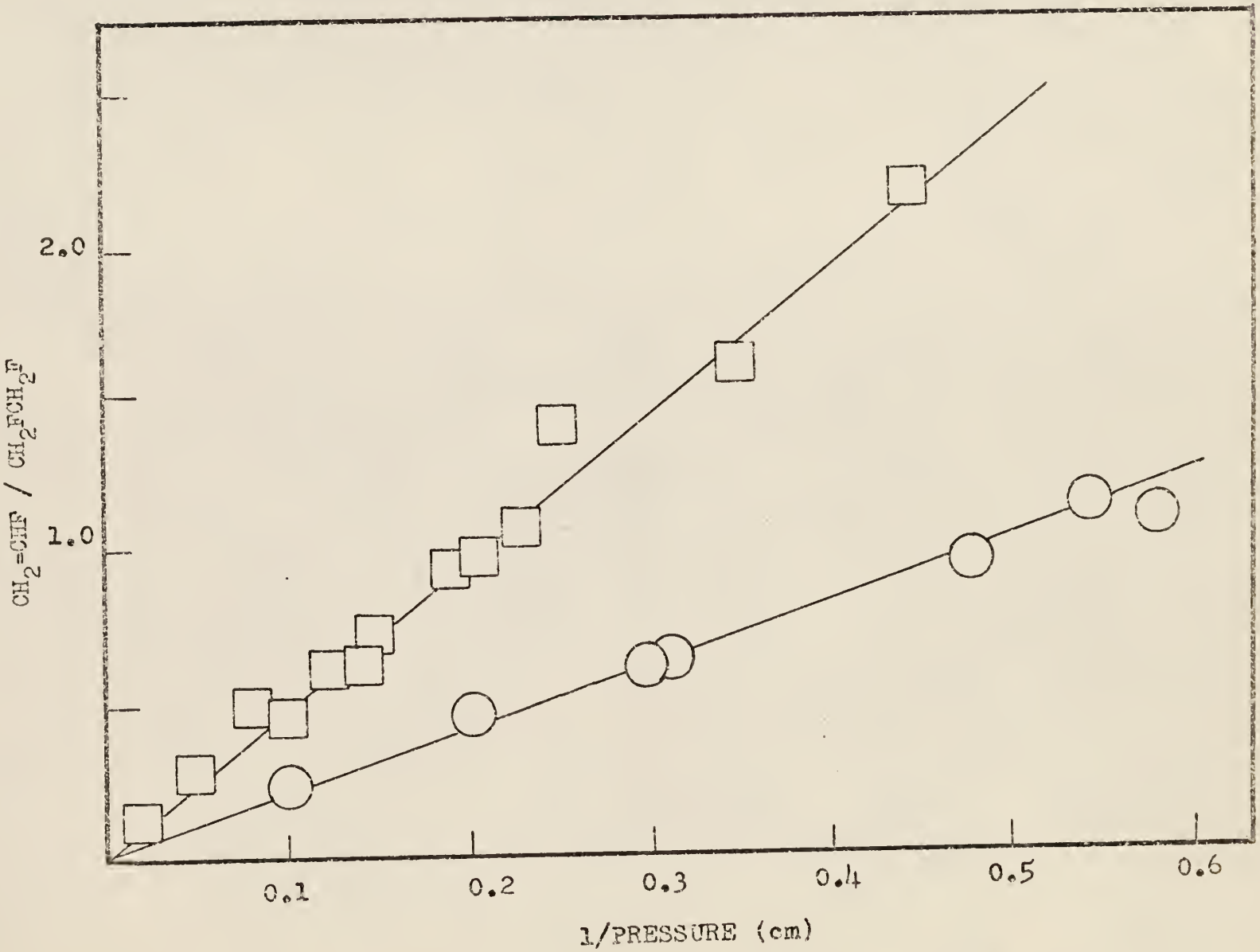

Fig. 3 D/S vs 1/P for CH_2FCH_2F at high pressure O-300°K, □ - 473°K.

temperature, μ reduced mass and σ collisional diameters.

At low pressure, where D/S is greater than two, a plot of D/S vs. 1/P does not give straight line, as shown in fig. 4. Therefore, in order to explain the low pressure data, it is necessary to introduce a collisional deactivation model other than a strictly unit deactivation model which is implied by equations 5a and 5b (to be discussed later). The collisional deactivation model reflects highly the curvature of this plot, and, hence, high accuracy of D/S measurements is important to fix the detailed aspects of the deactivation model. Unfortunately there were some experimental problems at low pressures. The consumption of propene in the lower pressure experiments was greater than in the high pressure experiments presumably due to the greater extent of decomposition of the excited propene molecule produced by Hg ($^3P_1$). In the high temperature experiments the consumption of propene was even greater due to increased rate of radical (CH_2F) additions to propene. It was necessary to maintain a large excess of propene throughout the run in order to prevent the loss of decomposition product (CH_2=CHF) by reaction 8. This was done by shortening the reaction times and increasing the amount of C_3H_6 to above 10 % of the sample. Care was taken to discard the results from a run if the ratio of propene/CH_2=CHF was not greater than 2. However, even so the low pressure points from higher temperature data tend to be less reliable than the set at the lower temperature.

Further treatment of the data, especially the low pressure data, is discussed in a later section which deals the collisional deactivation model.

Photolyses of CH_3COCH_3 and CH_2FCOCH_2F at 358°K. The photolysis of mixtures of CH_3COCH_3 and CH_2FCOCH_2F gave the following products; CH_3F,

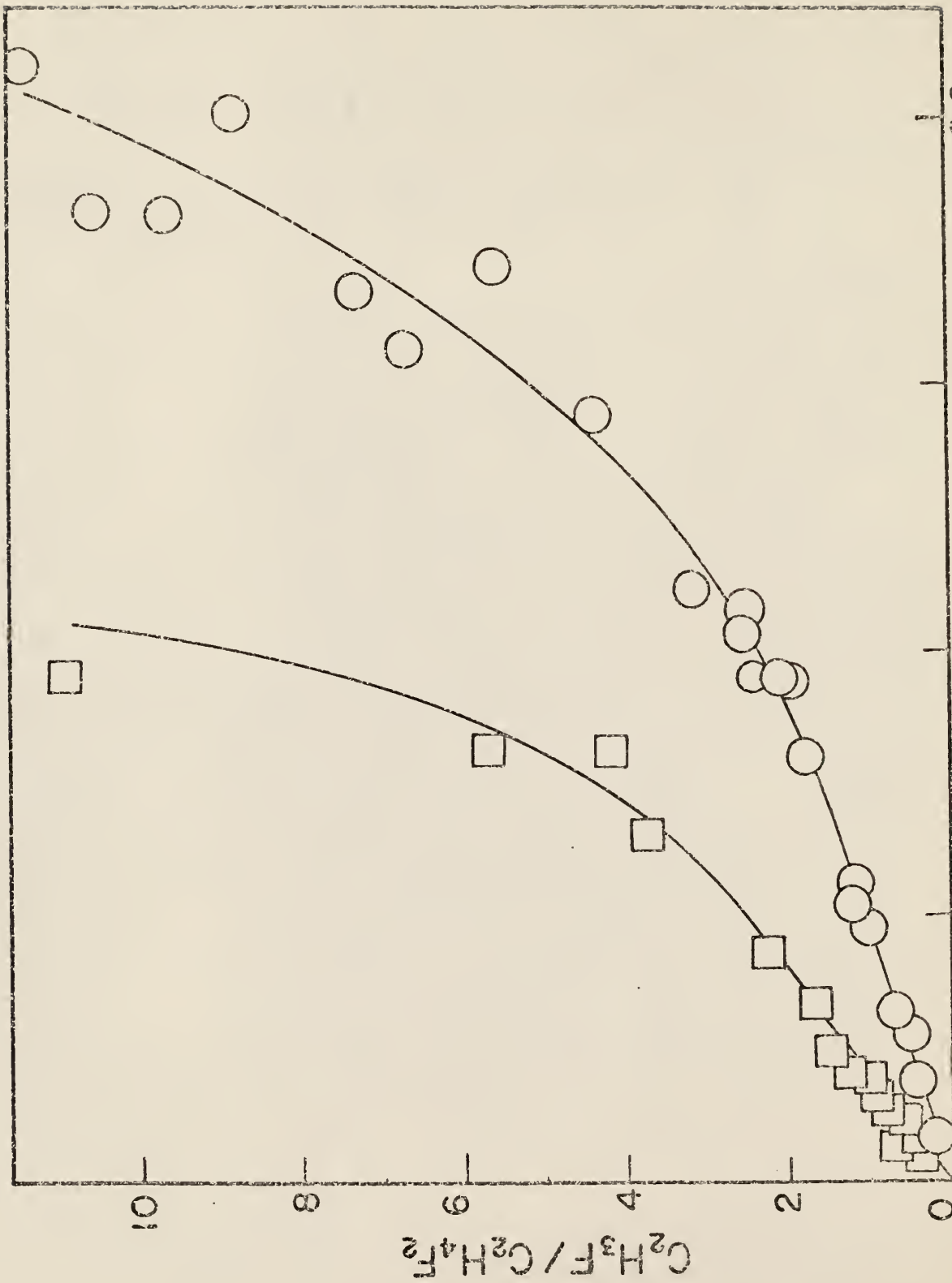

Fig. 4 Summary of all data for CH_2FCH_2F ○ - 300°K, □ - 473°K

C_2H_4, C_2H_6, C_2H_5F, and CH_2FCH_2F. The products were identified by comparing their g. c. retention times with those of known compounds. Table V shows typical yields. Quantitative analysis was done only for CH_3CH_2F and $CH_2{=}CH_2$ because our main interest was the rate constant for CH_3CH_2F elimination.

Table V. Typical data for ethyl fluoride decomposition (358°K).

Pressure cm-Hg	C_2H_4(x10^2 cc)	C_2H_5F(x10^2 cc)	$\frac{C_2H_4}{CH_3CH_2F}$
65.41	0.283	0.637	1.97
50.24	0.505	1.50	0.337
39.79	0.646	1.73	0.373
36,59	0.606	1.43	0.424
35.46	0.556	1.77	0.314
19.21	1.33	1.73	0.769
15.58	2.79	2.57	1.09
14.46	2.06	2.05	1.00
12.68	2.63	2.30	1.14
9.70	2.73	1.72	1.59
8.32	4.75	2.50	1.90

The following reaction scheme is consistent with the observed products. The photodecomposition reactions of CH_3COCH_3(13) and CH_2FCOCH_2F (8) are known to follow the scheme;

$$(CH_3)_2CO + h\nu = CH_3 + CH_3CO \qquad (11)$$

$$(CH_2F)_2CO + h\nu = CH_2F + CH_2FCO \qquad (12)$$

At high temperature these reactions are succeeded by

$$(CH_2F)CO = CH_2F + CO \qquad (13)$$

$$(CH_3)CO = CH_3 + CO \qquad (14)$$

$$CH_2F + CH_2FCOCH_2F = CH_3F + CHFCOCH_2F \quad (15)$$

$$CH_2F + CH_3COCH_3 = CH_3F + CH_2COCH_3 \quad (16)$$

$$CH_3 + CH_2FCOCH_2F = CH_4 + CHFCOCH_2F \quad (17)$$

$$CH_3 + CH_3COCH_3 = CH_4 + CH_2COCH_3 \quad (18)$$

$$CH_3 + CH_3 \overset{k_1}{=} CH_3CH_3^* \overset{\omega}{=} CH_3CH_3 \quad (19)$$

$$CH_2F + CH_2F \overset{k_2}{=} CH_2FCH_2F^* \overset{\omega}{=} CH_2FCH_2F \quad (20a)$$

$$\overset{k_a}{=} HF + CH_2{=}CHF \quad (20b)$$

$$CH_3 + CH_2F \overset{k_3}{=} CH_3CH_2F^* \overset{\omega}{=} CH_3CH_2F \quad (21a)$$

$$\overset{k_a}{=} HF + CH_2{=}CH_2 \quad (21b)$$

where k_1, k_2, and k_3 are the rate constants for the radical combination reactions. A steady state treatment of reactions (19), (20a), and (21a) at high pressure predicts

$$\frac{\left((CH_3CH_3)(CH_2FCH_2F) \right)^{\frac{1}{2}}}{(CH_3CH_2F)} = \frac{(k_1k_2)^{\frac{1}{2}}}{k_3} \quad (22)$$

Collisional theory with same values of cross sections for CH_3 and CH_2F and with no activation energy gives this ratio as 0.5. Previously it has been shown that systems with CH_3 and CH_2Cl (3), CH_3 and CH_2F (8), and CF_3 and CH_2F (44) gave 0.47, 0.48 and 0.47, respectively, for the ratio similar to eq. 22 while the system studied in this thesis gives 0.66. This close agreement also supports the mechanism suggested above.

Again a plot of $CH_2{=}CH_2/CH_3CH_2F$ vs. 1/P should give a straight line. This is shown in fig. 5. From a least squares analysis it was found that $k_a = 17.2 \pm 0.1$ cm. Equation 10, together with collisional diameters of 4.7 Å, 5 Å, and 4.0 Å for CH_3COCH_3 (22), CH_2FCOCH_2F, and CH_3CH_2F (the

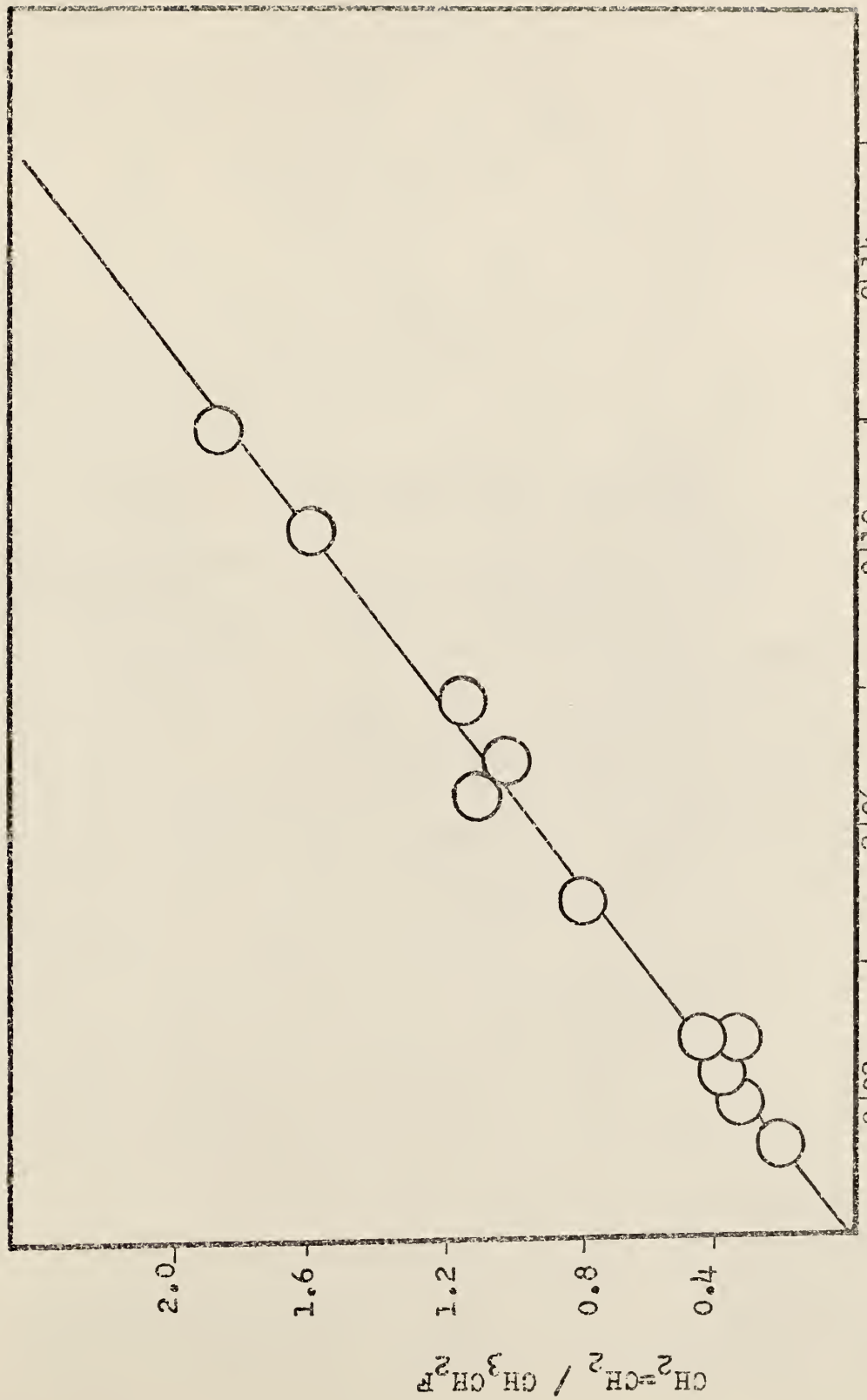

Fig. 5 D/S vs 1/P for CH_3CH_2F

values for the last two were estimated by comparing with CH_3COCH_3), respectively, gives $k_a=(1.44 \pm 0.01) \times 10^9$ sec^{-1}.

No effort was made to measure the rate constant of CH_2FCH_2F decomposition in these experiments because of the high pressure needed to obtain useful D/S ratio for CH_3CH_2F.

CALCULATIONS

(I) RRKM Formulation.

The Rice-Ramsperger-Kassel-Marcus formulation has been thoroughly discussed elsewhere (23). A brief outline of the equations will be reviewed in the following pages.

(a). Terminology.

ω ; Collision frequency.

ϵ ; Active energy of the molecule.

ϵ^+ ; Active energy of the activated complex.

ϵ_o ; Critical energy of the reaction, thus $\epsilon^+ = \epsilon - \epsilon_o$.

$\epsilon_v, \epsilon_{vr}$; Active vibrational and vibrational-rotational energy, respectively, of the molecule.

$\epsilon^+_v, \epsilon^+_{vr}$; Same as the preceding quantities, but for the activated complex.

k_ϵ ; Specific dissociation probabilities.

$P^+(\epsilon)$; Sum of energy eigenstates of the active degrees of freedom for the complex at energy ϵ^+.

$N^*(\epsilon)$; The density of energy eigenstates of the active degrees of freedom for the molecule at energy ϵ.

Z_1^+, Z_1^* ; Partition function for adiabatic degrees of freedom of the complex and molecule, respectively.

r^+, r^* ; Number of active rotational degrees of freedom for the complex and molecule, respectively, including internal rotation.

$f(\epsilon)$; The energy distribution for the system of interest.

$K(\epsilon)$; Thermal Boltzman distribution function.

σ' ; Reaction path degeneracy.

(b) Relationships of the terms and computations. When two radicals combine to form a vibrationally excited molecule, the molecule can either be stabilized by collision, undergo reverse dissociation or decompose by some lower energy path, if one is available.

$$R_1 + R_2 \underset{k_\epsilon}{\rightleftarrows} R_1\text{-}R_2^* \xrightarrow{M} R_1\text{-}R_2 \quad (S) \qquad (23a)$$

$$R_1\text{-}R_2^* \xrightarrow{k_a} M_1 + M_2 \quad (D) \qquad (23b)$$

The specific rate constant (or probability) k_ϵ for a unimolecular reaction is given by

$$k_\epsilon = \frac{\sigma' Z_1^+ \sum P(\epsilon_{vr}^+)}{h Z_1^* \; N^*(\epsilon_{vr}^*)} \qquad (24)$$

where

$$\sum_{\epsilon_{vr}^+=0}^{\epsilon_{vr}^+} P(\epsilon_{vr}^+) = \frac{Z_r^+}{(kT)^{r^+/2}\,\Gamma(1+r^+/2)} \sum_{\epsilon_v^+=0}^{\epsilon^+} P(\epsilon_v^+)(\epsilon^+ - \epsilon_v^+)^{r^+/2} \quad ; \; r^+ \neq 0 \qquad (25)$$

$$= \sum_{\epsilon_v^+=0}^{\epsilon_v^+} P(\epsilon_v^+) \quad ; \; r^+ = 0$$

$$N^*(\epsilon) = \frac{Z_r^*}{(kT)^{r^*/2}\,\Gamma(r^*/2)} \sum_{\epsilon_v=0}^{\epsilon_v} P(\epsilon_v^*)(\epsilon - \epsilon_v)^{r^*/2-1} \quad ; \; r^* \neq 0 \qquad (26)$$

$$= \frac{\partial}{\partial \epsilon}\left(\sum_{\epsilon_v=0}^{\epsilon_v} P(\epsilon_v^*)\right) \quad ; \; r^* = 0$$

For all calculations of this thesis $r^+ = r^* = 0$ except for the association complex which has $r^* = 1$. The value of $\sum P(\epsilon_{vr}^+)$ was calculated by a computer using the direct sum by Harrington's method at low energies (24) and the

Haarhoff approximation (25) at high energies.

In a real system, the molecules are formed with a distribution of energies. In order to compare the theoretical specific rate constant with the experimental rate constant, the specific rate constant must be averaged according to the energy distribution function appropriate to the experiment. In a chemical activation system where molecules are formed by association of two radicals which are in thermal equilibrium with the bath molecules, the energy distribution function is given by

$$f(\epsilon_{vr})d\epsilon_{vr} = \frac{k'_{\epsilon} K(\epsilon_{vr})d\epsilon_{vr}}{\int_{\epsilon_{min}}^{\infty} k'_{\epsilon} K(\epsilon_{vr})d\epsilon} \qquad (27)$$

The rate constant, k'_{ϵ}, refers to the decomposition reaction of the molecules into radicals which is the reverse of the activating reaction.

The apparent rate constant, which is the averaged specific rate constant, can be expressed as the ratio of probabilities of stabilization and decomposition. For a unit deactivation model this is simply:

$$k_a = \omega D/S = \omega \frac{\int_{\epsilon_{min}}^{\infty} \frac{k_{\epsilon}}{k_{\epsilon}+\omega} f(\epsilon)d\epsilon}{\int_{\epsilon_{min}}^{\infty} \frac{\omega}{k_{\epsilon}+\omega} f(\epsilon)d\epsilon} \qquad (28)$$

The formulation for a cascade collisional mechanism is considered in sec. III of CALCULATED RESULT.

(II) Models

In order to carry out the calculations of eq. 24-28, molecular models for the transition states of the radical association reactions and decompo-

sition reactions must be selected. Models of the molecules are also needed. In all cases the overall rotations are taken as adiabatic and all internal degrees of freedom are active.

(a) Association activated complex. The association complex is defined as the transition state for the following reaction

$$R_1 - R_2 \quad \underset{k_r}{\overset{k_f}{\rightleftharpoons}} \quad R_1 + R_2$$

where k_f and k_r are the macroscopic rate constant for the forward and reverse reactions, respectively.

If k_r, the bimolecular combination rate constant for the radicals, is expresses as $P\frac{1}{4}\overline{\sigma}^2\left(\frac{8\pi kT}{\mu}\right)^{\frac{1}{2}}$, where P is the steric factor, σ is the collisional diameter and $\frac{1}{4}$ is the electronic steric factor, it is found that for most radical combination reactions P ranges from 0.1 to 0.01 (26). It is possible to assume that the combination rate constant, k_r, is defined by these limits, and combine these limiting rate constant with the known equilibrium constant to obtain an estimation for the limits of the unimolecular rate constant, k_f. Once this is done, the model for the association complex can be fixed through the magnitude of the preexponential factor for k_f. The procedure is illustrated in the following equations. First the equilibrium constant is obtained from a quantum statistical calculations,

$$K_{eq} = \frac{q_{R_1}/N \; q_{R_2}/N}{q_{R_1-R_2}/N} \; e^{-\Delta\epsilon_o^\circ/RT} \qquad (29)$$

where q_{R_1}, q_{R_2} and $q_{R_1-R_2}$ are partition functions of radicals R_1 and R_2, and molecule R_1-R_2, respectively. The unimolecular reaction rate constant,

k_f, is obtained by

$$k_f = k_r K_{eq}$$

$$k_f = P \frac{\sigma^2}{4} \left(\frac{8\pi kT}{\mu}\right)^{\frac{1}{2}} \frac{q_{R_1}/N \; q_{R_2}/N}{q_{R_1-R_2}/N} e^{-\Delta\epsilon^\circ/RT} \tag{30}$$

Now the absolute rate theory form of a unimolecular reaction is

$$k_f = \frac{\sigma' kT}{h} \frac{q_r^+ q_v^+}{q_r^* q_v^*} e^{-\Delta\epsilon^\circ/RT} \tag{31}$$

$$= A_f e^{-\Delta\epsilon^\circ/RT}$$

Therefore we can equate the two preexponential factors and this gives A_f.

$$\frac{\sigma' kT}{h} \frac{q_r^+ q_v^+}{q^* q_v} = P \frac{\sigma^2}{4} \left(\frac{8\pi kT}{\mu}\right)^{\frac{1}{2}} \frac{q_{R_1}/N \; q_{R_2}/N}{q_{R_1-R_2}/N} \tag{32}$$

where q_r is the rotational partition function for total rotational degree of freedom, q_v is the total vibrational partition function, + and * refer to the complex and molecule, respectively. σ' is the reaction path degeneracy, and h is Planck's constant. Since the partition functions of the radicals and molecule can be calculated, eq. 32 gives the magnitude of the partition functions for the complex which serves to roughly define the model of the association complex.

In this study the model for the association complex was constructed first by analogy with chloroethane case and P factors calculated from this model with eq. 32 were compared with the limiting value of 0.1 to 0.01.

For the reaction

$$CH_3 + CH_2F \rightarrow CH_3 \cdots CH_2F$$

a model for the complex is as follows: each radical was assumed to be planar with the two planes separated by 3 Å. The other bond lengths were assumed to be same as in the molecules, CH_3CH_2F and CH_2FCH_2F. The angles H-C-H and H-C-F were assumed to be 120°. The vibrational frequencies of the complex were chosen to be six frequencies from each radical (12 frequencies altogether) and four C-C bending frequencies. The torsional motion was treated as an internal rotation. The frequencies of CH_3 are available (27), those of CH_2F were estimated from CH_2FCH_2F. Four low bending frequencies for C-C are critical and were chosen to obtain the assumed steric factor (Table VII). These models are similar to those used previously for the distribution function of chloroethane (3). Frequencies are shown in Table VI.

In order to determine the effect of the model on the energy distribution function, a less tightly bound complex for CH_2FCH_2F (C-C=4.5 Å) with bending frequencies 120 cm^{-1} and 80 cm^{-1} was tried. However, the change in the average energy of the activated molecule is only 0.1 kcal mol^{-1} with the one using a less tight complex having a higher average energy and all the calculations were presented in terms of the models of Table VI.

Table VI Vibrational frequencies (in cm^{-1} unit) of the radicals and association complex.

	CH_3	CH_2F	$CH_3...CH_2F$	$CH_2F...CH_2F$
CH_3 stretch	3056 (3)	3056(2)	3056 (5)	3056 (4)
CH_3 bend	1400 (2)	1435 (1)	1430 (1)	1435 (2)
			1400 (2)	
CH_3 out-of-plane	730 (1)[a]		730 (1)[a]	
H-C-F bend		1365 (1)	1365 (1)	1365 (2)
C-F stretch		1171 (1)	1171 (1)	1171 (2)
CH_2F out-of-plane		600 (1)	600 (1)	600 (2)
low bending			240 (2)	151 (2)
			150 (2)	100 (2)
Torsion			1 rotor	1 rotor
grouped			3056 (5)	3056 (4)
frequencies			1400 (4)	1400 (4)
			1171 (1)	1171 (2)
			662 (2)	600 (2)
			240 (2)	151 (2)
			150 (2)	100 (2)
			1 rotor	1 rotor

a. A more recently measured value is 610 cm^{-1} (27) but the difference is not important since there are several frequencies which are lower than 610 cm^{-1} present in the complex.

Table VII Steric factor P (800°K).

complex	k_r (sec^{-1})	K_{eq} (atoms/cc)[a]	k_f (cc/atoms sec)	P
$CH_3...CH_2F$	8.48×10^{-10}	1.16×10^{-2}	1.82×10^{-10} P	0.054
$CH_2F...CH_2F$	2.31×10^{-9}	1.54×10^{-3}	1.4×10^{-10} P	0.025

a. $K_{eq} = \frac{k_f}{k_r}$.

(b) Activation complex The activated complex is defined here as the transition state for HF elimination reaction of the vibrationally excited fluoroethane molecule. It has been found by Pritchard and co-workers with the chemical activation system of CH_2F and CD_3 (28), and by Tang and Rowland in recoil tritium experiments with CH_3CD_2F and CD_3CH_2F (29) that only α,β HF elimination occurs. Two fluorine atoms on the same carbon atom seem to be necessary for α,α elimination. For example both α,α and α,β eliminations occur from chemically activated 1,1-CH_3CHF_2 (28). The α,β elimination reaction proceeds by a simultaneous breaking of the C-X and C-H bonds and formation of C-C double bond and H-X bond. Because of these simultaneous processes, the complex has been called a four centered model. Pictorially it can be represented as

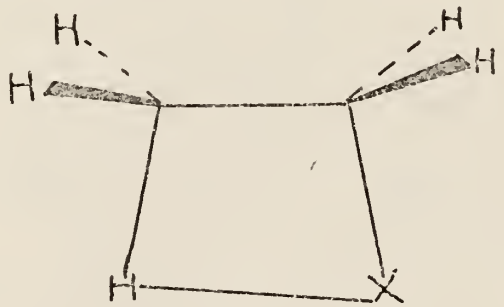

A model for this complex has been constructed by using kinetic data from the reactions of chlorine and bromine substituted ethanes, and the calculated results were in good agreement with experimental results which include thermal activation (2), chemical activation (4) and H/D kinetic isotope (5) effects for both methods of activation. The model was varied until the best simultaneous fit to all the data was obtained. Since the thermochemistry is well known for CH_3CH_2Cl and CH_3CH_2Br, and since the molecular parameters of the molecules are known, the data could be used to design the model. In order to obtain the frequencies of the complex, the model was divided

into three categories, that is, ring frequencies, ring puckering and out-of-ring frequencies. The four centered model for the chloroethane and bromoethane reactions was formulated in terms of the bond order of the four changing bonds in order to calculate the ring frequencies. Therefore it is a simple matter to transfer this model to the fluoroethane. The out-of-ring C-H frequencies were chosen by analogy with ethylene and cyclobutane for the CH_3CH_2X cases. The ring puckering frequency was a parameter and varied to fit the data.

i) Ring frequencies. The in-plane-ring frequencies were calculated by the Wilson F. G. matrix method by using force constants obtained from Johnston's force constant formula (30), with bond length calculated from Pauling's correlation of bond length with bond order (31). Johnston's force constant relationship and its constants are given as follows,

$$\log f = \left(\frac{a-d}{b}\right) \times 10^5 (\text{dynes cm}^{-1}) \qquad (33)$$

Bond	a	b
C-C	1.85	0.55
C-F	1.85	0.55
H-F	1.46	0.56
H-C	1.46	0.56

In this equation, d is the bond length given by Pauling's correlation

$$d = d_o - 0.711 \log n$$

where n is the fractional bond order and d_o is the bond length with bond order 1. Since the fluoroethane complex is not expected to have a significantly different structure from the chloroethane complex, bond orders 1.9 (C-C), 0.9 (C-F), 0.1 (H-F), and 0.1(H-C) shown to be the best for

simultaneously fitting all the chloroethane (3) and bromoethane data (4) were used to obtain frequencies given in Table VIII.

ii) Out-of-ring frequencies. The CH_2 frequencies for the complex of CH_3CH_2F were chosen to be same as those used for CH_3CH_2Cl and CH_3CH_2Br which in turn, were based upon frequencies of $CH_2=CH_2$. For the complex of the CH_2FCH_2F reactions the appropriate frequencies from $CH_2=CHF$ were used.

iii) Ring puckering. It is not possible to even guess this frequency due to the lack of knowledge concerning the frequencies associated with H atoms in weakly bound rings. Ring puckering frequencies for the eight membered ring formed by hydrogen bonds have been reported (32). However, little similarity between four membered rings and eight membered rings is expected. For chloroethane and bromoethane this frequency was taken previously to be an adjustable parameter whose value was determined by matching calculations with experimental results (4). It was found that 400 cm^{-1} gave the best result for the chloroethane and 300 cm^{-1} for the bromoethane molecule. Since fluoroethane is lighter than the chloroethane or bromoethane molecule, 450 cm^{-1} was arbitrarily used. The frequencies of the complexes were grouped and are shown in Table VIII.

iv) Moments of inertia. Moments of inertia were calculated by assigning the geometry of the complexes as follows; the geometry of the ring was fixed by placing all four atoms in a plane with bond lengths calculated from Pauling's correlation equation on the basis of single bond lengths of C-C = 1.54 Å, C-F = 1.38 Å, H-F = 0.93 Å and H-C = 1.09 Å. The out-of-ring geometry was assigned to have bond orders of unity, and the angle between H-C-H plane and the C-C bond equal to 150°, the H-C-H angle was set equal to 115°. The calculated moments of inertia from this geometry are also shown in Table VIII.

Table VIII Frequencies and moments of inertia of the complex.

Complex	Moments of inertia (amu Å)	2 ring freq. (cm^{-1})	ring puck.(cm^{-1})	out-of-ring (cm^{-1})	group
	17.02	1418		3050 (4)	3050 (4)
	40.30	1143		1390 (2)	1405 (3)
	50.50	962	450	1025 (2)	1057 (3)
CH_3CH_2F		616		948 (2)	927 (5)
		33[a]		890 (2)	616 (1)
					450 (1)
	33.6	1222		3050 (3)	3050 (3)
	75.2	1132		1400 (2)	1337 (3)
	127.0	961	450	1000 (2)	1034 (3)
CH_2FCH_2F		604		920 (2)	920 (5)
		29[a]		905 (2)	604 (1)
				483 (1)	466 (2)

a. The frequency corresponding to the reaction coordinate which drops out of the calculation of k_ϵ.

III Comparison of models for CH_2XCH_2X. The reactions and the activated complex for the four 1,2 dihaloethanes shown in Table IX have been examined. The interesting feature is the change in the out-of-ring C-X frequencies in these different cases.

Table IX Comparison of Models.

		CH_2FCH_2F (cm^{-1})	CH_2ClCH_2Cl[a] (cm^{-1})	CH_2BrCH_2Cl[b] (cm^{-1})	CH_2BrCH_2Br[b] (cm^{-1})
Out-of	C-H stretch	3050 (3)	3100 (3)	3050 (3)	3050 (3)
ring	CH_2 deform	1400 (2)	1400 (2)	1400 (2)	1400 (2)
	twist	1000 (2)	1000 (2)	1000 (2)	1000 (2)
	wag & rock	920 (2)	920 (2)	920 (2)	920 (2)
	C-X stretch & C-C-X rock	905 (2)	700 (2)	610 (2)	610 (2)
	C-X bend	483 (1)	400 (1)	345 (1)	345 (1)

Continuation of Table IX.

	CH_2FCH_2F (cm^{-1})	CH_2ClCH_2Cl[a] (cm^{-1})	CH_2BrCH_2Cl[b,c] (cm^{-1})	CH_2BrCH_2Br[b] (cm^{-1})
Ring	1222	946	1001	1001
	1132	918	915	871
	961	835	834	797
	604	574	573	446
Ring puckering	450	400	400	300

a. Reference 3, b. Reference 4, c. For HCl elimination.

The out-of-ring C-H frequencies of CH_3CH_2X molecules are the same for all halogens. The model for dihalogen substituted ethane was constructed from mono-substituted one by exchanging three C-H type vibrations with three C-X type vibrations. The effect of this exchange is clearly shown at the three lower out-of-ring frequencies. Of particular importance is the low C-X bending frequency which is partially fixed by the magnitude of the unimolecular preexponential factors for the unimolecular reaction. These are 13.31, 13.34, and 13.23 for CH_2FCH_2F, CH_2ClCH_2Cl and CH_2BrCH_2Br at 800°K, respectively, and are internally consistent.

(IV) Molecules. All molecular parameters (frequencies and moments of inertia) were taken from the literature (33), and they are shown in Table X. Frequencies have been grouped by taking the geometric mean of sets of frequencies with similar magnitude. The computation of the density of states was done on the basis that the frequency patterns were those of harmonic oscillators. Anharmonicity correction to the density of eigen states are difficult to calculate because the anharmonicity constants are not known for most vibrational frequencies. It has been shown (34), however, that for the

Table X Frequencies and Moments of Inertia for C_2H_5F and $C_2H_4F_2$.

Molecule	moments of inertia	frequencies[b] (cm^{-1})		grouped freq. (cm^{-1})
		^{o}[2a]		
	14.00 amu A	C-H stretch	3000,3000	2947 (5)
	53.93 "	"	2941,2915	1430 (5)
	61.58 "	"	2874	1277 (1)
		CH_2 def.	1479	1082 (3)
C_2H_5F		CH_3 asy.def.	1449,1449	844 (2)
		CH_3 sym.def.	1395	415 (1)
		CH_2 wag.	1365	
		CH_2 twist	1277	243 (1)
		CH_3 rock.	1048,880	
		C-C stretch	1108	
		CH_2 rock.	811	
		C-CF stretch	1171	
		C-C-F bend	415	
		torsional	243[c]	
	18.6[d]	C-H stretch	2962,2994[d]	2975 (4)
	123.8	"	2990,2951	1372 (4)
	141.0	CH_2 deform.	1416,1415	1056 (3)
		"	1376,1235	852 (3)
CH_2FCH_2F		"	1079	542 (2)
		C-F stretch	1049,1065	320 (1)
		CH_2 deform.	897	196 (1)
		C-C stretch	858	
		CH_2 rock	804,652	
			450,320	
		torsion	196	

a. Ref. 33a. b. Ref. 33b. c. Ref. 33c. d. Ref. 33d.

energies in question the changes in the $N^{*}(\epsilon)$ and $\sum P(\epsilon^{\dagger})$ due to anharmonicity corrections tend to cancel and are not an important factor for determining k_a.

The torsional degree of freedom was treated as a vibration for all calculations except for the CH_3CH_2F equilibrium thermal activation rate constant at high pressures for which the partition function was calculated on the basis of a hindered internal rotor by Wilson's method (35). In this method the partition function is evaluated directly:

$$Q = \sum_r g_r \, e^{-\epsilon_r / kT}$$

g_r is the degeneracy of the r^{th} energy level, k is Boltzmann's constant, T is the absolute temperature and ϵ_r is the individual internal rotational energy level given by

$$\epsilon_r = \left| \frac{m^2 h^2}{32 I_r} \right| a_r \qquad (34)$$

where m is the internal rotational symmetry number, h is Planck's constant, I_r is the reduced moment of inertia of the internal rotation, and a_r is determined for a given value of θ as a function of the quantum number r. θ can be calculated from the following equation;

$$\theta = \frac{8\pi^2 I_r U_o}{m^2 h^2} \qquad (35)$$

U_o is the potential barrier to the internal rotation. In this study a_r for $r \leqslant 6$ were taken from Wilson's tables (35) and a_r for $r > 6$ were calculated from the following approximate formula:

$$a_r = r^2 + \tfrac{1}{2} \frac{\theta}{r^2 - 1} \qquad (36)$$

The degeneracy is one for levels below 3.31 kcal mol^{-1} and 2 for those above. The calculation for CH_3CH_2F at 800°K is shown in Table XI.

Table XI Partition function calculation for Hindered internal rotation.

U_o = 3.31 kcal mol^{-1} (36)
I_r = 4.36 x 10^{-40} g cm^2 (37)
θ = 20.3
Q = 3.52 (at 800°K)

r	a_r	ϵ_r (kcal mol^{-1})
o	-31.85	0.
1	-14.9	0.7
2	1.25	1.37
3	15.32	1.95
4	27.6	2.46
5	40.7	3.0
6	42.2	3.06
7	49.2	3.35
8	64.2	3.97
9	81.1	4.67
10	100.1	5.46
11	121.1	6.32
12	144.1	7.32
13	169.1	8.30
14	196.1	9.42
15	225.1	10.61
16	256.1	11.92

The partition function calculated with the above energy levels for the hindered rotation is 3.52 compared to 2.86 for a vibration with frequency of 243 cm^{-1} at 800°K. Thus there is a factor of 0.813 at 800°K for the difference in the preexponential factor of k_{th}^{∞} for the torsional motion treated as a hindered rotation relative to treating it as a vibration.

(V) thermochemistry. In order to calculate the RRKM specific rate constant, the average energy of the chemically activated molecules must be known. The average energy at any given temperature can be calculated from

the following relationship;

$$\langle\epsilon\rangle = \Delta H_f^o(M) - \Delta H_f^o(R_1) - \Delta H_f^o(R_2) + \epsilon_a' + \epsilon_{th}' = E_{min} + \epsilon_{th}' \qquad (37)$$

where $H_f^o(\ )$ is the heat of formation of the molecule or radicals at 0^oK,

ϵ_a' is the energy of the activation of the radical combination reaction,

ϵ_{th}' is the average thermal energy in the active degrees of freedom of the molecule. ϵ_{th}' can be calculated from the nonequilibrium distribution function, $f(\epsilon)d\epsilon$.

The heats of formation of CH_3CH_2F, CH_2FCH_2F, CH_3 and CH_2F were estimated as follows.

Ethyl fluoride. No direct experimental value is available. The value, -63 kcal mol^{-1} at 300^oK (-59.4 kcal mol^{-1} at 0^oK) used in this study was obtained by Bernstein's group additivity method (38). This method seems to agree well with the experimental values for other molecules; the heat of formation of ethane can be estimated to be -20 kcal mol^{-1} at 298^oK by this method compared to -20.2 kcal mol^{-1} reported by the National Bureau of Standard (39). Another example is ethyl chloride; Bernstein's method gives -26 kcal mol^{-1} at 298^oK compared to -25.8 kcal mol^{-1} measured by the hydrogenation of ethyl chloride (40).

Methyl radical. The heat of formation of the methyl radical is well established and need no further consideration. The value used in this study was based on the most recent value of the C-H bond dissociation energy in methane ($D(CH_3-H)$=104 kcal mol^{-1} at 298^oK) which gives $\Delta H_f^o(CH_3)$=34 kcal mol^{-1} at 298^oK and $\Delta H_f^o(CH_3)$=34.9 kcal mol^{-1} at 0^oK.

CH_2F radical. The heat of the formation of CH_2F presents a problem. The

only available direct experimental value is ~0.95 ev (~21 kcal mol^{-1}) which was obtained by the mass spectroscopic method (41). However, this value gives the unreasonably small value of $D(CH_3-CH_2F)$ of 76 kcal mol^{-1} at 298°K. In this study the heat of formation of CH_2F was obtained from the consideration of the following reaction.

$$CH_2F - H = CH_2F + H$$

If the heat of formation of H and CH_3F, and the bond dissociation energy, $D(CH_2F-H)$, are known, the heat of formation of CH_2F can be simply calculated by

$$\Delta H_f^\circ(CH_2F)_{0^\circ K} = -D(CH_2F-H)_{0^\circ K} + \Delta H_f^\circ(CH_3F)_{0^\circ K} - \Delta H_f^\circ(H)_{0^\circ K}$$

$\Delta H_f^\circ(H)_{0^\circ K}$ is known to be 51.63 ± 0.06 kcal mol^{-1} (42). The heat of formation of CH_3F has been calculated to be -55.9 ± 0.8 kcal mol^{-1} at 298°K from Allen's parameters by Lacher and Skinner (43). From a study of the bromination of methane and methyl fluoride, Whittle and co-workers (44) found that $D(CH_2F-H)$=101 kcal mol^{-1} at 200°C. In the same work the C-H bond energy in CH_4 was taken to be 103 kcal mol^{-1}. This is smaller than the currently accepted value of 104 kcal mol^{-1}, but close enough so that their $D(CH_2F-H)$=101 kcal mol^{-1} at 200°C was used with no correction. It should also be noted that $D(CH_2F-H)$ was estimated to be the same as $D(CHF_2-H)$ in the same work. With 200°C values for $D(CH_2F-H)$=101 kcal mol^{-1}, $\Delta H_f^\circ(H)$=52.35 kcal mol^{-1} and $\Delta H_f^\circ(CH_3F)$= -57.1 kcal mol^{-1} (converted to 473°K by calculations of $H^\circ - H_o^\circ$ from partition functions for CH_3F and its components) (see Table XV), the heat of formation of CH_2F radical is -8.48 kcal mol^{-1}. This in turn, gives $\Delta H_f^\circ(CH_2F)_{0^\circ K}$ = -7.1 kcal mol^{-1}

from $H^{\circ} - H_{o}^{\circ}$ listed in Table XV. With $\Delta H_{f}^{\circ}(CH_3CH_2F)_{0^{\circ}K}$ = -59.4 kcal mol^{-1}, $\Delta H_{f}^{\circ}(CH_3)_{0^{\circ}K}$ = 34.9 kcal mol^{-1} and $\Delta H_{f}^{\circ}(CH_2F)_{0^{\circ}K}$ = -7.1 kcal mol^{-1}, $D(CH_3-CH_2F)$ became 87.2 kcal mol^{-1} at 0°K.

Perona (45) has measured $D(CHF_2-H)$ from the activation energies of the reaction between CHF_2 and CH_4 and its reverse reaction, and his value was 96.1 kcal mol^{-1} at 298°K. If $D(CH_2F-H)$ is equal to $D(CHF_2-H)$ as estimated in reference 44, Perona's $D(CHF_2-H)$=96.1 kcal mol^{-1} at 298°K gives $D(CH_3-CH_2F)$=84.6 kcal mol^{-1} at 0°K. A choice between these two values can be reached by considering the activation energies of the abstraction reactions of bromine atoms (46), CH_3 radical (47) and CF_3 radical (47) with various halogen substituted methanes.

Table XII Comparison of activation energies.

RH	Br abstraction	CH_3 abstraction	CF_3 abstraction
CH_4	18.6 kcal mol^{-1}	14.8 kcal mol^{-1}	11.2 kcal mol^{-1}
CH_3F	16.1	11.4	11.2
CH_2F_2	16.6	10.2	11.2
CH_3Cl	14.7	11.4	10.6

From the above table one can estimate that $D(CH_2F-H)$ and $D(CHF_2-H)$ lie somewhere between $D(CH_3-H)$ (104 kcal mol^{-1}) and $D(CH_2Cl-H)$ (99 kcal mol^{-1}) at 298°K. Whittle's value $D(CH_2F-H)$=99.9 kcal mol^{-1} at 298°K is indeed between $D(CH_3-H)$ and $D(CH_2Cl-H)$, while Perona's value $D(CHF_2-H)$=96.1 kcal mol^{-1} is a little smaller than $D(CH_2Cl-H)$. Thus the value $D(CH_2F-H)$=99.9 kcal mol^{-1} is favored.

CH_2FCH_2F. The average energy of the vibrationally excited molecule, CH_2FCH_2F is more obscure than that of ethyl fluoride due to the lack of

the information concerning the heat of formation of CH_2FCH_2F and to the uncertainty in the heat of formation of CH_2F radicals which enters twice into $D(CH_2F-CH_2F)$. Bernstein's tables give -53 kcal mol^{-1} for the contribution of the CH_2F radical toward the heat of formation of the molecule containing this radical (38). Since CH_2FCH_2F has two CH_2F radicals, $\Delta H_f^\circ(CH_2FCH_2F)_{298^\circ K}$ is -106 kcal mol^{-1}. Using $H^\circ - H_o^\circ$ of CH_2FCH_2F and its components, the heat of formation of CH_2FCH_2F at $0^\circ K$ becomes -102.8 kcal mol^{-1}, and this value gives $D(CH_2F-CH_2F)$=88.6 and 84.6 kcal mol^{-1} with Whittle's $D(CH_2F-H)$=101 kcal mol^{-1} and Perona's $D(CHF_2-H)$=96.1 kcal mol^{-1}, respectively.

Another method of obtaining $\Delta H_f^\circ(CH_2FCH_2F)$ is to consider the heat of a redistribution reaction (43). For example, consider the redistribution reaction

$$\tfrac{1}{2}\,(CH_3CH_3 + ClCH_2CH_2Cl) = CH_3CH_2Cl \qquad \Delta H_r = -0.6 \pm 0.6 \text{ kcal mol}^{-1}$$

Eq's (iii) & (vii) of Table 5 of reference 43 show that the difference in the heats of redistribution between fluorine compounds and chlorine counterparts should be negligible. Thus the following reaction should also have -0.6 ± 0.6 kcal mol^{-1} for the heat of the redistribution reaction.

$$\tfrac{1}{2}\,(CH_3CH_3 + FCH_2CH_2F) = CH_3CH_2F \qquad \Delta H_r = -0.6 \pm 0.6 \text{ kcal mol}^{-1}$$

If the heats of formation of CH_3CH_3 and CH_3CH_2F at 25°C are -20.2 and -63 kcal mol^{-1}, respectively, the heat of formation of CH_2FCH_2F will be -106.4 kcal mol^{-1}, in good agreement with the value from Bernstein's method. Table XIII summarizes the heats of formation and bond energies that will be used in the following sections of this thesis.

Table XIII Thermochemistry of the radicals and molecules.

Species	Heat of formation ($0^{\circ}K$)	Bond energy ($0^{\circ}K$)	E^{a}_{min} ($0^{\circ}K$)
CH_3	34.9 kcal mol^{-1}		
CH_2F	-9.7[b]		
	-7.1[c]		
CH_3CH_2F	-59.4	84.6[b] kcal mol^{-1}	85.6[b] kcal mol^{-1}
		87.2[c]	88.2[c]
CH_2FCH_2F	-102.8	83.4[b]	84.4[b]
		88.6	89.6[c]

a. With ϵ'_a = 1 kcal mol^{-1}.

b. With Perona's $D(CHF_2 - H)$=96 kcal mol^{-1} at $298^{\circ}K$.

c. With Whittle's $D(CH_2F - H)$=101 kcal mol^{-1} at $473^{\circ}K$; these are the preferred values.

These estimated bond energies $D(CH_3CH_2F)$ and $D(CH_2FCH_2F)$ can be compared with the known bond energies of $D(CH_3-CH_3)$, $D(CH_3CH_2-CF_3)$, $D(CH_3-CHF_2)$, $D(CH_3-CF_3)$, and $D(CF_3-CF_3)$. The bond energies of these compounds are as follows at $298^{\circ}K$ and $0^{\circ}K$.

$D(CH_3-CH_3)$=88 kcal mol^{-1} (Calculated from the known heats of formation
" =86.3 of CH_3 and CH_3CH_3)

$D(CH_3-CHF_2)$=91.8 (Based upon $\Delta H^{\circ}_f(CH_3CHF_2)$= -118 kcal mol^{-1} at
" =90.2 $298^{\circ}K$ (43) and $D(CHF_2 - H)$=101 kcal mol^{-1} at $473^{\circ}K$ (44))

$D(CH_3CH_2-CF_3)$=89.5 (48)
" =87.8

$D(CH_3-CF_3)$=99.7 (Based upon $\Delta H^{\circ}_f(CH_3CF_3)$= -178.3 kcal mol^{-1} at $298^{\circ}K$
" =97.9 and $D(CF_3-H)$=106 kcal mol^{-1} (46))

$D(CF_3-CF_3)$=96.6 kcal mol^{-1} (From the study of equilibria for the

" =94.8 following reactions (49)

$$Br_2 + CF_3H = HBr + CF_3Br$$

$$Br_2 + C_2F_6 = 2\ CF_3Br$$

where $D(CF_3-H)$ was used as 106.3 kcal mol^{-1} at 298°K)

Apparently fluorine always tends to increase the bond energy and one expects the bond energy of CH_2FCH_2F to be close to $D(CH_3CH_2-CF_3)$ and $D(CH_3-CF_3)$. Therefore this argument favors the higher value of $D(CH_3-CH_2F)$ and $D(CH_2F-CH_2F)$.

Table XIV gives the E_{min} for various halogen substituted ethanes. Even though in all cases considered previously, the C-C bond energies are not known exactly but the estimated values for E_{min} are all in the range of 85 kcal mol^{-1} to 90 kcal mol^{-1}; fluoroethanes are higher than the others. In all cases a value of one kcal mol^{-1} has been used as the activation energy for radical combination.

Table XIV Comparison of E_{min}.

Molecule	CH_3CH_2F	CH_2FCH_2F	CH_3CH_2Cl	CH_2ClCH_2Cl	CH_3CH_2Br	CH_2BrCH_2Br
E_{min}(kcal mol^{-1})	88.2	89.6	87.8[a,b]	85.3[a]	87.8[a,b]	85.3[a]

a. Reference 4.

b. The E_{min} values for these compounds differ by 0.6 kcal mol^{-1} from those reported in reference 4 because the conversion of $\Delta H_f^o(CH_3)$ to 0°K was done in a slightly different way.

Table XV $H^{\circ} - H_{o}^{\circ}$ values (kcal mol^{-1}).

Species	T=298°K	T=473°K
CH_3CH_2F	3.1	6.5
CH_2FCH_2F	3.5	6.9
CH_3CHF_2	3.3	6.6
CH_3CF_3	3.6	7.4
CF_3CF_3	4.8	9.8
CH_2F	2.5	4.3
CHF_2	2.5	4.5
CF_3	2.8	5.1

CALCULATED RESULTS AND COMPARISON TO EXPERIMENT

(I) Critical Energy (or Activation Energy). The activation energy of the reaction is defined as the difference between the average energy of the activated complex and that of reactants while the critical energy is defined as the difference between the lowest vibrational levels in the activated and initial states. This is shown in fig.6.

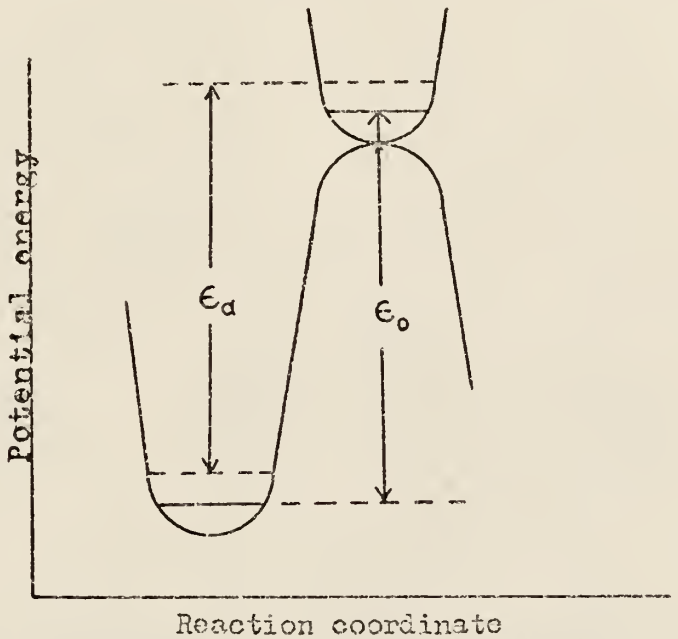

Fig. 6 Potential energy vs reaction coordinate

The difference between the activation energy and the critical energy for a unimolecular reaction can be given by

$$\epsilon_a = \epsilon_o + RT^2 \left(\frac{\ln Q^+_{vib}}{T} - \frac{\ln Q^*_{vib}}{T} + \frac{1}{T} \right) \qquad (38)$$

where * and + represent the molecule and activated complex, respectively.

Critical energies for reactions studied in this work are not known. This is mainly because thermal pyrolysis experiments with CH_3CH_2F and CH_2FCH_2F are not possible due to the occurrence of heterogeneous reactions. Therefore, the critical energies were obtained by using ϵ_o as a parameter and fitting the calculations to the experimental results. This was done

as follows; numerical values of the nonequilibrium rate constants for various ϵ_o were calculated according to eq. 24 from the model of the previous section and the appropriate E_{min} values., The results are shown in figs. 7 & 8 and Tables XVI & XVII. The distribution functions are also plotted and the average values of $\langle\epsilon\rangle$ indicated on the figures; the calculated rate constants for the appropriate value of $\langle\epsilon\rangle$ that numerically matched the experimental rate constants fix the critical energy.

For CH_3CH_2F, the calculated rate constants with E_{min}=88.2 kcal mol^{-1} and calculated average energy at 358°K of 3.3 kcal mol^{-1} above E_{min} (see Table XXII), are as follows: 1.9×10^9 sec^{-1} with ϵ_o=56 kcal mol^{-1}, 1.47×10^9 sec^{-1} with ϵ_o=57 kcal mol^{-1}, 1.10×10^9 sec^{-1} with ϵ_o=58 kcal mol^{-1} and 6.0×10^8 sec^{-1} with ϵ_o=60 kcal mol^{-1}. By comparing these calculated rate constants with the experimental rate constant of 1.44×10^9 sec^{-1}, which was assumed to be unit deactivation rate constant,* ϵ_o=57 kcal mol^{-1} was found to give best fit. For a lower E_{min} of 85.6 kcal mol^{-1}, an ϵ_o of 55 kcal mol^{-1} seems to give best fit. Therefore, values of 57 $\pm$ 1 and 55 $\pm$ 1 kcal mol^{-1} tend to be upper and lower limits. However, from the general trend of the experimentally known critical energies for HX elimination from halogen substituted ethanes (CH_3CH_2Br = 52 kcal mol^{-1}, CH_3CH_2F = 55 kcal mol^{-1}) the upper limit for CH_3CH_2F is favored. From the point of view of the reliability of the thermochemistry, the higher E_{min} value is also more favored than the lower value.

For CH_2FCH_2F with the higher value of E_{min}, 89.6 kcal mol^{-1}, and 2.9 kcal mol^{-1} of average energy at 300°K, the calculated rate constants at a total energy of 92.5 kcal mol^{-1} but with different critical energies are as follows: 9.0×10^8 sec^{-1} with ϵ_o=56 kcal mol^{-1}, 5.0×10^8 sec^{-1} with ϵ_o=58 kcal mol^{-1}, 2.8×10^8 sec^{-1} with ϵ_o=60 kcal mol^{-1} and 1.55×10^8

* See the footnote c. of Table XXII for the correction of k_a for CH_3CH_2F.

Table XVI Calculated k_ϵ[a] for ethyl fluoride.

ϵ_o	ϵ (kcal mol^{-1})	k_ϵ(sec^{-1})	$P(\epsilon_v^+)$	$N(\epsilon)$ states cm^{-1}
56	89	1.28×10^{9}	5.79×10^{6}	2.03×10^{8}
	90	1.48×10^{9}	7.66×10^{6}	2.32×10^{8}
	91	1.70×10^{9}	1.00×10^{7}	2.66×10^{8}
	92	1.95×10^{9}	1.32×10^{7}	3.04×10^{8}
	93	2.22×10^{9}	1.71×10^{7}	3.47×10^{8}
	94	2.53×10^{9}	2.22×10^{7}	3.95×10^{8}
57	89	9.58×10^{8}	4.35×10^{6}	2.03×10^{8}
	90	1.11×10^{9}	5.79×10^{6}	2.32×10^{8}
	91	1.29×10^{9}	7.66×10^{6}	2.66×10^{8}
	92	1.48×10^{9}	1.00×10^{7}	3.04×10^{8}
	93	1.70×10^{9}	1.32×10^{7}	3.47×10^{8}
	94	1.94×10^{9}	1.71×10^{7}	3.95×10^{8}
58	89	7.22×10^{8}	3.26×10^{6}	2.03×10^{8}
	90	8.42×10^{8}	4.35×10^{6}	2.32×10^{8}
	91	9.80×10^{8}	5.79×10^{6}	2.66×10^{8}
	92	1.13×10^{9}	7.66×10^{6}	3.04×10^{8}
	93	1.30×10^{9}	1.00×10^{7}	3.47×10^{8}
	94	1.50×10^{9}	1.32×10^{7}	3.95×10^{8}
60	89	4.01×10^{8}	1.81×10^{6}	2.03×10^{8}
	90	4.72×10^{8}	2.44×10^{6}	2.32×10^{8}
	91	5.51×10^{8}	3.26×10^{6}	2.66×10^{8}
	92	6.44×10^{8}	4.35×10^{6}	3.04×10^{8}
	93	7.51×10^{8}	5.79×10^{6}	3.47×10^{8}
	94	8.72×10^{8}	7.66×10^{6}	3.95×10^{8}

a. Reaction path degeneracy = 2

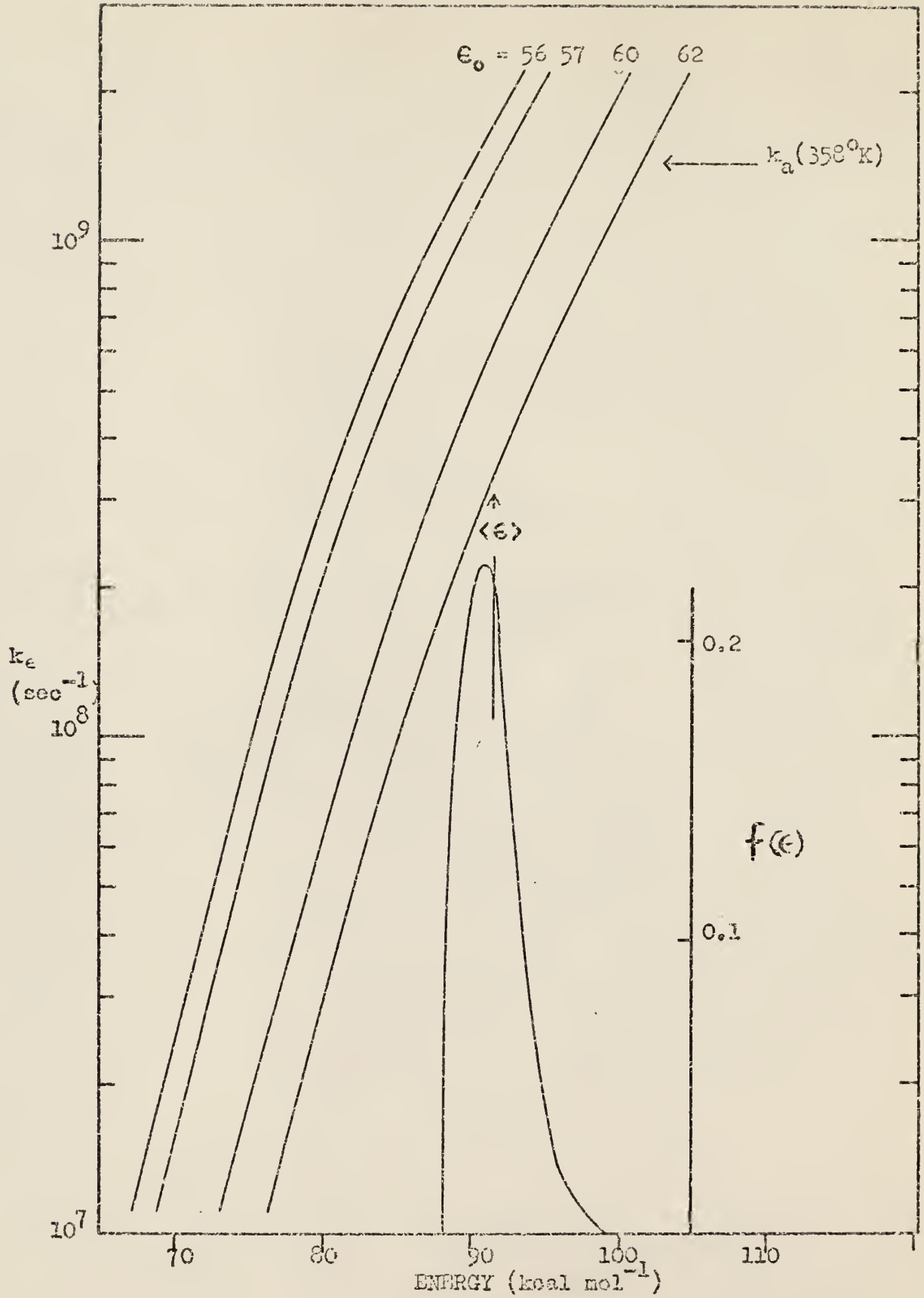

Fig. 7 k_ϵ vs energy for CH_3CH_2F with various critical energies and a distribution function at 358°K.

Table XVII Calculated k_ϵ^a for CH_2FCH_2F.

ϵ_0	ϵ(kcal mol^{-1})	k_ϵ(sec^{-1})	$P(\epsilon_v^+)$	N(ϵ) states cm^{-1}
	89	5.37×10^{8}	1.88×10^{7}	4.00×10^{9}
	90	6.25×10^{8}	2.52×10^{7}	4.60×10^{9}
56	91	7.23×10^{8}	3.36×10^{7}	5.29×10^{9}
	92	8.33×10^{8}	4.45×10^{7}	6.08×10^{9}
	93	9.58×10^{8}	5.87×10^{7}	6.98×10^{9}
	94	1.10×10^{9}	7.70×10^{7}	8.00×10^{9}
	95	1.25×10^{9}	1.00×10^{8}	9.16×10^{9}
	89	2.94×10^{8}	1.03×10^{7}	4.00×10^{9}
	90	3.46×10^{8}	1.40×10^{7}	4.60×10^{9}
58	91	4.05×10^{8}	1.88×10^{7}	5.29×10^{9}
	92	4.73×10^{8}	2.52×10^{7}	6.08×10^{9}
	93	5.48×10^{8}	3.36×10^{7}	6.98×10^{9}
	94	6.34×10^{8}	4.45×10^{7}	8.00×10^{9}
	95	7.30×10^{8}	5.87×10^{7}	9.16×10^{9}
	89	1.57×10^{8}	5.51×10^{7}	4.00×10^{9}
	90	1.87×10^{8}	7.57×10^{7}	4.60×10^{9}
	91	2.22×10^{8}	1.03×10^{7}	5.29×10^{9}
60	92	2.62×10^{8}	1.40×10^{7}	6.08×10^{9}
	93	3.07×10^{8}	1.88×10^{7}	6.98×10^{9}
	94	3.60×10^{8}	2.52×10^{7}	8.00×10^{9}
	95	4.18×10^{8}	3.36×10^{7}	9.16×10^{9}
	89	8.15×10^{7}	2.86×10^{7}	4.00×10^{9}
	90	9.87×10^{7}	3.98×10^{7}	4.60×10^{9}
	91	1.19×10^{8}	5.51×10^{7}	5.29×10^{9}
62	92	1.42×10^{8}	7.57×10^{7}	6.08×10^{9}
	93	1.69×10^{8}	1.03×10^{7}	6.98×10^{9}
	94	1.99×10^{8}	1.40×10^{7}	8.00×10^{9}
	95	2.34×10^{8}	1.88×10^{7}	9.16×10^{9}

a. Reaction path degeneracy=4.

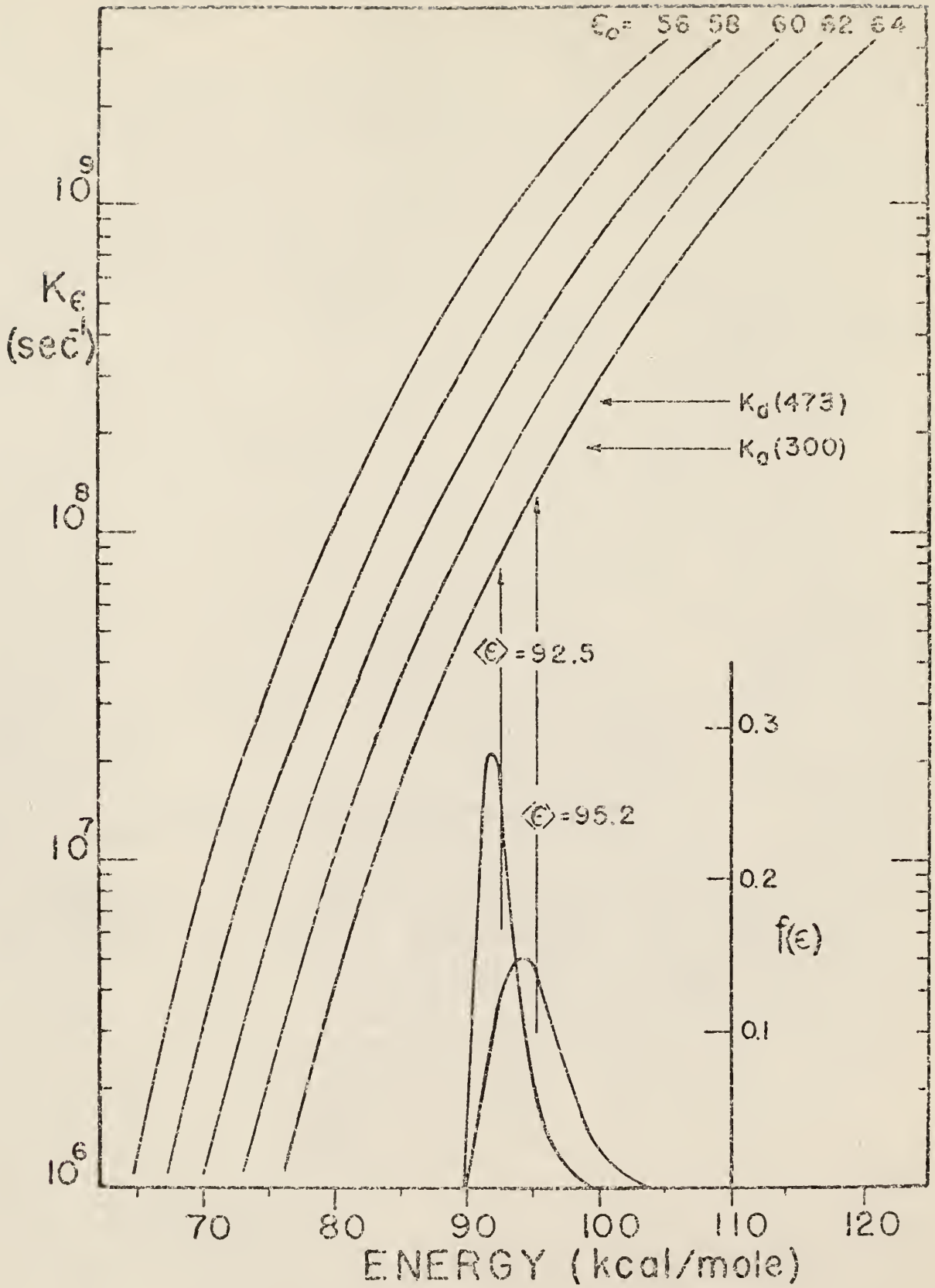

Fig. 8 k_ϵ vs Energy for CH_2FCH_2F with various critical energies and distribution functions at 300°K and 473°K.

sec^{-1} with ϵ_o=62 kcal mol^{-1}. By comparing these calculated rate constants with the experimental rate constant at 300°K(1.8×10^8 sec^{-1})which was reduced by a factor of 0.89 to account for the fact that unit efficiency in deactivation is not followed (to be discussed later), it was found that the best fit was obtained with ϵ_o=62kcal mol^{-1}. With the lower E_{min} of 84.4 kcal mol^{-1}, ϵ_o=57 kcal mol^{-1} gives best agreement between calculated and experimental rate constants. Since none of the critical energies of HX elimination from dihalogen substituted ethanes are known, it is not possible to determine the more favored value from a known trend such as the argument used for CH_3CH_2F. Previously critical energies for monochloroethane (3) and monobromoethane (4) of 55 kcal mol^{-1} and 52 kcal mol^{-1}, respectively, have been used. Although there was good agreement between the experimental rate constant (1.7×10^9 sec^{-1}) and the calculated value (1.5×10^9 sec^{-1}) for dibromoethane,this was not the case for CH_2ClCH_2Cl (experimental value was 1.79×10^8 sec^{-1} compared to the calculated value 9.57×10^8 sec^{-1}). However, the calculation with the critical energy of 60 kcal mol^{-1} for CH_2ClCH_2Cl done by Dees (3) shows better agreement between the experimental rate constant (1.79×10^8 sec^{-1}) and the calculated value (1.99×10^8 sec^{-1}). Better agreement was also found for the nonequilibrium isotopic effects using a higher value for ϵ_o. Therefore it seems that the dihaloethane may have a higher critical energy than the corresponding monohaloethane. If this was true, the upper limit 62 kcal mol^{-1} would be more favored value for CH_2FCH_2F. Also the higher E_{min} is favored from the thermochemical consideration.

These values, 57 kcal mol^{-1} for CH_3CH_2F and 62 kcal mol^{-1} for CH_2FCH_2F, are compared with the critical energies for the dehydrohalogenation of other chloro and bromoethanes in Table XVIII.

Table XVIII Critical energy and preexponential factors

Molecule	Critical energy (kcal mol^{-1})	Preexponential factor[a]
CH_3CH_2F	57	13.20
CH_2FCH_2F	62	13.31
CH_3CH_2Cl[b]	55	13.16
CH_2ClCH_2Cl[b]	55	13.34
CH_3CH_2Br[b]	52	13.20
CH_2BrCH_2Br[b]	52	13.23

a. Calculated at 800°K in terms of partition function ratios.

b. Reference 4.

Maccoll (50) has noticed that a linear relationship exists between the RX activation energies for dehydrohalogenation and the heterolytic bond dissociation energies $D(R^+X^-)$

$$E(H\text{-}X) = 0.29\ D(R^+X^-) \qquad (39)$$

Tsuda and Hamill (51) have shown that the lowest appearance potential of R^+ in RX is $D(R^+X^-)$. With this relationship and measurements by Tsuda and Hamill (51) of the appearance potential for $CH_3CH_2^+$ of ethyl chloride (8.5 ev), bromide (8.2 ev) and iodide (7.8) and together with Maccoll's calculated value, $D(CH_3CH_2^+F^-) = 9.5$ ev, the trend in the critical energy values for CH_3CH_2F, CH_3CH_2Cl and CH_3CH_2Br shown in Table XVIII is to be expected. Benson has shown (52) that a fully developed ion pair is not to be taken as a literal description of the four centered transition state. There is, however, apparently sufficient polar character to make the above correlation with $D(R^+X^-)$ valid.

As mentioned in reference 4 with the comparison of the activation energies of CH_3CH_2Cl (56.5 kcal mol^{-1}), 1,2 $C_3H_6Cl_2$ (54.9 kcal mol^{-1}) and i-C_3H_7Cl (50.5 kcal mol^{-1}), the activation energy (or the critical energy) for 1,2 dihaloethanes should be equal to or greater than for the corresponding monohaloethane. Indeed, Table XVIII shows not only that the fluoroethane has a higher critical energy than chloro or bromoethane, but also that the CH_2FCH_2F has a higher critical energy than CH_3CH_2F. Hence CH_2FCH_2F has the highest critical energy in the series shown above.

(II) Preexponential factor. The preexponential factors in terms of the ratio of partition functions of the molecule and activated complex obtained at 800°K from eq. 31, the thermal equilibrium rate constant expression, are shown above in Table XVIII. As mentioned earlier in the CALCULATION SECTION, the preexponential factor for CH_3CH_2F was calculated using a hindered internal rotor to represent the torsional degree of freedom, while for CH_2FCH_2F the torsion was treated as a vibrational degree of freedom. Since the preexponential factor is just the ratio of the partition function of the molecule to that of the activated complex, and since the molecular structures of halogen substituted ethanes and their complexes are similar, the preexponential factors are very similar.

Previously it has been shown that the calculated preexponential factors for CH_3CH_2Cl (13.16 sec^{-1}), CH_3CH_2Br (13.20 sec^{-1}) were in good agreement with the experimental numbers, 13.09 and 13.04 sec^{-1}, respectively (4). This good agreement, together with the fact that the calculated preexponential factors of fluoroethanes are similar in magnitude to CH_3CH_2Cl and CH_3CH_2Br gives some confidence that the models chosen for the CH_3CH_2F four centered complex are approximately correct.

(III) Collisional Inefficiency. As mentioned earlier, and as shown in fig. 4, a rapid increase in the decomposition product sets in at low pressure due to the cascade collisional deactivation of the excited molecules. The result is a deviation from linearity in the D/S vs. 1/P plots. Rabinovitch and co-workers (53) have proposed a model, the stepladder model, from which it is possible to calculate k_a as a function of step size, the average energy lost in a single collision. A brief description of this model is as follows.

The steady state population of the i^{th} state of the energized molecule can be described by the transport equations

$$\frac{dn_i}{dt} = \omega\left(\sum_{j\neq i} P_{ij}n_j - \sum_{j\neq i} P_{ji}n_i\right) - k_{\epsilon i}n_i + Rf_{\epsilon i}(\epsilon) = 0 \qquad (40)$$

or

$$\frac{dn_i}{dt} = \omega\left(\sum_{j\neq i} P_{ij}n_j\right) - (k_{\epsilon i} + \beta_i\omega)n_i + Rf_{\epsilon i}(\epsilon) = 0 \qquad (41)$$

where P_{ji} is the probability per collision that a molecule in state i will undergo a transition to state j, so that $\sum_j P_{ji} = 1$,

n_i is the steady-state population of the i^{th} state,

β_i is the effective collision factor $(1 - P_{ii})$; then $\beta_i = 1$, if $P_{ii}=0$; β_i is taken constant for all i, equal to β,

$k_{\epsilon i}$ is the specific decomposition probability per second for state i,

R is the total rate of chemical activation,

$f(\epsilon)$ is the activation distribution function, with the normalization $\sum f_i = 1$.

In the above expressions the i^{th} state is not a well defined quantum state but just represents the i^{th} energy region which depends upon the grain size chosen for the active energy region, which were 100 cm^{-1} increments. From the defi-

nitions of k_ϵ, n_i and R, the yields of decomposition products D, and of stabilization products, S, become functions of n_i and $k_{\epsilon i}$ and hence depend upon p_{ji} as shown in the following expressions

$$D=\Sigma k_{\epsilon i} n_i \qquad S = R - \Sigma k_{\epsilon i} n_i \tag{42}$$

For the simple stepladder cascade model the energy loss per collision in kcal mol^{-1} is constant and transitions to upper states by collision are not allowed, that is,

$$P_{ij} = 1 \quad \text{if } j - i = s \tag{43}$$

$$P_{ij} = 0 \quad \text{if } j - i \neq s \tag{44}$$

If T is the number of transitions in the active region, the S, D and k_a can be expressed as follows.

$$S_T = \prod_{t=1}^{T} \left(\frac{\beta\omega}{\beta\omega + k_{\epsilon t}} \right) \qquad D_T = 1 - S_T \tag{45}$$

$$k_a = \left(\frac{1}{\beta\omega}\right)^T \prod_{t=1} (\beta\omega + k_{\epsilon t}) - 1 \tag{46}$$

At high pressure $\omega \gg k_{\epsilon t}$ and by expanding $\prod_{t=1} (\beta\omega + k_{\epsilon t})$ and dropping terms of $k_{\epsilon t}^2$ and higher

$$k_a = \frac{1}{\beta} \sum_{t=1}^{T} k_{\epsilon t} \tag{47}$$

The experimental and calculated results were compared on plots of k_a/k_a^∞ vs. S/D. Such plots are shown in fig. 9. The experimental points are obtained by first finding a high pressure rate constant, k_a^∞, from the data of fig. 3. Next each low pressure point is found by calculating k_a from $\omega(D/S)$ and dividing it by the k_a^∞ value. The calculated lines are obtained from the computer output which lists $k_a = \omega D/S$ values and S/D for each pressure and various

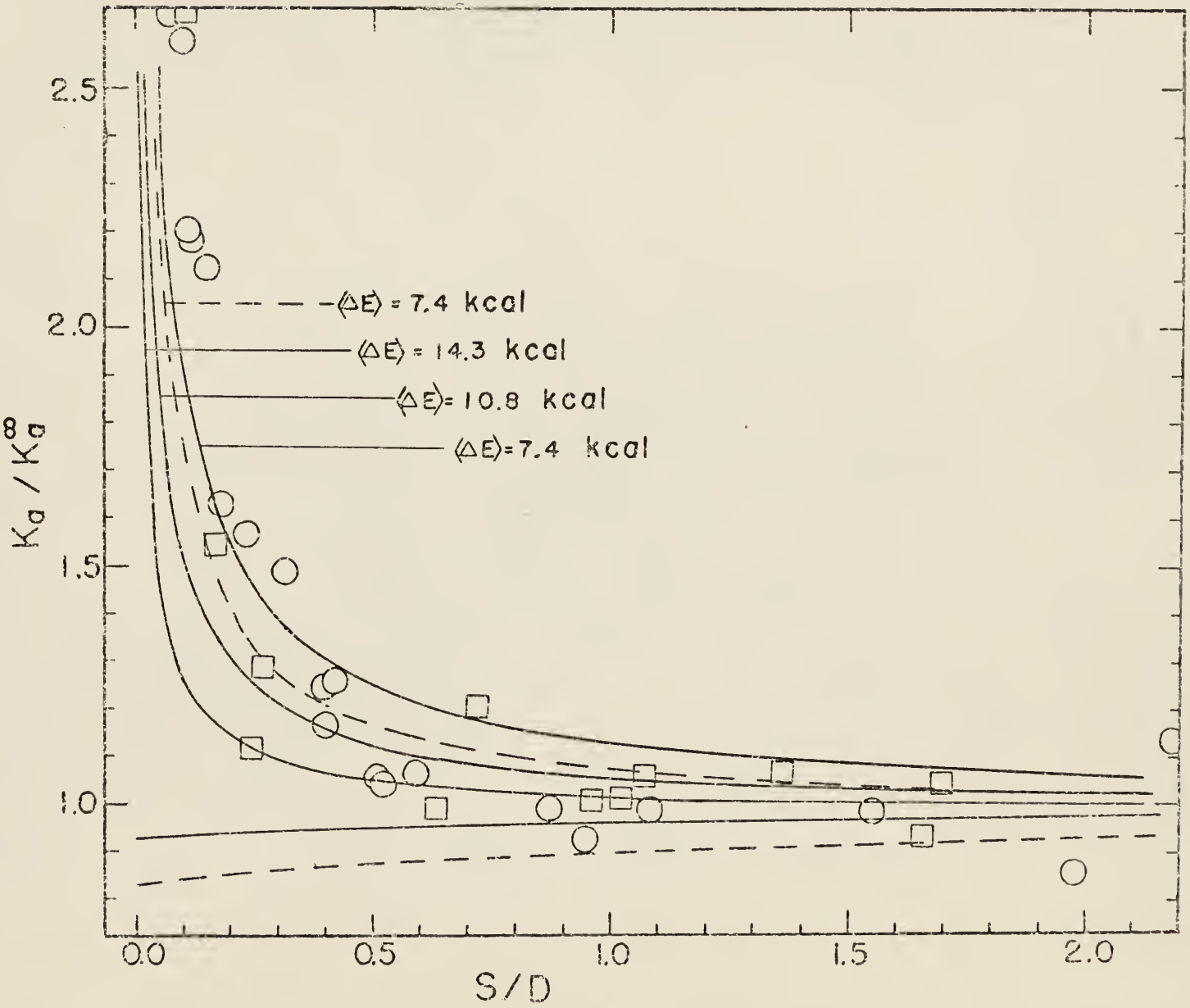

Fig. 9 Low pressure data (○ - 300 K, □ - 473 K) and calculated curves for simple stepladder cascade deactivation with energy increments <ε> kcal mol^{-1}. The solid and dotted lines are calculated results for 300° and 473°K, respectively. Two bottom curves are the unit deactivation curves.

s value (average energy losses per collision). $k_a^s/k_{a\infty}^s$ was obtained by simply dividing the k_a^s by the high pressure limiting value for each s.

From the general curvature of the experimental data in fig. 9, collisional inefficiency certainly exists, and the energy loss per collision is equal to 11 ± 3 kcal mol^{-1}; the quoted error limits apply to both sets of data. This value can be compared with the corresponding value of 11-14 kcal mol^{-1} per collision for vibrationally excited 1,2-$C_2H_4Cl_2$ in the presence of the bath gas, CH_2Cl_2 (3). The detailed agreement between experimental points and calculated curves is not very good. As shown in fig. 9, experimental rate constants increase more rapidly at low S/D than the calculated values. The data are not highly accurate, and it is premature to judge that a simple cascade model is inadequate description for the transition probabilities.

The temperature dependence of the collisional inefficiency can not be clearly deduced due to scatter in the experimental data. However, raising the temperature causes the calculated curves to turn upward at lower values of S/D shown in the following table which was taken from s=11 kcal mol^{-1} curves. This arises due to the higher average energy and to increased spread of the distribution function which is apparent from the change in the two unit deactivation curves at the two temperatures.

Table XIX $k_a^{s=11} / k_{a\infty}^{s=11}$ with different S/D values.

S/D		0.13	0.53	1.1
$k_a^{s=11} / k_{a\infty}^{s=11}$	(300°K)	1.36	1.09	1.03
	(473°K)	1.25	1.02	0.98

The scatter of the experimental data allows no clear selection of the

experimental temperature dependence of the collisional inefficiency of the system studied in this thesis. It would be expected that the efficiency would decrease according to the results with sec-butyl radical (54).

Because of the fact that the consumption of propene increased rapidly as the pressure was lowered, there is some doubt as to whether or not the olefin was completely protected from Cl atom addition at low pressure. This limitation of the experimental method insures that the data provide an upper estimation to the values of s. The data clearly show that the unit deactivation is not valid; just the fact most of the experimental points below S/D = 0.5 lie above s = 14 kcal mol^{-1} certainly proves that one should not use a unit deactivation model.

The above arguments showed that CH_2FCH_2F colliding with CH_2FCl loses 11 $\pm$ 3 kcal mol^{-1} in a single collision. One should, therefore, compare the experimental k_a with calculated values of k_a using s=11 kcal mol^{-1} rather than with the unit deactivation model used in the previous section to deduce the critical energy. However, the tabulated values of the limiting high pressure values of k_a for step size from 5.7 kcal mol^{-1} to unit deactivation show that the high pressure rate constant is not very dependent upon the exact cascade step size for the larger values of s. Therefore, another way of comparing the experimental and calculated rate constant, which is easier, is to convert the experimental rate constant into the unit deactivation rate constant. These correction factors, 0.89 for 300°K and 0.86 for 473°K, were calculated from the following table and were used in the previous section to convert the experimentally measured rate constant to the unit deactivation experimental rate constant.

Table XX k_a^∞ for different energy losses per collision

	energy loss (kcal mol^{-1})							unit deact.	$\frac{k_a^{unit}}{k_a(s=11)}$
	s=5.7	s=7.4	s=9.2	s=11	s=13	s=14	s=16		
k_a^∞ (300°K) x 10^{-8}	2.30	2.02	1.86	1.75	1.69	1.65	1.62	1.55	0.89
k_a^∞ (473°K) x10^{-8}	4.02	3.49	3.18	2.98	2.85	2.77	2.71	2.57	0.86

(IV) Temperature dependence of nonequilibrium unimolecular rate constants. The temperature dependence of the rate constant at high pressure may be assigned to three things: i) variation of the collisional deactivation mechanism, ii) variation of average energy of the formed molecules, and iii) variation of the collision cross section. In the previous section it was shown that within experimental error the deactivation mechanism did not change for the two temperatures investigated, and for reasonably efficient gases ($s \geq 10$ kcal mol^{-1}) a unit deactivation formulation was sufficient. Therefore, the temperature dependence of the rate constants arises mainly from the change of average energy of the reacting molecules with temperatures which can be calculated from the distribution function $f(\epsilon)$.

$$k_a = D/S = \omega \frac{\int_{\epsilon_{min}}^{\infty} \frac{k_\epsilon}{k_\epsilon + \omega} f(\epsilon) d\epsilon}{\int_{\epsilon_{min}}^{\infty} \frac{\omega}{k_\epsilon + \omega} f(\epsilon) d\epsilon} \qquad (28)$$

At high pressure where $\omega >> k_\epsilon$ the definition of the theoretical k_a reduces to a simple form which is just the average k_ϵ and is independent of ω .

$$k_a = \frac{\int_{\epsilon_{min}}^{\infty} f(\epsilon) k_\epsilon \, d\epsilon}{\int_{\epsilon_{min}}^{\infty} f(\epsilon) d\epsilon} = \langle k_\epsilon \rangle \qquad (48)$$

The temperature dependence of the distribution function can be easily seen by the following equation.

$$f(\epsilon) = \frac{k'_\epsilon K_\epsilon}{\int_{\epsilon_{min}}^{\infty} k'_\epsilon K_\epsilon} = \frac{k'_\epsilon N^*_{\epsilon_{vr}} e^{-\epsilon_{vr}/kT}/Q^*_{vr}}{\int_{\epsilon_{min}}^{\infty} k'_\epsilon N^*_{\epsilon_{vr}} e^{-\epsilon_{vr}/kT}/Q^*_{vr}\, d\epsilon_{vr}} \qquad (49)$$

With the computer, calculations of the nonequilibrium rate constant, k_ϵ, using the distribution function gives the theoretical values of the k_a in a natural and easy way.

In order to obtain the temperature dependence of the rate constants from experimental data which follow the unit deactivation mechanism, it is necessary only to convert the rate constants measured in pressure units into absolute values by using some sort of collision cross section.

$$k_a = \omega(\text{decomposition})/(\text{stabilization})$$

$$\omega = N S^2 \left(\frac{8\pi kT}{\mu}\right)^{\frac{1}{2}} \qquad (10)$$

In the above collisional frequency expression N, the concentration of the bath molecules, and T, the reaction temperature, can be taken into account just by using appropriate values. However, the temperature dependence of the collisional cross section, S^2, presents a problem. This problem was attacked by considering the omega integral (55).

Hirshfelder et al. defined the reduced cross section $S^l(K)$ as the ratio of the gas kinetic cross section to the cross section of the rigid sphere. The reduced cross section is given by

$$S^l(K) = 4/\left(2 - \frac{1+(-1)^l}{1+l}\right) \int_0^\infty (1-\cos\chi)\, \rho\, d\rho \qquad (50)$$

where $l = 2$ for the usual transport cross section such as viscosity and and heat conductivity,

= 1,4 for other kinetic properties.

K is the relative kinetic energy at large separations of the colliding molecules along the line of centers in units of ϵ, ϵ is energy difference between the separated molecules and the molecules in the configuration for which they have the maximum energy of attraction, i. e., the Lennard-Jones value. β is the distance of closest approach of the molecules in units of S_o. If there were no interaction potential between molecules, S_o would be the radius of the hard sphere, and χ is the angle of deflection. The integral is over all values of β, i. e., for all values of the impact parameter. Since the average value of this reduced cross section is desired, the expression must be averaged over the kinetic energy range as follows.

$$\omega^{(l)}(n;x) = \frac{1}{8}\left(2 - \frac{1 + (-1)^l}{1 + l}\right) x^{n+2} \int_0^\infty e^{-xK} K^{n+1} S^l(K)\,dK \qquad (51)$$

For viscosity cross section, n=2 and $x = \frac{1}{kT}$ with k being the Boltzmann's constant. Hirschfelder et. al. related these functions to omega integral as follows.

$$\Omega^{(l,n)}\left(\frac{kT}{\epsilon}\right) = S_o^2 \left(\frac{2\pi kT}{\mu}\right)^{\frac{1}{2}} \omega^l(n;x) \qquad (52)$$

In the reference 22 the omega integral is tabulated in terms of the reduced omega integral, which is the same as the average reduced cross section as shown below.

$$\Omega^{*(2,2)}\left(\frac{kT}{\epsilon}\right) = \frac{\Omega^{(2,2)}\left(\frac{kT}{\epsilon}\right)}{\Omega^{(2,2)}_{\text{rig. sph.}}\left(\frac{kT}{\epsilon}\right)} \qquad (53)$$

$$= \frac{S_o^2 \left(\frac{2\pi kT}{\mu}\right)^{\frac{1}{2}} \omega^l(n;x)}{S_o^2 \left(\frac{2\pi kT}{\mu}\right)^{\frac{1}{2}} \omega^l_{\text{rig. sph.}}(n;x)}$$

$$= \frac{\omega^{(1)}(n;x)}{\omega^{(1)}_{\text{rig. sph.}}(n;x)}$$

$$= \frac{\frac{1}{8}(2-2/3)\,x^4 \int_0^\infty e^{-xK} K^3 S^{(2)}(K)\,dK}{\frac{1}{8}(2-2/3)\,x^4 \int_0^\infty e^{-xK} K^3 S^{(2)}_{\text{rig. sph.}}(K)dK}$$

For rigid sphere $S^{(2)}_{\text{rig. sph.}} = 1$

$$= \frac{\int_0^\infty e^{-xK} K^3 S^{(2)}(K)dK}{\int_0^\infty e^{-xK} K^3\,dK}$$

$$= \langle S^{(2)}(K) \rangle$$

$$= \frac{S^2(T)}{S_o^2} \quad \text{(By definition of } S^1(K)\text{)}$$

Therefore, $S^2(T) = S_o^2\ \Omega^{*(2,2)}(\frac{kT}{\epsilon})$

The reduced omega integrals $\Omega^{*(2,2)}$ taken from table 1-M of reference 22, which have been calculated with the Lennard-Jone's 12-6 potential and viscosity coefficients, are plotted as a function of kT/ϵ in fig. 10. In order to find the reduced omega integral as a function of T for a specific system, it is necessary only to know the ϵ value for that system. However, the values for CH_2FCl, CH_2FCH_2F and CH_3CH_2F are not known. Therefore values for similar molecules were investigated. Most of hydrocarbons have ϵ/k = 200-400°K (see Table 1-A of the reference 22) and for this reason two different values ϵ/k =283°K and ϵ/k =400°K were examined, and it was found that the reduced omega integral becomes unity at 950°K and 1,400°K with ϵ/k = 283°K and ϵ/k = 400°K, respectively. In other words S_o=S(950°K) or S_o= S(1,400°K). This implies that the experimental k_a^{300} calculated by

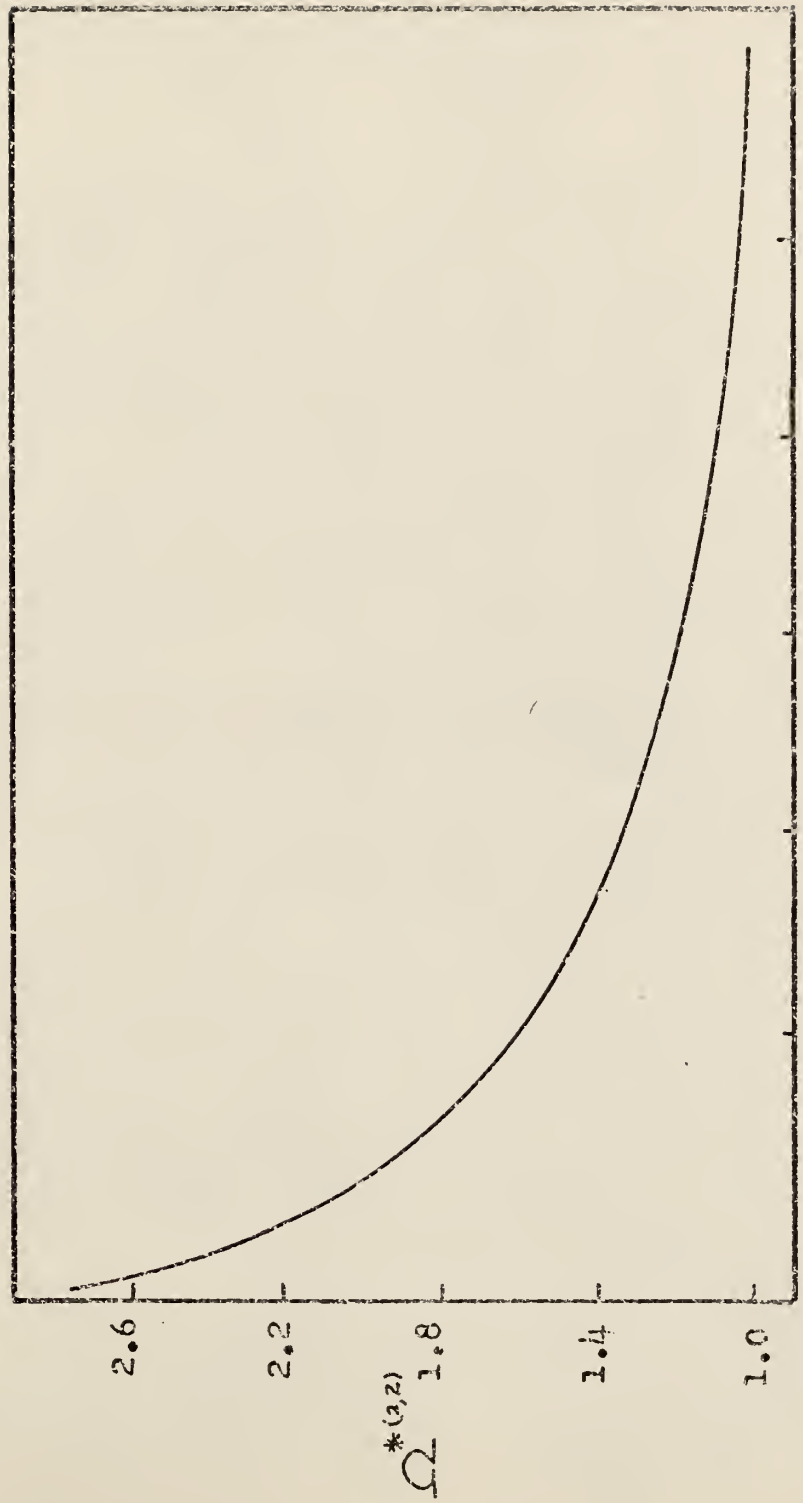

Fig. 10. $\Omega^{*(1,1)}$ vs $T^*(=kT/\epsilon)$

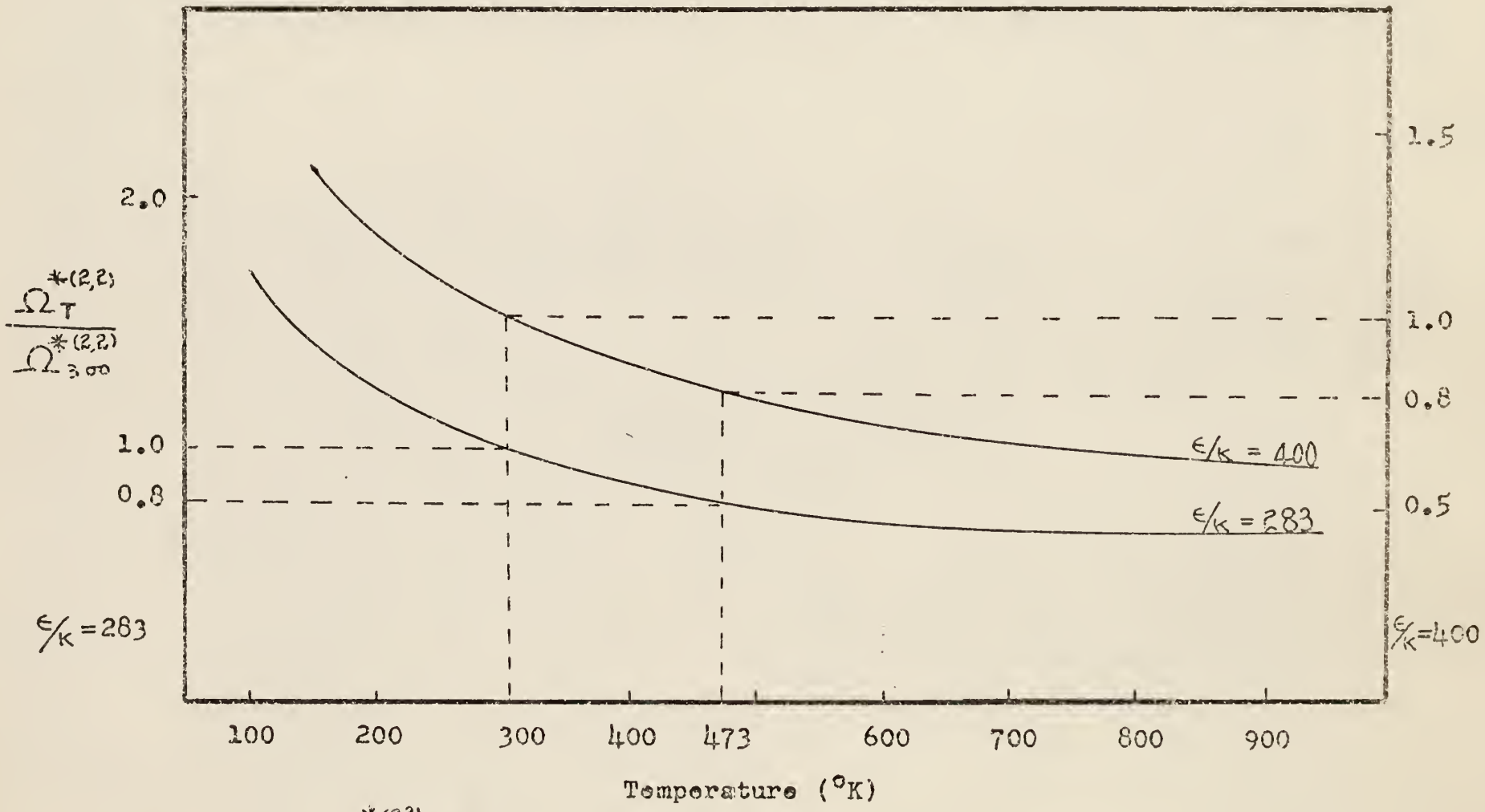

Fig. 11 $\Omega_T^{*(2,2)} / \Omega_{300°K}^{*(2,2)}$ vs Temperature

Table XXI The ratio of the omega integral.

Temp ($^{\circ}K$)	ϵ/k =283$^{\circ}K$			ϵ/k =400$^{\circ}K$		
	kT/ϵ	Ω^{*T}	$\frac{\Omega^{*T}}{\Omega^{*300}}$	kT/ϵ	Ω^{*T}	$\frac{\Omega^{*T}}{\Omega^{*300}}$
100	0.353	2.63	1.69	0.25		
150	0.530	2.20	1.41	0.375	2.55	1.40
200	0.706	1.90	1.22	0.500	2.25	1.24
250	0.883	1.70	1.09	0.625	2.00	1.10
300	1.06	1.56	1.00	0.750	1.82	1.00
350	1.24	1.40	0.90	0.875	1.68	0.92
400	1.41	1.34	0.86	1.000	1.58	0.87
450	1.59	1.28	0.82	1.125	1.50	0.82
473	1.67	1.25	0.80	1.18	1.46	0.80
500	1.77	1.23	0.79	1.25	1.44	0.79
550	1.94	1.18	0.76	1.375	1.36	0.75
600	2.12	1.16	0.74	1.5	1.3	0.71
650	2.29	1.12	0.72	1.625	1.26	0.69
700	2.47	1.09	0.70	1.75	1.22	0.67
750	2.65	1.06	0.68	1.875	1.2	0.66
800	2.82	1.04	0.67	1.9	1.19	0.65
850	3.00	1.03	0.66	2.125	1.15	0.63
900	3.18	1.02	0.65	2.15	1.14	0.63
950	3.35	1.00	0.64	2.375	1.1	0.6

use of S_o should be increased by a factor between 1.56 and 1.82 (see Table XXI). However, because of the following two reasons k_a^{300} with S_c can be used as a correct value: i) most of S_o(CH_2FCl, CH_2FCH_2F, and CH_3CH_2F) are not very well known and adjusting the absolute values does not have much significance, ii) the reduced omega integrals were calculated from the viscosity coefficient and it is not understood whether or not the S_o values from the viscosity coefficient are the appropriate cross sections for collisional deactivation. For purposes of evaluating the temperature dependence of the rate constants, one needs only to examine the relative values of the rate constants, that is, in this study values relative to k_a^{300}. Therefore, it is not critical to establish the exact absolute cross sections. It is necessary, however, to make some adjustment for the change of the cross section with temperature. A correction based upon viscosity data may not be the correct one but this is the best that can be done at the present time. Since the ϵ/k is not known for collisions between the molecules of interest in this study, calculations were done for ϵ/k=283 and 400°K. It was found that the temperature dependence of these two cases are very similar, although as noted above the absolute values are significantly different.

There are two ways for easy comparison of the experimental rate constants to the calculated values for unit deactivation gases. The first method is to use the high pressure rate constant and the second one is to use the low pressure rate constant. The difference between the rate constants and the average energies of reacting molecules of these two limits is shown below:

$$k_a = \omega \frac{\int_{\epsilon_{min}}^{\infty} \frac{k_\epsilon}{k_\epsilon + \omega} f(\epsilon)d\epsilon}{\int_{\epsilon}^{\infty} \frac{\omega}{k_\epsilon + \omega} f(\epsilon)d\epsilon} \quad ; \quad \langle \epsilon \rangle_R = \frac{\int_{\epsilon_{min}}^{\infty} \frac{\epsilon \; k_\epsilon}{k_\epsilon + \omega} f(\epsilon)d\epsilon}{\int_{\epsilon_o}^{\infty} \frac{k_\epsilon}{k_\epsilon + \omega} f(\epsilon)d\epsilon} \qquad (54)$$

At low pressure the collisional frequency becomes negligble compared to k_ϵ and the expressions take the form

$$k_a^o = \frac{\int_{\epsilon_{min}}^{\infty} f(\epsilon)d\epsilon}{\int_{\epsilon_{min}}^{\infty} \frac{f(\epsilon)d\epsilon}{k_\epsilon}} = \langle k^{-1} \rangle^{-1} \qquad \langle \epsilon \rangle_R^o = \frac{\int_{\epsilon_{min}}^{\infty} \epsilon \, f(\epsilon)d\epsilon}{\int_{\epsilon_{min}}^{\infty} f(\epsilon)d\epsilon} \qquad (55)$$

At high pressure the decomposition rate constant becomes negligible compared to the collisional frequency ω and

$$k_a = \frac{\int_{\epsilon_{min}}^{\infty} k_\epsilon f(\epsilon)d\epsilon}{\int_{\epsilon_{min}}^{\infty} f(\epsilon)d\epsilon} = \langle k_\epsilon \rangle \qquad \langle \epsilon \rangle_R^\infty = \frac{\int_{\epsilon_{min}}^{\infty} \epsilon \, f(\epsilon)d\epsilon}{\int_{\epsilon_{min}}^{\infty} f(\epsilon)d\epsilon} \qquad (56)$$

The difference between k_a^o and k_a^∞ is small at low temperature (for CH_2FCH_2F $k_a^o(300) = 1.44 \times 10^8$ sec^{-1}, $k_a^\infty = 1.55 \times 10^8$ sec^{-1}), but becomes significant at high temperature ($k_a^o(800) = 4.79 \times 10^8$ sec^{-1}, $k_a^\infty = 7.83 \times 10^8$ sec^{-1}). The difference comes from the increased spread in distribution function which increases the difference in the average energies of the reacting molecules at the P=0 and ∞ limits. This problem is not very important for the fluoroethane. However for larger molecules or if $E_{min} - E_o$ is small, then the difference between k_a^o and k_a^∞ becomes quite noticeable even for cases following the unit deactivating mechanism (for instance, for butyl radical system (11) at 300°K k_a^o differs from k_a^∞ by a factor of 1.6).

Therefore, one must decide which limiting value to use. In this study the high pressure values were chosen for the comparison; because, as shown in fig. 9, if the unit deactivation mechanism is not valid (i. e. cascade deactivation becomes important) the rate constant k_a^o increases markedly with decreasing pressure and the rate constant depends on the deactivation mechanism, that is, the collisionally less efficient molecule has higher k_a^o than the more efficient molecule. However, at high pressure this phenomenon becomes less important. Also it is simple, even for the unit deactivation case, to handle the variation of k_ϵ with $f(\epsilon)$ at high pressure since $k_a = \langle k_\epsilon \rangle$.

Table XXII contains a listing of the calculated and measured rate constants at various temperatures.

Table XXII Comparison of the calculated and experimental rate constants

T°K	CH_3CH_2F			CH_2FCH_2F		
	k_a calc'd	$\langle\epsilon\rangle$(kcal mol^{-1})	k_a exp	k_a calc'd	$\langle\epsilon\rangle$	k_a exp
300	1.32×10^9 sec^{-1}	2.48		1.55×10^8 sec^{-1}	2.87	1.80[a]
358	1.49	3.33	1.31[b,c]			
375	1.55	3.57		1.91	3.99	
450	1.84	4.71		2.39	5.21	
473	1.95	5.09		2.57	5.60	2.55[a,b]
500	2.08	5.56		2.80	6.08	
551	2.37	6.43		3.82	7.62	
640	3.00	8.10		4.49	8.84	
700	3.54	9.29		5.53	11.0	
800				7.83	12.3	

a. Converted to the unit deactivation rate constants by using factors of 0.89 for 300°K value and 0.86 for 473°K value.

b. The temperature dependence of the collisional cross section was taken into account by using a factor of 0.8 for CH_2FCH_2F and 0.91 for CH_3CH_2F relative to 300°K values.

c. No correction for collisional inefficiency was applied because the bath gas in this system was CH_3COCH_3 which has greater molecular complexity than CH_2FCl.

The calculated temperature dependence (1.66) agrees to within 15 % of the experimental dependence (1.42) for CH_2FCH_2F for the temperature range of 300°K to 473°K. The theoretical factor of 1.66 corresponds to a change in average energy of 2.73 kcal mol^{-1}. Although not an extensive test these results suggest that the energy dependence of the RRKM formulation is satisfactory for the fluoroethane models. Without the correction factor, 0.8 for the temperature dependence of the collisional cross section, the experimental ratio is 1.67 for the data at 300 and 473°K.

DISCUSSION

The critical energy of the HF elimination reaction from the vibrationally excited fluoroethane has not been directly measured by thermal activation. Some efforts (7)(8)(9)(10) have been made to estimate the critical energy from chemical activation data by using the classical, statistical mechanical RRK theory for interpreting the experimental data. However, the reliability of the experimental values of the rate constants in those studies as well as the calculated results from the RRK theory are in doubt. The experimental measurements (7)(8)(9) were done over too small a pressure range for most work in the literature, and this is the main source of possible error. Furthermore, the pressure used in the literature was too low for the studies of CH_3CH_2F. From the work of this thesis, CH_3CH_2F has a half quenching (D/S = 1) pressure of 17 cm-Hg, while the pressure range of the work reported in the literature was 6-7 cm-Hg. For this reason the measurements of the rate constant were repeated first in order to eliminate the uncertainty in the literature data and then to estimate the critical energy from well established experimental data together with RRKM calculation. The contributions of this work are threefold: first, this is the first attempt to generate the vibrationally excited 1,2 difluoroethane by mercury photosensitization, second, the experiments were done over a wide range of prssures which gave D/S ratio from 0.1 to 11 for CH_2FCH_2F and from 0.1 to 2 for CH_3CH_2F, third, this is the first interpretation of unimolecular reactions of the energized fluoroethane in terms of the RRKM formulation. The experimental data obtained in this thesis were interpreted according to the RRKM theory of unimolecular reactions in the preceding section. The conclusions were summarized on pages 49 - 73 . This section is mainly concerned with comparing the experimental results of this lab-

oratory and calculated results of RRKM theory with literature data and RRK calculations for fluoroethanes. Specifically the experimental results of this study will be compared to those of the literature, next, other data in the literautre will be interpreted according to the RRKM theoretical calculations, and the results from RRK calculation which have been previously published in the literature will be criticized.

(I) Comparison of experimental rate constants.

(a) CH_2FCH_2F. The HF elimination reaction rate constants have been reported by several workers, and the results that can be compared to the data of this study are shown in Table XXIII.

Table XXIII Rate constants for $C_2H_4F_2$

System	Temp(^oK)	k_a(cm)	$k_a(sec^{-1}) \times 10^8$
CH_2FCl	300	2.0 ± 0.1	2.0 ± 0.1
+			
($Hg(^3P_1)$)	473	4.6 ± 0.2	3.0[a](3.7) ± 0.2
CH_2FCOCH_2F[b]	300 ± 20	2.2	2.2
+			
hν	476 ± 4	4.5	2.9[a](3.6)
CH_3COCH_2F[c]	329	7.2	7.1 (7.4)
+			
hν	472 ± 12	9.0	6.2[a](7.7)
CH_2FCOCH_2F[d]	300	1.6	1.6
+			
hν	473	3.6	2.3[a](2.9)

a. The rate constant if a temperature dependence factor of 0.8 is applied to the Lennard Jone's cross section.
b. Pritchard et al.(9). c. Pritchard et al.(8).
c. Trotman-Dickenson et al.(7).

These rate constants were estimated from fig. 12 which was constructed from the experimental D/S values at the different pressures given in the literature cited above with exceptions of lines 1, 4, and 5. The latter three were obtained from the rate constants that were estimated from fig. 1 of the reference 7 and fig. 2 of the reference 8. The rate constants were converted from cm units to sec^{-1} by using the following collision diameters at 300°K; C_3H_6-4.7 Å (22), CH_2FCl-4.5 Å, CH_2FCOCH_2F-5 Å, CH_2FCH_2F-5 Å, and CH_3COCH_2F-5 Å (the last four were chosen by analogy with CH_2Cl_2 (4.8 Å) and CH_3COCH_3 (4.7 Å).

The results of the first row of Table XXIII were obtained in this laboratory. The experiments were done over a wide range of pressures and were analyzed under different conditions as described in the EXPERIMENTAL SECTION. There is an excellent agreement between the results of this study and those of the second in Table XXIII obtained by Pritchard and co-workers from the photolysis of 1,3 difluoroacetone. There is also a fairly good agreement between the first two sets of results and the last one which was obtained by Trotman-Dickenson and co-workers with the photolysis of 1,3 difluoroacetone. This good agreement between three sets of experiments done by three different groups and two different techniques, photolysis and Hg-photosensitization, leads to the conclusion that the rate constants obtained from this laboratory, $(2.0 \pm 0.1) \times 10^8$ sec^{-1} at 300°K and $(3.0 \pm 0.2) \times 10^8$ sec^{-1} at 473°K, are very reliable.

The third set of experiments of Table XXIII done by Pritchard and Thommarson with photolysis of CH_3COCH_2F is in disagreement with all the others including the second set of rate constants which were also measured in the same laboratory. The discrepancy between two sets of Pritchard's data exsits for all temperatures studied, 300-500°K, with the rate constants from

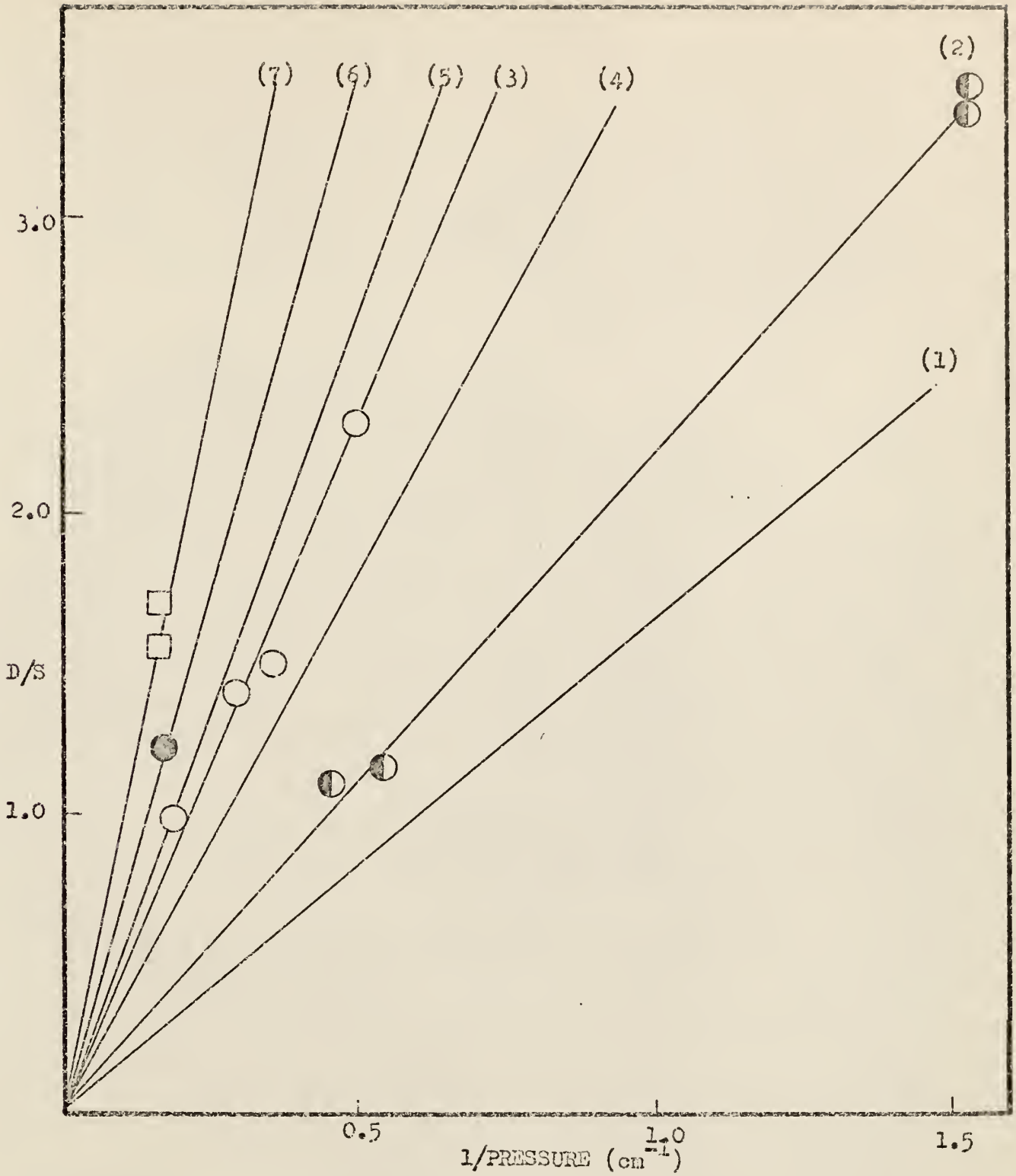

Fig. 12 Comparison of experimental rate constants.
(1), (4) Trotman-Dickenson (CH_3COCH_3 + CH_2FCOCH_2F) at 300°K & 473°K
(2) Pritchard et al. with CH_2FCOCH_2F at 300 ± 20°K. ◐
(3) Pritchard et al. with CH_2FCOCH_2F at 476 ± 4°K ○
(5),(6) & (7). Pritchard et al. with CH_3COCH_2F at 298, 329 & 472°K.
(○-329°K, □-472°K)

CH_3COCH_2F system being higher than those from CH_2FCOCH_2F system. The difference was attributed by the authors to the difference in quenching efficiencies of mono and difluoroacetone. The work of this thesis, however, shows that CH_2FCl removes as much as 11 ± 3 kcal mol^{-1} of energy per collision. Hence, CH_2FCOCH_3, which has a greater molecular complexity, should have higher quenching efficiency than CH_2FCl, which implies that the rate constants from fluoroketone system can not be higher than those from CH_2FCl systems. Furthermore the cross sections and reduced masses of difluoroacetone and monofluoroacetone are similar. Therefore, the disagreement in rate constants is not easily explained in terms of the different quenching efficiencies of the bath gas.

(b) CH_3CH_2F. Three different rate constants are available; one value comes from Trotman-Dickenson's studies (7) and three values from Pritchard and Thommarson (8). The rate constants were converted into sec^{-1} units with the following collision diameters; CH_3CH_2F-4 Å, CH_3COCH_2F-5 Å, and CH_3COCH_3-4.7 Å (22). These values were assumed as 300°K values.

Table XXIV Rate constants for CH_3CH_2F.

System	T°K	k_a(cm)	$k_a(sec^{-1})x10^9$
$CH_3COCH_3 + CH_2FCOCH_2F + h\nu$ [a]	358	17.2	1.31[d] (1.44)
$CH_3COCH_2F + h\nu$ [b]	329	34.2	2.95[d] (3.11)
	362	25.3	2.00[d] (2.20)
	405	27.0	1.91[d] (2.20)
$CH_3COCH_3 + CH_2FCOCH_2F + h\nu$ [c]	300	14.2	1.24

a. This study. b. Pritchard and Thommarson (8). c. Trotman-Dickenson and co-workers (7). d. Allowance was made for the temperature dependence of the cross section relative to 300°K.

The first row of Table XXIV is the result of this study, and the rate constant is the least square value from eleven D/S points at different pressure ranging from 8.3 to 64 cm-Hg. The temperature dependence of the cross section relative to 300°K was considered by multiplying the rate constant in sec^{-1} unit by a factor of 0.91 (see Table XXI). No detailed experimental data in the terms of D/S were given by reference 7; the rate constant was merely quoted in cm units for the temperature of the experiment. However, it is obvious from comparison of the rate constant in cm units that Trotman-Dickenson's data agree with the result of this thesis. If converting to sec^{-1} units, the rate constants can be compared at a common temperature and for unit deactivation efficiency. This was done simply by multiplying Trotman-Dickenson's rate constant, 1.24×10^9 sec^{-1}, by a factor of 1.13 which is the RRKM calculated value for the ratio of k_a (358°K) / k_a(300°K). This conversion results in a value of 1.40×10^9 sec^{-1} which agrees within 8 % with the value measured in this work, 1.31×10^9 sec^{-1}. The second row of Table XXIV was from data by Pritchard and Thommarson in the same study that the high rate constants for CH_2FCH_2F were measured. The rate constants in terms of sec^{-1} were calculated by this author from a single D/S value for each temperature cited in the reference 8. There were no more data given in the paper for this temperature range. The rate constants are inverted with respect to the expected temperature difference. Furthermore, much of these data is in the low pressure region where accurate measurements are hard to make. Since Pritchard's CH_3COCH_2F system gave no agreement for both CH_2FCH_2F and CH_3CH_2F, the rate constants measured in that study are not considered very reliable.

(II) Comparison of the calculated and experimental temperature dependence of the chemical activation rate constants.

(a) CH_2FCH_2F. The increase of the reaction temperature causes the distribution function to spread out, as shown in fig. 8, which increases the average energy of the energized molecules. Since k_a is defined as k_e averaged by the distribution function, the apparent rate constant k_a is expected to increase as the reaction temperature increases. Hence, a comparison of the theoretical and experimental k_a values constitutes a test of the energy dependence of k_a (11), providing the deactivation mechanism is independent of temperature. In this section comparison is made between RRKM calculations and the body of data available in the literature. Calculated rate constants used for the comparison are values at the high pressure limit for the reason given previously (see page 72).

The rate constants for CH_2FCH_2F have been measured for a variety of temperatures by Trotman-Dickenson and co-workers and by Pritchard and co-workers; the results are summarized in Table XXV. The rate constants from Trotman-Dickenson's data were calculated from fig. 1 of reference 7, while Pritchard's data were taken from Table III of reference 9. Pritchard's rate constants above 500°K were measured at low pressure where $S/D \geq 0.3$. It has been shown in this thesis that for CH_2FCl as the deactivating gas the measured rate constants (average-energy loss per collision of 11 $\pm$ 3 kcal mol^{-1}) correspond to unit deactivation if multiplied by a factor of 0.89 at 300°K and 0.86 at 473°K. Since data in the literature were obtained with molecules with greater complexity as bath gases than CH_2FCl, no such factors were applied to them. The temperature dependence of the collisional cross sections used in Table XXV were estimated, relative to 300°K, by use of the reduced omega integral.

In order to graphically compare the temperature dependence of the rate constants given in Table XXV, k_a^T / k_a^{300} was drawn against T (°K)

Table XXV Comparison of the Calculated and Experimental Rate Constants[a, b]. (CH_2FCH_2F).

T^oK	Calculated $k_a(sec^{-1})$	ratio	$\langle\epsilon\rangle$	This study $k_a(sec^{-1})$	ratio	Pritchard[c] $k_a(sec^{-1})$	ratio	Trotman-Dickenson[d] $k_a(sec^{-1})$	ratio
300	1.55	1.00	2.9	1.8[e]	1.0	2.2	1.0	1.6	1.0
325						2.2	1.0		
375	1.91	1.23	4.0			2.2	1.0		
426						2.9	1.3		
473	2.57	1.66	5.6	2.6[e]	1.4			2.3	1.4
476						2.9	1.3		
500	2.80	1.81	5.8					2.7	1.7
523						4.0	1.8		
550								3.2	2.0
551						7.4	3.4		
581						11.5	5.2		
593	3.82	2.46	7.9					3.8	2.4
639	4.49	2.90	8.6					5.4	3.4
700	5.53	3.57	10.1					8.8	5.5

a. All values for the rate constants must be multiplied by 10^8 sec^{-1}.

b. Temperature dependence of the cross section for experimental rate constants was allowed according to the omega integral.

c. Ref. 9. d. Ref. 7.

e. Corrected for unit deactivation rate constants by multiplying by a factor of 0.89 for 300°K and 0.86 for 473°K.

as shown in fig. 13; k_a^{300} is the rate constant at 300°K, while k_a^T is that of a given temperature T. Since the main concern is to see the relationship between variation of average energy and the rate constant, the experimental k_a^T was divided by the experimental k_a^{300} from the same set of data. Thus differences in absolute values of k_a(300°K) between the different laboratories become unimportant.

Up to a temperature of about 500°K there is excellent agreement between the experimental and calculated ratio for all data. The calculated ratio of 1.81 at 500°K corresponds to an average energy change of 3 kcal mol^{-1}; the agreement between theory and experiment suggests that the energy dependence of the theory is satisfactory. The temperature dependence of the collisional probabilities (average quantity of energy transferred per collision) could not be detected between 300° and 473°K. However, if previous work by Kohlmaier and Rabinovitch (54) is correct, the diminishing collisional efficiency at low pressure coupled with the fact that the experiments were done in the low pressure region could explain the deviation of experiment from the theoretical curve above 500°K.

Discussion of the possible variation of the collisional cross section with temperature is delayed until the end of the section.

(b) CH_3CH_2F. Since the rate constant was measured at only one temperature in this study, it is not possible to compare the temperature dependence of the calculated rate constants with our experimental values. However, previously studies have been done by Pritchard and Thommarson over the range from 329°K to 571°K with CH_3COCH_2F as a radical source (8). The reported D/S value at a given pressure and temperature was converted to the rate constant in sec^{-1} unit using the same collision diameters as previously listed and the reduced omega integral for the temperature dependence of the collisional cross section. This is shown in Table XXVI.

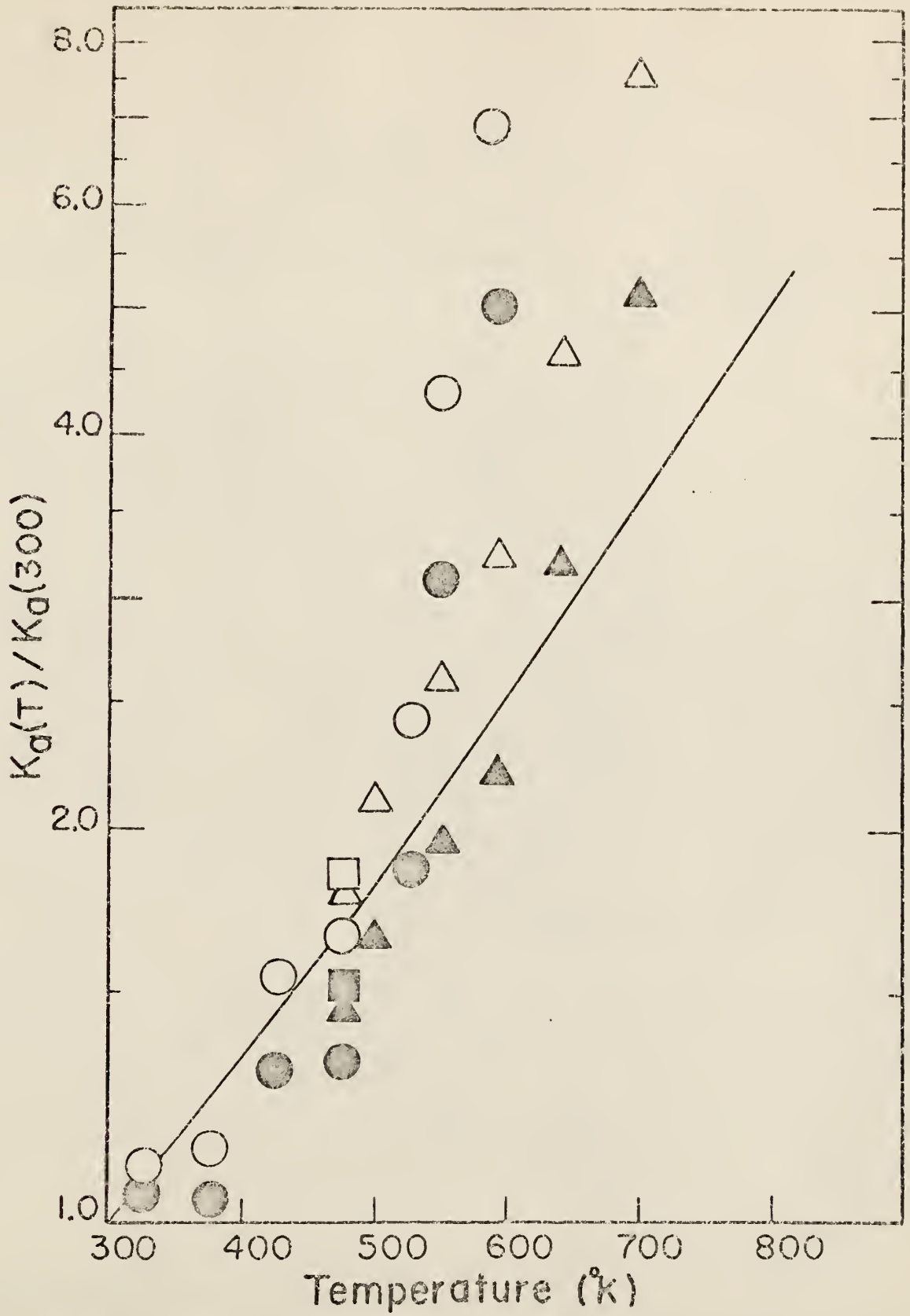

Fig. 13 Temperature dependence of rate constants for CH_2FCH_2F. □ - present work; O - photolysis of CH_2FCOCH_2F (ref 9); Δ - ref 7. Open and closed symbols correspond to temperature independent and dependent cross sections. The line is the RRKM computed rate constants.

Table XXVI Comparison of the Calculated and Experimental Rate Constants[a], (CH_3CH_2F)

T(°K)	Calculated k_a	Calculated ratio	$\langle\epsilon\rangle$ c	This Study k_a [b]	Trotman-Dickenson[d] k_a	Pritchard[e] k_a [b]	Pritchard[e] ratio
300	1.32	0.87	2.55		1.24		
329	1.40	0.93	2.93			2.95	1.51
358	1.49	0.99	3.33	1.31			
362	1.51	1.00	3.39			2.00	1.00
406	1.66	1.10	4.03			1.91	0.97
417	1.70	1.13	4.20			2.21	1.10
420	1.72	1.14	4.24			2.72	1.36
450	1.84	1.22	4.71			2.67	1.37
464	1.91	1.26	4.94			1.99	1.00
480	1.98	1.31	5.20			2.58	1.29
505						2.87	1.44
525	2.22	1.47	5.97			2.24	1.12
551	2.37	1.57	6.43			2.14	1.07
571	2.50	1.66	6.79			2.18	1.09
640	3.00	1.99	8.10				
700	3.54	2.34	9.30				

a. All values for the rate constants must be multiplied by 10^9 sec^{-1}.

b. Temperature dependence of the cross section was allowed according to the omega integral (see page 69).

c. The average energy of the molecule is 88.2 kcal $mol^{-1}(E_{min})$ + $\langle\epsilon\rangle$.

d. Reference 7. e. Reference 8.

Obviously there is a general increase in the rate constants as the temperature increases; however, the scatter in the data is very bad. In order to see the increase relative to one temperature, the rate constant at 362°K was used as a normalizing factor for both the calculated and experimental data. The relative increase is shown in fig. 14. Up to temperature of 480°K, the agreement between the calculated dependence, 1.31 (corresponds to energy increase of 1.9 kcal mol^{-1}) and experimental dependence, 1.29, is good although it is not any better than for CH_2FCH_2F. Above this limit the data are obviously in error since most of the values for the rate constant decline with increasing temperature. The error probably comes about from the fact that the rate constants were measured in the low pressure range, 5-6 cm-Hg and at this low pressure the decomposition product $CH_2=CH_2$ becomes a significant component of the reaction mixture and may have been consumed by radical reactions during the reaction. This points out the need to always do a D/S vs. 1/P plot before assigning confidence to a measured value of k_a.

(c) CH_3CHF_2. The enhancement of the chemical activation rate for 1,1 difluoroethane over 1,2 difluoroethane is expected due to the higher frequencies of CH_3CHF_2 which lowers the $N^*(\epsilon)$ in eq. 24. In addition, additional reaction channels are available due to the competitive α,α and α,β HF elimination. Experimental data obtained by Trotman-Dickenson and co-workers (56) from co-photolyses of CH_2F_2 and ketene (half quenching pressure is 20 cm at 290°K) and acetone and tetrafluoroacetone (half quenching pressure is 20 cm at 300°K) along with Bryant and Pritchard's half quenching pressure, 24.8 cm at 460°K measured in the co-photolysis system of acetone and tetrafluoroacetone (57) support this prediction.

In this section Trotman-Dickenson's experimental data which are more

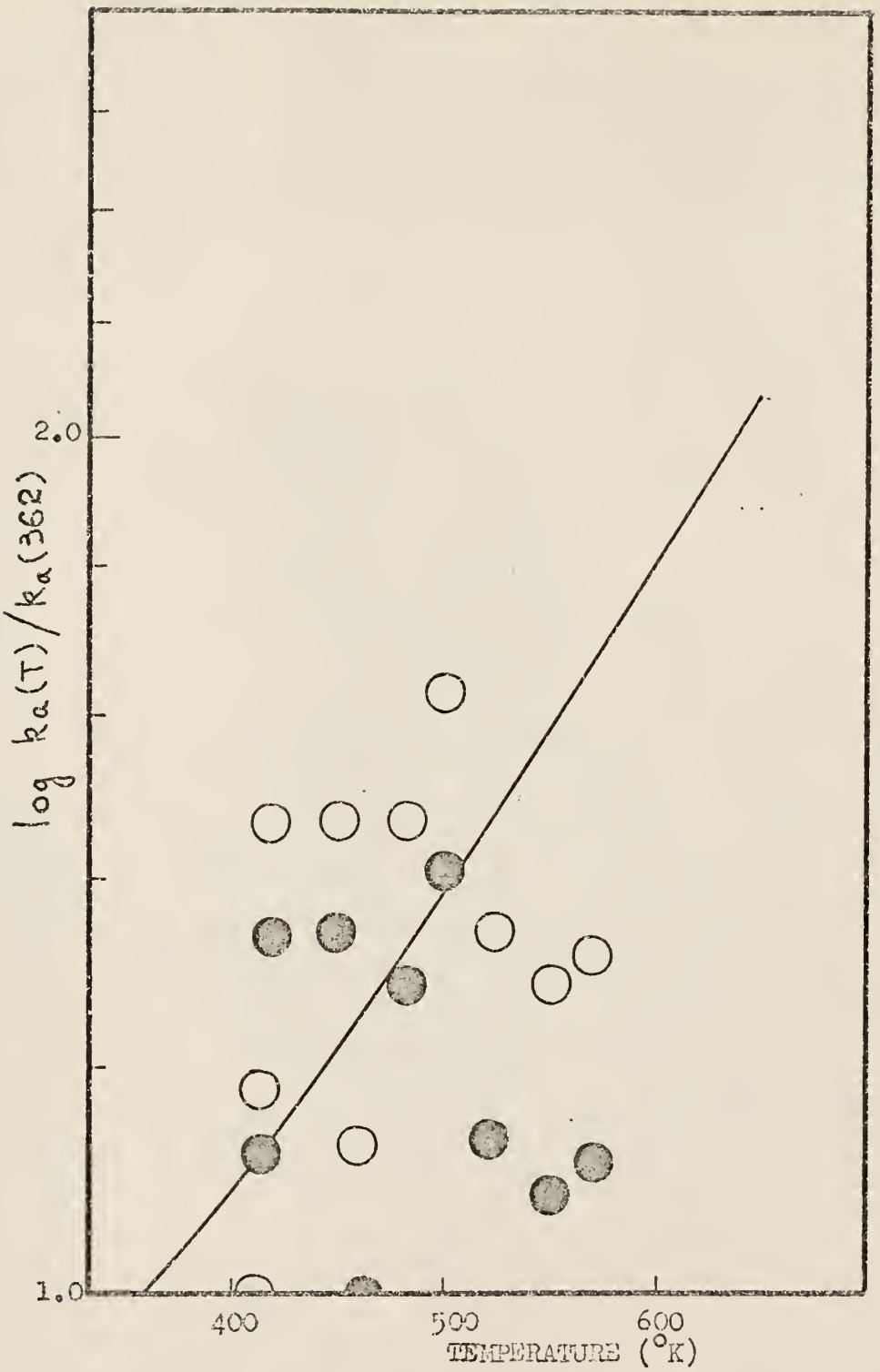

Fig. 14. Temperature dependence of rate constants for CH_3CH_2F. Open and closed symbols correspond to temperature independent and dependent cross section, respectively.

extensive than Pritchard's data are compared with RRKM values calculated using same distribution function and activated complex as for 1,2 $C_2H_4F_2$ but the known frequencies for 1,1 $C_2H_4F_2$. Table XXVII shows this comparison. Experimental rate constants were converted from cm units to sec^{-1} units with following collisional diameters; CH_2F_2- 4.4 Å (22), CH_3CHF_2- 5 Å, and CHF_2COCHF_2- 5 Å; the latter two were assumed. For the RRKM calculation one of the needed thermochemical values, E_{min} of 91.2 kcal mol^{-1} was obtained from $\Delta H_f^\circ(CH_3)$=34.9 kcal mol^{-1} at 0°K, $\Delta H_f^\circ(CH_3CHF_2)$=-118 kcal mol^{-1} at 298°K (43) with appropriate $H^\circ-H_o^\circ$ listed in Table XV and $\Delta H_f^\circ(CHF_2)$=59.3 kcal mol^{-1} which was estimated using $\Delta H_f^\circ(CH_2F_2)$=-106.4 kcal mol^{-1} at 0°K (43), and $D(CHF_2-H)$=101 kcal mol^{-1} at 473°K (44). Another thermochemical value necessary for the calculations is the critical energy, and the value of 57 kcal mol^{-1} was obtained by matching Trotman-Dickenson's experimental rate constants to calculated k_ϵ curves with the critical energy as a variable parameter as in fig. 7. The critical energy which gave agreement was 57 kcal mol^{-1}, which is 5 kcal mol^{-1} lower than for CH_2FCH_2F. This lower critical energy also contributes to the cause of increased rate constant (a factor of three) for 1,1 $C_2H_4F_2$ compared to 1,2 $C_2H_4F_2$. This value for the critical energy can be compared to ϵ_o of 53 kcal mol^{-1} and 47-48 kcal mol^{-1} estimated by Bryant and Pritchard (57) and Kerr, Phillips and Trotman-Dickenson(56), respectively. The reason for this disagreement is due to their use of a lower E_{min},(85 kcal mol^{-1}) in the classical RRK formulation.

The temperature dependence of the Trotman-Dickenson's experimental rate constants is shown in the plot of k_a^T / k_a^{300} vs T in fig. 15. The open and closed symbols correspond to the temperature independent and dependent cross sections, respectively. The solid line corresponds to the RRKM calculated value and lies exactly between the two types of treatment of

Table XXVII Comparison of Calculated and Experimental Rate Constants[a,b,c]

(CH_3CHF_2)

T°K	Calculated $k_a(sec^{-1})$	ratio	$CH_2CO+CH_2F_2$ $k_a(sec^{-1})$	ratio[d]	$CH_3COCH_3+CHF_2COCHF_2$ $k_a(sec^{-1})$	ratio
290	2.42	0.98	1.95	1.00		
300	2.47	1.00			1.75[e]	1.00
333			2.10	1.08		
373	2.89	1.17	2.30	1.18		
386	2.98	1.21			2.09	1.19
428	3.29	1.33	2.48	1.27		
448	3.46	1.40			2.26	1.29
471			2.45	1.25		
478	3.73	1.51			2.40	1.36
500			2.70	1.38		
525	4.21	1.70	2.76	1.41		
529	4.25	1.72			2.81	1.61
620	5.43	2.20			3.36	1.92

a. Ref. 56.

b. All values for the rate constants must be multiplied by 10^9 sec^{-1}.

c. Temperature dependence of the cross section was allowed according to the omega integral.

d. Used k_a (290°K) as a normalizing factor.

e. Extrapolated.

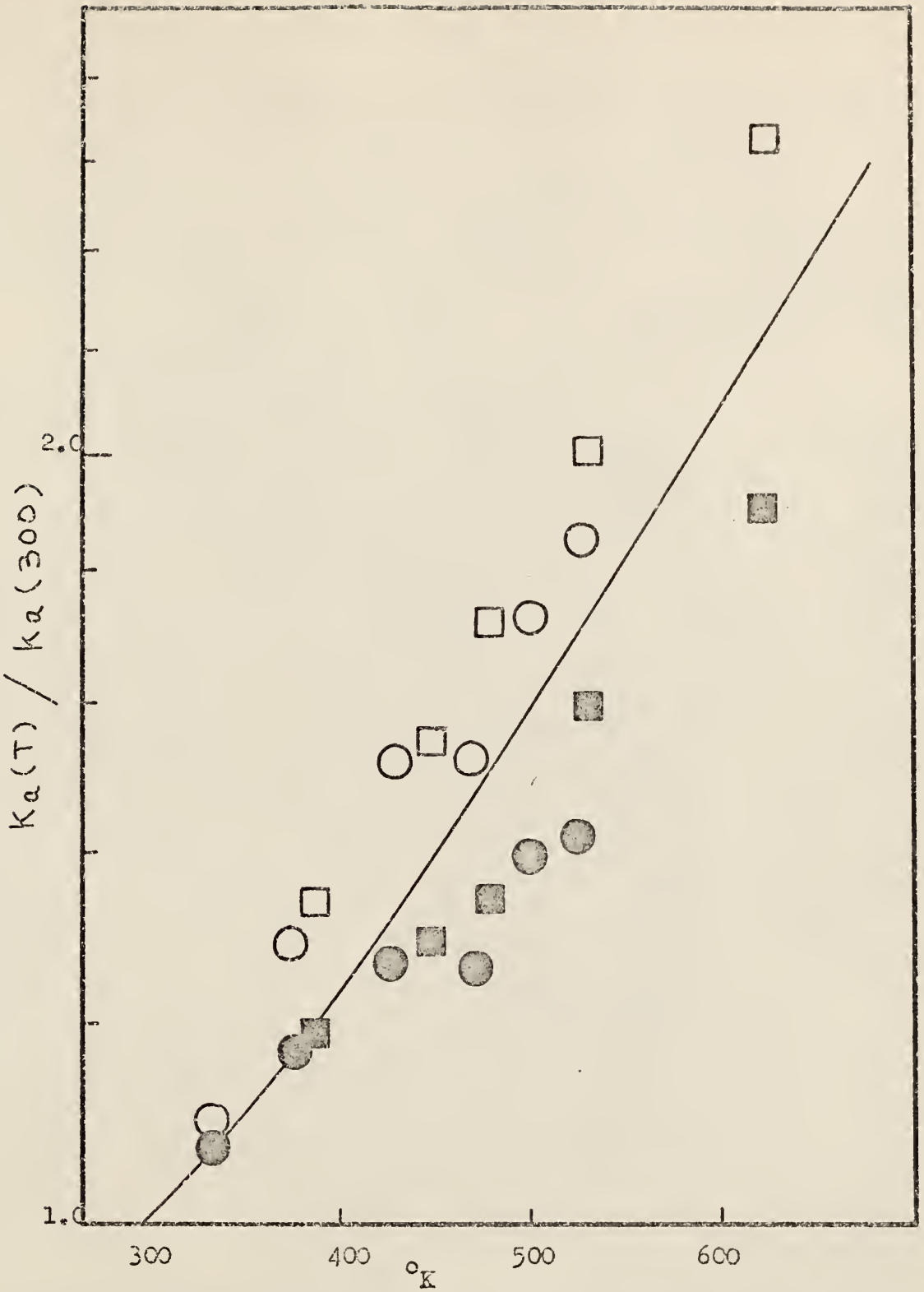

Fig. 15 Temperature dependence of rate constants for CH_3CHF_2. Open and closed symbols correspond to temperature independent and dependent cross section, respectively. ○ - photolysis of ketene, □ - photolysis of acetones.

of collisional diameters.

Therefore, the energy dependence of the elementary specific rate constants seems to be about right, and the remaining problem is to assign the correct form of the temperature dependence of the collision cross section. It seems from figs. 13, 14, and 15, that a less temperature dependent cross section than that given by the omega integral would give better agreement with experimental and calculated results. It is premature to reach a firm conclusion due to the lack of the sufficient knowledge about the deactivation mechanism (value of energy transferred per collision) of the bath gases.

A similar test of the energy dependence of the RRKM rate constants has been done by Rabinovitch and his co-workers with sec-butyl radicals at 195 to 298°K (11). In this case it is known that unit deactivation is followed. They have found good agreement between experimental and calculated temperature dependence of the rate constants with no provision for a temperature dependent cross section. As an example, the experimentally measured ratio of decomposition rate constant of sec-butyl radical formed by the addition of H atom to butene-1 at 195°K and 298°K was 2.2 compared to the theoretically calculated value of 2.1. This ratio corresponded to an average energy change of 1.4 kcal mol^{-1}. No corrections were made for a change in cross section with temperature. For collisions between s-butyl radicals and butene, ϵ/k would be about 300°K. It is clear that the experimental rate constant ratio of 1.8 using a temperature dependent cross section gives a worse agreement than that of a temperature independent cross section. Thus, these data also indicate that the temperature dependence of the collisional deactivation cross section is probably less than that given by the omega integral.

(III) Rate constants of energized fluoroethane generated by different activating reactions. So far discussion has been focused on $CH_3CH_2F^*$ and $CH_2FCH_2F^*$ generated by the combination of CH_3 and CH_2F radicals. However, other reactions for the formation of the energized molecules are also known; two examples are insertion and abstraction reactions.

Insertion : $CH_3F + CH_2 = CH_3CH_2F$

Abstraction: $CH_3CH_2 + F_2 = CH_3CH_2F + F$

$CH_2FCH_2 + F_2 = CH_2FCH_2F + F$

Trotman-Dickenson and co-workers have measured the rate constants for the HF elimination reaction from above energized molecules and they are shown in Table XXVIII.

Table XXVIII Rate Constants of Different Kinds of Chemical Activation System.

		$k_a(sec^{-1})$	E from RRKM (kcal mol^{-1})	Heat of reaction (kcal mol^{-1})
$C_2H_5F^*$	Insertion[a]	1.6×10^{10}	113	99.4
	Abstraction[a]	6.3×10^{6}	67	70.8
$C_2H_4F_2^*$	Abstraction[b]	5.4×10^{4}	67.5	68.2

a. Ref. 58, b. Calculated from k_a=0.00055 cm using cross sections 4 Å and 5 Å for CH_3CH_2F and CH_2FCH_2F, respectively, with CH_3CH_2F as a bath gas (see Ref 7).

In the first line of Table XXVIII $CH_3CH_2F^*$ was formed from the insertion of CH_2 into CH_3F; CH_2 was generated by the photolysis of ketene in the presence of large amounts of oxygen using the full light of a medium pressure mercury arc. The data were obtained over the pressure range from 22 cm to 380 cm-Hg. The nonequilibrium decomposition rate constant of 1.6×10^{10} sec^{-1} corresponds to 113 kcal mol^{-1} of energy according to the RRKM calculated values of k_ϵ tabulated in fig. 7. This may be compared with

an estimate from the thermochemistry of the system. The thermochemical data, $\Delta H_f^o(CH_2) = 93.9$ kcal mol^{-1} (59), $\Delta H_f^o(CH_3F) = 53.9$ kcal mol^{-1} (43) and $\Delta H_f^o(CH_3CH_2F) = -59.4$ kcal mol^{-1} at 0°K give the energy of the activated molecule formed by insertion as $E = 99.4$ kcal mol^{-1}. Adding 2.6 kcal mol^{-1} as the thermal energy (same as that from radical combination system at 300°K) plus 7.3 kcal mol^{-1} from the photo-partitioning of the excess energy of the absorbed quantum of energy gives 109.3 kcal mol^{-1}. The photo-partitioning of the energy was estimated by assuming that i) the light source is mainly 3200 Å and ii) all excess energy goes to the CH_2. With these two assumptions and $E_{excess\ energy} = \Delta H_f^o(CH_2CO) + h\nu - \Delta H_f^o(CO)$ (60) together with $\Delta H_f^o(CH_2CO) = -14.6$ kcal mol^{-1}, $\Delta H_f^o(CH_2) = 93.9$ kcal mol^{-1} and $\Delta H_f^o(CO) = 26.4$ kcal mol^{-1} (59) at 300°K, the excess energy of 7.3 kcal mol^{-1} was obtained. This value, in turn, gives 109.3 kcal mol^{-1} for the energy of the activated molecules. RRKM calculation with the experimental rate constant gives 113 kcal mol^{-1} for this energy. This is probably not too serious a disagreement since the energy difference of 4.7 kcal mol^{-1} only corresponds to a difference of a factor of 0.6 in the rate constant which may be difficult to measure accurately in a oxygen scanved system.

In the second line of Table XXVIII the $CH_3CH_2F^*$ molecules were formed by the F abstraction from F_2 by CH_3CH_2. According to the RRKM calculation the rate constant 6.3×10^6 sec^{-1} corresponds to 67 kcal mol^{-1} of energy. ΔH_{RX} of this system with $\Delta H_f^o(F) = 18.9$ kcal mol^{-1}, $\Delta H_f^o(CH_3CH_2) = 26.7$ kcal mol^{-1} (59) and $\Delta H_f^o(CH_3CH_2F) = -63$ kcal mol^{-1} at 300°K is 70.8 kcal mol^{-1}. From these two values (67 kcal mol^{-1} from RRKM calculation and 70.8 kcal mol^{-1} for the heat of reaction) it can be said that ~95 % of energy is in the internal degree of freedom of the ethyl fluoride.

The last line of the Table XXVIII is the F abstraction from F_2 by

CH_2FCH_2 to form energized molecule $CH_2FCH_2F^*$. Trotman-Dickenson's rate constant 0.00055 cm was converted to 5.4×10^4 sec^{-1} by using cross sections 4 Å and 5 Å for CH_3CH_2F and CH_2FCH_2F, respectively. According to RRKM calculation the rate constant 5.4×10^4 sec^{-1} corresponds to 67.5 kcal mol^{-1} for the energy content of the energized molecule, $CH_2FCH_2F^*$. The heat of the reaction using $\Delta H_f^o(CH_2FCH_2F) = -106$ kcal mol^{-1} (38), $\Delta H_f^o(F) = 18.9$ kcal mol^{-1} (42) and $\Delta H_f^o(CH_2FCH_2) = 18.9$ kcal mol^{-1} (calculated from $CH_2FCH_2F = CH_2FCH_2 + F$ with $D(CH_2FCH_2 - F)$ assumed to be same as $D(CH_3 - F)$) is 68.2 kcal mol^{-1}. These two values imply that 93.9 % of the heat of the reaction is distributed in the energized molecule $CH_2FCH_2F^*$. Amazingly good agreement regarding partitioning of the energy by the abstraction reaction exists between these two sets of data. This implies that in such transfer reactions the newly formed molecules are acquiring nearly all of the potential energy released by the reaction.

(IV) RRK Theory.

Since most of the experimental data in the literature have been interpreted according to the RRK theory, it is pertinent to review this theory and compare those interpretations to the ones deduced from the RRKM theory.

The Rice-Ramsperger-Kassel theory gives the rate constant of the unimolecular decomposition as a function of energy content of the molecule in a classical statistical form:

$$k_{decomp} = A_r \left(\frac{E - \epsilon_o}{E} \right)^{s-1} \qquad (57)$$

where A_r is a constant called frequency factor, ϵ_o is a critical energy of the reaction, E is the energy content of the energized molecule, which

is a function of temperature, and s is the number of effective classical oscillators. For fluorine substituted ethanes Benson (10) related the rate of deactivation to the collision number, Z, and to the probability of complete deactivation per collision, λ, by

$$k_{deact} = \lambda Z \quad ; \quad \frac{1}{P}\frac{S}{D} = \frac{k_{deact}}{k_{decomp}} \tag{58}$$

The λ is essentially a parameter less than unity which measures the effective collisional cross section. The Z may be substituted by ω/P where ω is the collisional frequency, $N\bar{S}_o^2 (8\pi kT/\mu)^{\frac{1}{2}}$, where N is the number of molecules per cc at pressure P. Therefore, the following relationship will hold

$$\frac{1}{P}\frac{S}{D} = \frac{k_{deact}}{k_{decomp}} = \frac{\lambda Z}{A_r}\left(\frac{E}{E-\epsilon_o}\right)^{s-1} = \frac{\lambda\omega'/P}{A_r}\left(E/E-\epsilon_o\right)^{s-1} \tag{59}$$

or in the units used in this thesis

$$1/k_a(sec^{-1}) = \lambda/A_r\,(E/E-\epsilon_o)^{s-1} \quad \text{or} \quad k_a = \frac{A_r}{\lambda}\left(\frac{E-\epsilon_o}{E}\right)^{s-1} \tag{60}$$

In practice other investigators have plotted the experimental points as $\log(1/P)\frac{(S)}{(D)}$ vs. T. The theoretical curves are compared to experiments by treating ϵ_o, s and $\log \lambda/A_r$ values as parameters to get a best fit. In this approach E must be known and it was found by assigning a E_{min} value at 300°K, and then estimating the increase in energy due to the increasing temperature by using the difference in heat capacities of radicals between 300°K and T°K of interest. For example

$$CH_3 + CH_2F \longrightarrow CH_3CH_2F$$

$$E(T)=E(300^\circ) + \frac{3}{2}R(T-300^\circ) + \frac{3}{2}R(T-300^\circ) + \Delta C_{vib}(T-300^\circ) \quad (61)$$

where one $\frac{3}{2}R(T-300^\circ)$ corresponds to conversion of 3 degrees of translation into vibrations and the other corresponds to the conversion of 3 rotations into vibrations. The calculated critical energies obtained in this way are shown in Table XXIX; also included are values calculated in this study from the RRKM formulation.

Table XXIX Critical and average energy[a] at 300°K.

Molecule	This study		Pritchard[b]		Benson[c]	
		E		E		E
CH_3CH_2F	57	90.8	59 (s=10)	85.4	62 (s=10.5)	85.4
CH_2FCH_2F	62	92.5	59 (s=11)	85.4	62 (s=12)	85.4

a. Energies in kcal mol^{-1}. b. Reference 9. c. Reference 10.

The critical energy 57 kcal mol^{-1} for CH_3CH_2F agrees with Pritchard's value 59 kcal mol^{-1}; Benson's 62 kcal mol^{-1} would give k_a values that are too low if it was used in the RRKM formulation. Benson's critical energy for CH_2FCH_2F, 62 kcal mol^{-1}, is in good agreement with the value estimated in this study for CH_2FCH_2F while Pritchard's 59 kcal mol^{-1} value is too low.

Although there is good agreement between the critical energies obtained in this study and those reported in the literature, the values of the energy content of the energized molecules do not agree as shown in the above table. If one uses common E values, the RRK treatment would give higher ϵ_o than the RRKM treatment.

In general for CH_2FCH_2F the method for calculating the average energy of the energized molecule from heat capacity relationship mentioned in the previous page gives higher values than the distribution function of eq. 27. For example $\langle E \rangle_{550} - \langle E \rangle_{300}$ was 6.9 kcal mol^{-1} according to the heat capacity relationship but is only 4.2 kcal mol^{-1} when calculated from $f(\epsilon)$.

In the section below calculated s values for CH_3CH_2F and CH_2FCH_2F were estimated by comparing the rate constant curves obtained from RRKM calculations to those from RRK calculations. The method used is the same as Benson and Pritchard used to fit experiments to RRK results. The curves for RRKM rate constants were obtained by using the values of k_a that have been calculated and listed in other sections of this thesis. The RRK curves were obtained by using the average energies calculated from the distribution function, which were tabulated in Tables XXV and XXVI, and ϵ_o values estimated in this study. The intercepts of the RRK curves were fixed in such a way that all RRK curves meet the RRKM curves at 300°K. As shown in figs. 16 and 17, s=10 with $A_r/\lambda = 10^{10.52}$ and $10^{12.99}$ for CH_2FCH_2F and CH_3CH_2F, respectively give the best fit to the theoretical RRKM curves from 300 to 700°K, which cover an energy range from 92.5 to 99.7 kcal mol^{-1} for CH_2FCH_2F and from 90.8 to 97.5 kcal mol^{-1} for CH_3CH_2F.

However, for a chemical activation system with a lower E_{min}, the same treatment would give different s values. In order to show this change

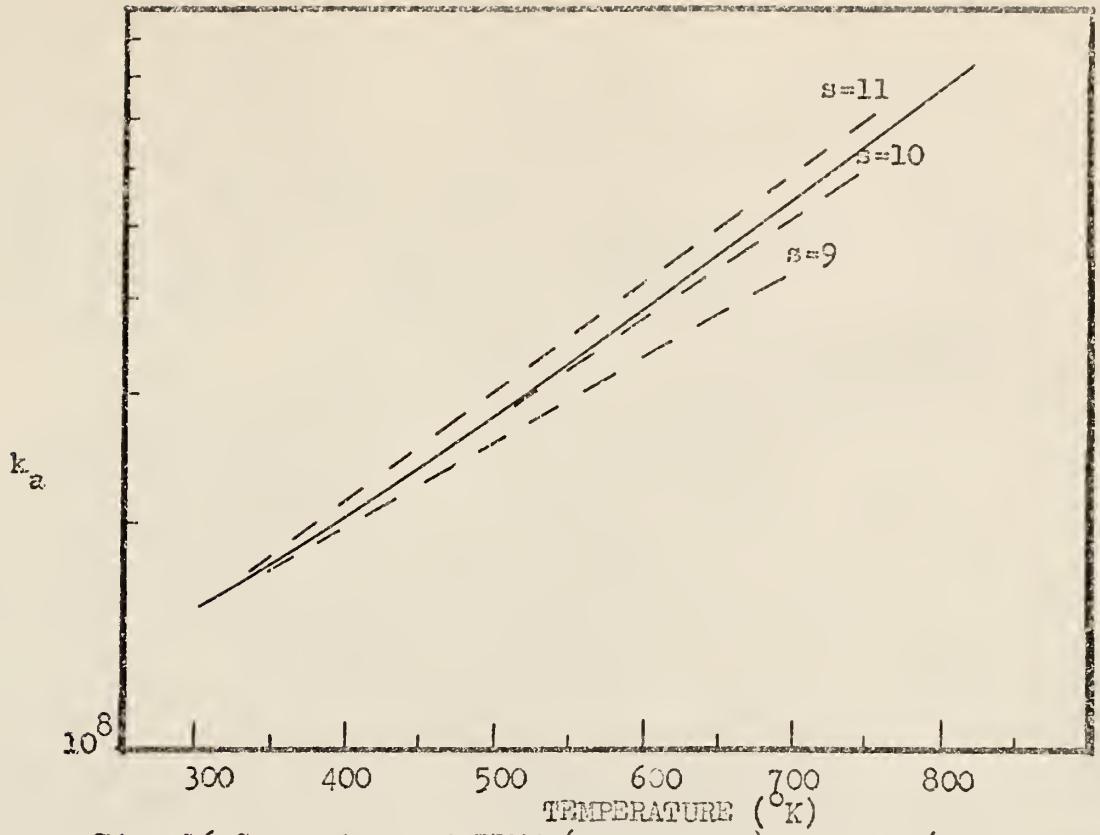

Fig. 16 Comparison of RRKM (solid line) and RRK (broken line) for CH_2FCH_2F

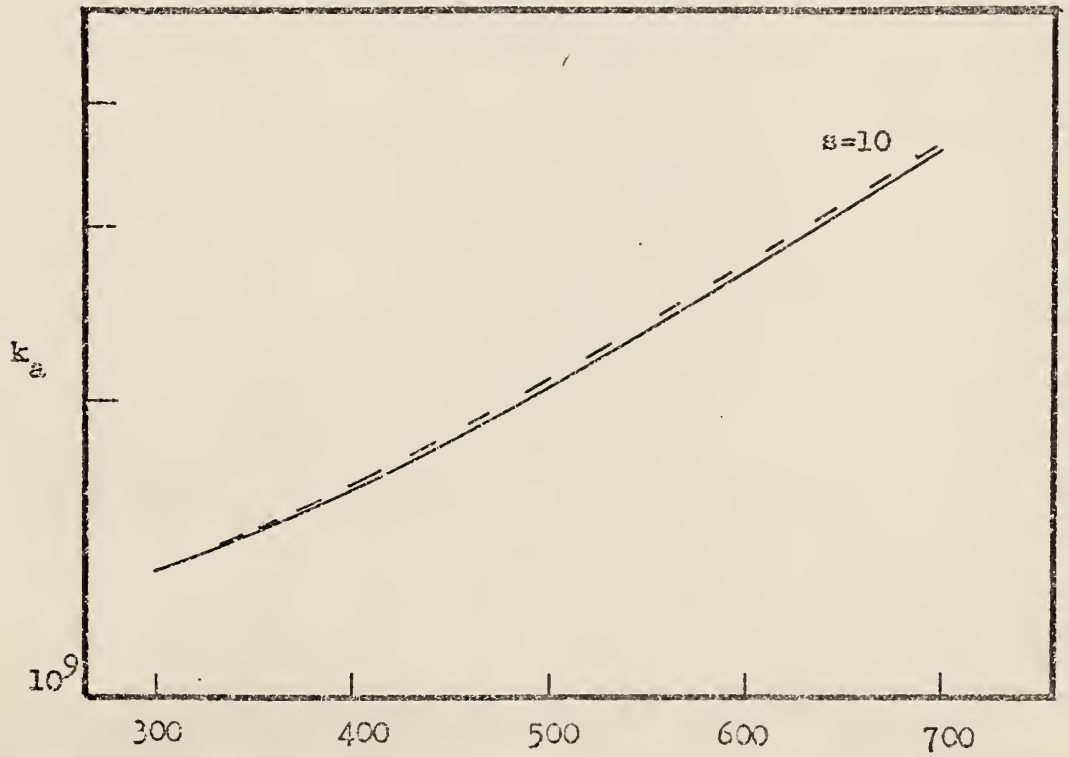

Fig. 17 Comparison of RRKM (solid line) and RRK (broken line) for CH_3CH_2F

in s dramatically, E_{min} was arbitrarily chosen as 65 kcal mol^{-1} for CH_2FCH_2F. The comparison of rate constant curves from RRKM and RRK calculations are shown in fig. 18. The broken line in fig. 18 which was obtained from RRK calculations with s=5.5 and $A_r/\lambda = 10^{9.82}$ gave best fit to the RRKM curve. Therefore, it is meaningless to give any physical significance to s, the number of the classical effective oscillators without mentioning energy content of the molecule. It also should be recognized that those A_r/λ factors are much lower than the measured Arrhenius preexponential factors for these HX elimination reactions. However, this is not surprising since they were used as empirical parameters. Also figs. 16 and 17 show that RRK curve with s=10 fits almost exactly to the RRKM curve for CH_3CH_2F, while for CH_2FCH_2F RRKM curve is slightly higher than RRK curve with s=10. Therefore a fractional change in s is expected.

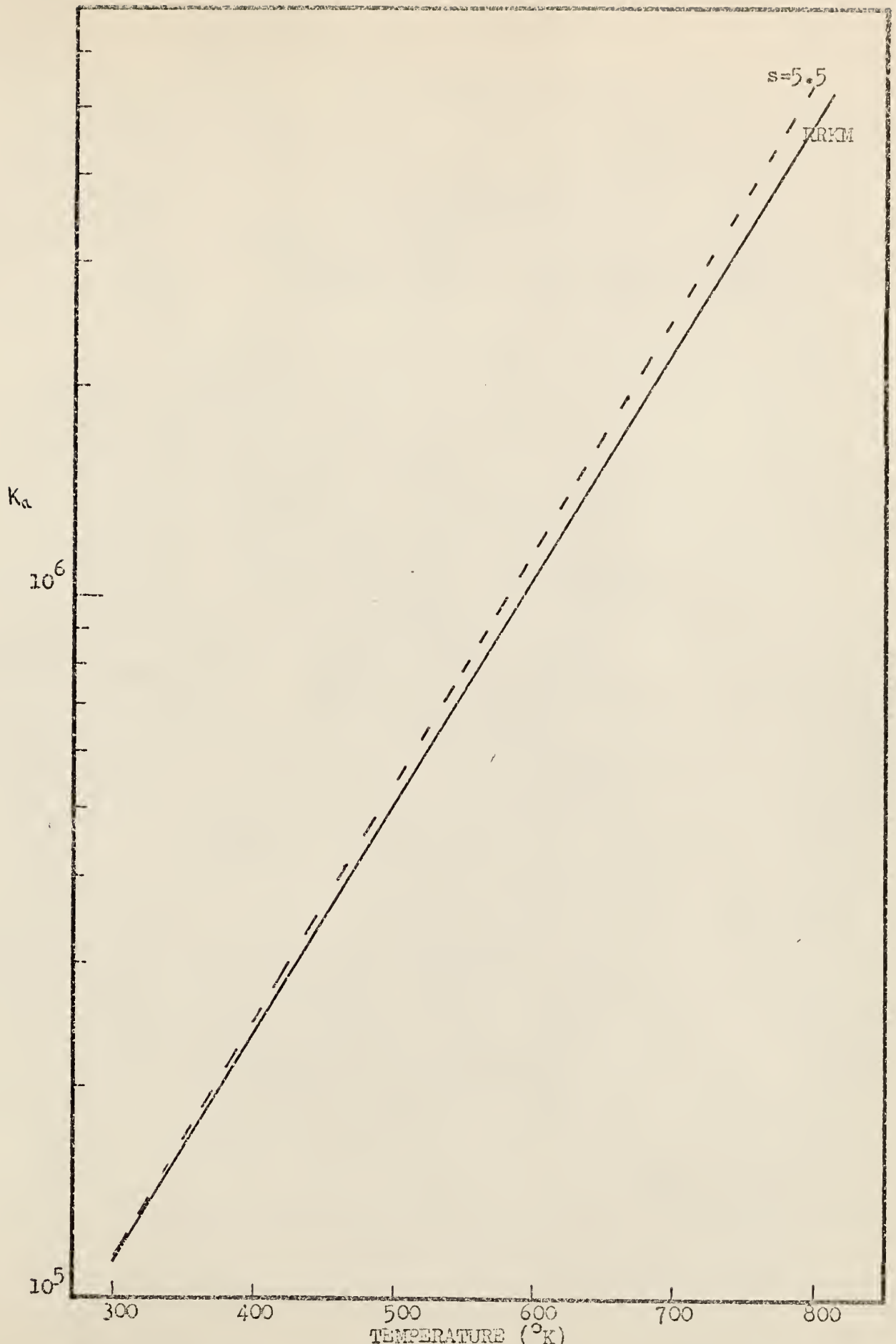

Fig. 18 Comparison of RRKM (solid line) and RRK (broken line) calculations with E_{min}=65 kcal mol^{-1}

CONCLUSION

Careful experiments were done under various conditions (different temperatures with a wide range of pressures with carefully calibrated analytical techniques) to obtain reliable rate constants for HF elimination from chemically activated CH_3CH_2F and CH_2FCH_2F. Since RRKM theory together with an empirical four centered model has been proved successful for correlating unimolecular reactions of chloroethane and bromoethane, it was applied to the fluoroethanes. The critical energies of the CH_3CH_2F and CH_2FCH_2F reactions were estimated, the experimental temperature dependence of the rate constants was examined, and the collisional inefficiency of CH_2FCH_2F at two temperatures was determined.

The following conclusions were obtained from this study:

(a) the experimental chemical activation rate constant for HF elimination from CH_3CH_2F is 1.4×10^9 sec^{-1}. This may be compared to 4.6×10^9 for HCl elimination from CH_3CH_2Cl and 7.6×10^9 sec^{-1} for HBr elimination from CH_3CH_2Br. The increase in the rate constant is due mainly to the decrease in critical energy in going from F to Br in the series.

(b) the critical energies of CH_3CH_2F and CH_2FCH_2F were estimated to be 57 kcal mol^{-1} and 62 kcal mol^{-1}, respectively.

(c) the average loss of energy per collision for the chemically activated CH_2FCH_2F with CH_2FCl was measured as 11-14 kcal mol^{-1}.

(d) the RRKM formulation was applied to the nonequilibrium rate constants which have been measured over the temperature range from 300 to 500°K by other laboratories. The experimental and calculated temperature dependence of the rate constants was in good agreement. Above 500°K it was not possible to test the calculated results because of the lack of good data.

(e) The temperature dependence of collisional deactivation cross sections was examined. The evidence is incomplete but the temperature dependence seems to be less than the temperature dependence of the appropriate (viscosity) omega integrals which are based upon Lennard-Jones interaction potentials.

FOOTNOTE. After this thesis was completed two papers related to the work done here were published by Trotman-Dickenson and co-workers. These are i) Kinetics of the Thermal Decomposition of Ethyl Fluoride (58) and ii) the Elimination of Hydrogen Fluoride from Chemically activated Ethyl Fluoride as a Function of Energy (61). In the first paper the activation energy of 58.2 kcal mol^{-1} with preexponential factor of 13.31 for HF elimination reaction of CH_3CH_2F were measured in the thermal activation system with a temperature range from 683.5 to 738.5°K. Since the data were reproducible, heterogeneous reactions obviously did not occur after seasoning the reaction vessel with ethyl fluoride at 450°C for 14 days. The perfect agreement between the reported activation energy of 58.2 kcal mol^{-1} with preexponential factor of 13.31 and our value of 58.5 kcal mol^{-1} with preexponential factor of 13.20, which was obtained from critical energy of 57 kcal mol^{-1} together with eq. 38, implies that our model for the complex (four centered model) was a good description for the transition state. Also it shows that RRKM calculation can be successfully applied to deduce thermochemical values if reliable experimental data and good models for the molecule and transition state are available. This good agreement also gives some confidence on the critical energy of 62 kcal mol^{-1} for CH_2FCH_2F.

In the second paper RRKM theory was used to interpret chemical activation data of ethyl fluoride formed by i) radical combination of CH_3 and CH_2F produced by photolysis of acetone and 1,3 difluoroacetone (k_a=1 x 10^9 sec^{-1}), ii) F abstraction from F_2 by C_2H_5 (k_a = 6.3 x 10^6 sec^{-1}). The values of k_ϵ calculated in this thesis are smaller than those of Trotman-Dickenson by a factor of 0.75 for the energy range from

70 to 90 kcal mol^{-1}. The difference comes mainly from two sources i) the overall rotational partition function ratio and ii) $\Sigma P(\epsilon)$ terms. Our rotational partition function ratio is larger (0.86) than theirs (0.6) by a factor of 1.4 whereas their $\Sigma P(\epsilon)$ term is larger than ours by a factor of 1.9. This rather large discrepancy in the $\Sigma P(\epsilon)$ term is understandable if the frequencies of the two complexes are examined. In the exchange of chlorine by fluorine in the complex three frequencies (from 861, 629 and 650 cm^{-1} to 1143, 962 and 616 cm^{-1}) should change rather than only one (280 to 310 cm^{-1}).

ACKNOWLEDGEMENT

The author wishes to express his deep appreciation to Professor D. W. Setser for his great encouragement and endless patience, without which this work would not have been possible.

The author wishes to thank Dr. R. L. Johnson for helpful discussions in the early stages of the experiments, and Dr. M. Perona for his grammatical advice.

The author also expresses his thanks to Messrs. K. Dees and W. Richardson for their help with the computations.

Finally, the author wishes to thank the National Science Foundation for support during the period of this study.

LITERATURE CITED

1. B. S. Rabinovitch and D. W. Setser, Advan. Photochem., 3, 48 (1964).
2. J. C. Hassler and D. W. Setser, J. Chem. Phys., 45, 3246 (1966).
3. K. Dees, Master's thesis, Kansas State University, 1968.
4. R. L. Johnson and D. W. Setser, J. Phys. Chem., 71, 4366 (1967).
5. K. Dees and D. W. Setser, J. Chem. Phys., 49, 1193 (1968).
6. C. W. Larson, D. C. Tardy and B. S. Rabinovitch, J. Chem. Phys., 49, 299 (1968).
7. J. A. Kerr, A. W. Kirk, B. V. O'Grady, C. C. Phillips and A. F. Trotman-Dickenson, Disc. Faraday Soc., 44, 263 (1967).
8. G. O. Pritchard and R. L. Thommarson, J. Phys. Chem., 71, 1674 (1967).
9. G. O. Pritchard, M. Venugopalan and T. F. Graham, J. Phys. Chem., 68, 1786 (1964).
10. S. W. Benson and G. Haugen, J. Phys. Chem., 69, 3898 (1965).
11. B. S. Rabinovitch, R. F. Kubin, and R. E. Harrington, J. Chem. Phys., 38, 405 (1963).
12. D. W. Setser and J. C. Hassler, J. Phys. Chem., 71, 1364 (1967).
13. J. G. Calvert and J. N. Pitts, Jr., "Photochemistry" John Wiley & Sons, Inc., New York, N. Y., 1967.
14. R. J. Cvetanovic, "Progress in Reaction Kinetics" vol. 2, The Macmillan Company, New York, N. Y., 1964.
15. M. G. Bellas, O. P. Strausz, and H. E. Gunning, Can. J. Chem., 43, 1022 (1965).
16. a. C. Cillien, P. Goldfinger, G. Huybrechts, and G. Martens, Trans. Faraday Soc., 63, 1631 (1967).
    b. D. Giles, L. M. Quick, and E. Whittle, Trans. Faraday Soc., 63, 662 (1967).
17. D. W. Setser, J. Am. Chem. Soc., 90, 582 (1968).
18. P. B. Ayscough, F. S. Dainton, and B. E. Fleischfresser, Trans. Faraday Soc., 62, 1838 (1966).
19. a. F. M. Scott and K. R. Jennings, Chem. Comm., 700 (1967).
    b. J. D. Allen and M. C. Flowers, Trans. Faraday Soc., 64, 3300 (1968).
20. M. Avarahami and P. Kebarle, J. Phys. Chem., 67, 354 (1963).
21. B. S. Rabinovitch and R. W. Diesen, J. Chem. Phys., 30, 735 (1959).

22. J. O. Hirschfelder, C. F. Curtis, and R. B. Bird, "Molecular Theory of Gases and Liquids", John Wiley & Sons, Inc., 1965.

23. a. R. A. Marcus and O. K. Rice, J. Phys. & Colloid Chem., 55, 894 (1951).
b. R. A. Marcus, J. Chem. Phys., 20, 359 (1952).
c. R. A. Marcus, J. Chem. Phys., 43, 2658 (1965).

24. R. E. Harrington, B. S. Rabinovitch, and R. W. Diesen, J. Chem. Phys., 32, 1245 (1960).

25. P. C. Haarhoff, J. Mol. Phys., 6, 337 (1963).

26. D. F. Eggers, Jr., N. W. Gregory, G. D. Halsey, Jr., and B. S. Rabinovitch, "Physical Chemistry " John Wiley & Sons, Inc., 1964.

27. D. E. Milligan and M. E. Jacox, J. Chem. Phys., 47, 5146 (1967).

28. M. J. Perona, J. T. Bryant, and G. O. Pritchard, J. Am. Chem. Soc., 90, 4782 (1968).

29. Yi-Noo Tang and F. S. Rowland, J. Am. Chem. Soc., 90, 570 (1968).

30. H. S. Johnston, J. Am. Chem. Soc., 86, 1643 (1964).

31. L. Pauling, "The Nature of Chemical Bond" 3rd Ed. Cornell University Press, Ithaca, N. Y. 1960.

32. R. J. Jakobsen, Y. Mikawa, and J. W. Brasch, Spectrochim. Acta, 234, 2199 (1967).

33. a. J. Kraitchman and B. P. Dailey, J. Chem. Phys., 23, 184 (1955).
b. D. C. Smith, R. A. Saunders, J. Rud. Nielsen, and E. B. Ferguson, J. Chem. Phys., 20, 847 (1952).
c. E. Catalano and K. S. Pitzer, J. Phys. Chem., 62, 873 (1958).
d. P. Klaboe and J. Rud Nielsen, J. Chem. Phys., 33, 1764 (1960).

34. F. W. Schneider and B. S. Rabinovitch, J. Am. Chem. Soc., 84, 4215 (1962).

35. E. B. Wilson, Chem. Rev., 27, 17 (1940).

36. D. R. Herschbach, J. Chem. Phys., 25, 358 (1956).

37. D. N. Minkin and A. A. Vvedenskii, Russian J. Phys. Chem., 41, 840 (1967).

38. H. J. Bernstein, J. Phys. Chem., 69, 1550 (1965).

39. "Selected Values of Chemical Thermodynamic Properties" part II. U. S. Department of Commerce, National Bureau of Standards, Circular 500, part II.

40. J. R. Lacher, E. Emory, E. Bohnfalk, and J. D. Park, J. Phys. Chem., 60, 492 (1956).

41. C. Lifshitz and F. A. Long, J. Phys. Chem., 69, 3731 (1965).
42. "JANAF Thermochemical Tables" U. S. Department of Commerce, National Bureau of Standards.
43. J. R. Lacher and H. A. Skinner, J. Chem. Soc., (A) 1033 (1968).
44. A. M. Tarr, J. W. Coomber, and E. Whittle, Trans. Faraday Soc., 61, 1182 (1965).
45. M. J. Perona, Ph.D. thesis, University of California at Santa Barbara, (1968).
46. J. C. Amphlett and E. Whittle, Trans. Faraday Soc., 64, 2130 (1968).
47. R. D. Giles, L. M. Quick, and E. Whittle, Trans. Faraday Soc., 63, 662 (1967).
48. P. Cadman, D. C. Phillips, and A. F. Trotman-Dickenson, Chem. Comm., 796 (1968).
49. J. W. Coomber and E. Whittle, Trans. Faraday Soc., 63, 1394 (1967).
50. A. Maccoll, Disc. Faraday Soc., 44, 283 (1967).
51. Satoru Tsuda and W. H. Hamill, J. Chem. Phys., 41, 2713 (1964).
52. H. E. O'neal and S. W. Benson, J. Phys. Chem., 71, 2903 (1967).
53. R. E. Harrington, B. S. Rabinovitch, and M. R. Hoare, J. Chem. Phys., 33, 744 (1960).
54. G. H. Kohlmaier and B. S. Rabinovitch, J. Chem. Phys., 38, 1692 (1963).
55. J. O. Hirschfelder, R. B. Bird, and E. L. Spotz, J. Chem. Phys., 16, 968 (1948).
S. Chapman and T. G. Cowling, "Mathematical Theory of non-uniform Gases", Cambridge University Press, Teddington, 1939.
56. J. A. Kerr, D. C. Phillips, and A. F. Trotman-Dickenson, J. Chem. Soc., (A), 1086 (1968).
57. J. T. Bryant and G. O. Pritchard, J. Phys. Chem., 71, 3439 (1967).
58. M. Day and A. F. Trotman-Dickenson, J. Chem. Soc., (A), 233 (1969).
59. "Selected Values of Chemical Thermodynamic Properties", 270-3 U. S. Department of Commerce, National Bureau of Standards.
60. D. W. Setser and B. S. Rabinovitch, Can. J. Chem., 40, 1425 (1962).
61. A. W. Kirk, A. F. Trotman-Dickenson, and B. L. Trus, J. Chem.Soc., (A), 3058 (1968).

NON-EQUILIBRIUM UNIMOLECULAR REACTIONS of CHEMICALLY ACTIVATED FLUOROETHANE

by

HEH WON CHANG

B. S. Yonsei University, Seoul, Korea, 1961

AN ABSTRACT OF A MASTER'S THESIS

submitted in partial fulfillment

of the requirements for the degree

MASTER OF SCIENCE

Department of Chemistry

KANSAS STATE UNIVERSITY

Manhattan, Kansas

1969

ABSTRACT

The Rice-Ramsperger-Kassel-Marcus formulation of unimolecular reactions with a four centered empirical model of the transition state has been used to estimate the critical energies and the temperature dependence of the HF elimination rate constants from vibrationally excited CH_2FCH_2F and CH_3CH_2F. The fluoroethanes were generated with about 90 kcal mol^{-1} of vibrational energy by mercury photosensitization of CH_2FCl and co-photolysis of CH_2FCOCH_2F and CH_3COCH_3. The experimental rate constants were $2.0 \pm 0.1 \times 10^8$ sec^{-1} at 300°K and 1.44×10^9 sec^{-1} at 358°K. These rate constants correspond to critical energies of 62 kcal mol^{-1} and 57 kcal mol^{-1} for CH_2FCH_2F and CH_3CH_2F, respectively. The increase in the temperature from 300°K to 473°K caused the average energy of the energized molecule (CH_2FCH_2F) to increase 2.73 kcal mol^{-1}, which increases the rate constant from $2.0 \pm 0.1 \times 10^8$ sec^{-1} to $3.7 \pm 0.2 \times 10^8$ sec^{-1} or $3.0 \pm 0.2 \times 10^8$ sec^{-1} depending upon whether or not the change of collisional diameter with temperature is considered. Simple stepladder deactivation model was used to deduce the collisional inefficiency of CH_2FCH_2F from low pressure data. It was found that the average amount of energy lost by an activated CH_2FCH_2F molecule is 11-14 kcal mol^{-1} per collision, which is in good agreement with a previously obtained value for chloroethanes and cyclopropane at a similar level of energy. A comparison between RRKM and RRK formulations was made for CH_3CH_2F and CH_2FCH_2F, and it was found that s, the number of classical effective oscillators, varies with energy content of the molecule.